

AD-A089 312

NAVAL RESEARCH LAB WASHINGTON DC
THE NRL PROGRAM ON ELECTROACTIVE POLYMERS.(U)
SEP 80 R B FOX
NRL-MR-4335

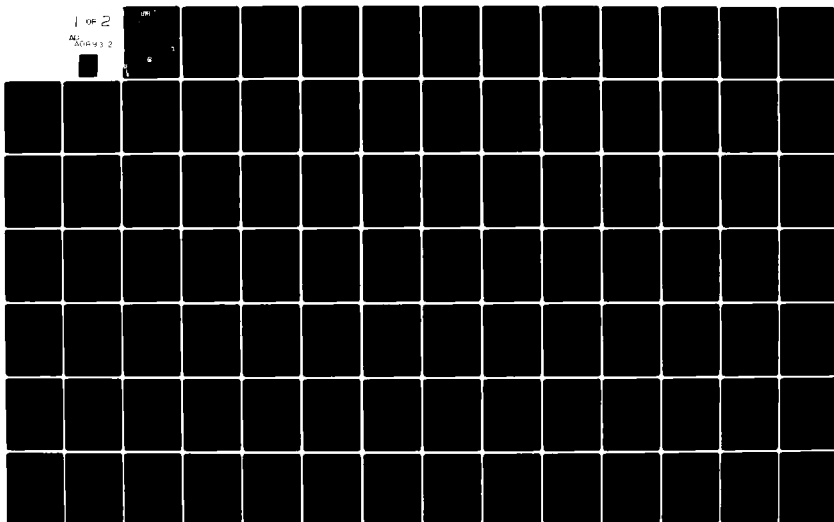
F/G 11/9

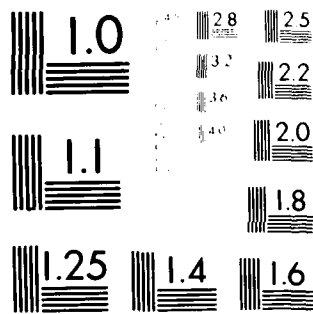
UNCLASSIFIED

NL

1 OF 2

200432





MICROCOPY RESOLUTION TEST CHART
NATIONAL BUREAU OF STANDARDS-1963-A

AD A089312

SECURITY CLASSIFICATION OF THIS PAGE (When Data Entered)

REPORT DOCUMENTATION PAGE		READ INSTRUCTIONS BEFORE COMPLETING FORM
1. REPORT NUMBER NRL Memorandum Report 4335	2. GOVT ACCESSION NO. AD-A089 312	3. RECIPIENT'S CATALOG NUMBER
4. TITLE (and Subtitle) THE NRL PROGRAM ON ELECTROACTIVE POLYMERS SECOND ANNUAL REPORT	5. TYPE OF REPORT & PERIOD COVERED 1979 Progress Report	
7. AUTHOR(s) Robert B. Fox Editor	6. CONTRACT OR GRANT NUMBER(s) 1215	
9. PERFORMING ORGANIZATION NAME AND ADDRESS Naval Research Laboratory Washington, D. C. 20375	10. PROGRAM ELEMENT, PROJECT, TASK AREA & WORK UNIT NUMBERS 61-0025-0-0	
11. CONTROLLING OFFICE NAME AND ADDRESS Naval Research Laboratory Washington, D. C. 20375	12. REPORT DATE September 15, 1980	
14. MONITORING AGENCY NAME & ADDRESS (if different from Controlling Office) Office of Naval Research Arlington, Va 22217	13. NUMBER OF PAGES 157	
	15. SECURITY CLASS. (of this report) UNCLASSIFIED	
16. DISTRIBUTION STATEMENT (of this Report) Approved for public release; distribution unlimited.		
17. DISTRIBUTION STATEMENT (of the abstract entered in Block 20, if different from Report)		
18. SUPPLEMENTARY NOTES		
19. KEY WORDS (Continue on reverse side if necessary and identify by block number) Organic semiconductors Charge transfer Tetracyanoquinodimethane Sulfur nitrides Polyconjugated polymers Intercalation Inorganic polymers Polyacetylene Organic polymers Paste electrodes		
20. ABSTRACT (Continue on reverse side if necessary and identify by block number) <input checked="" type="checkbox"/> The electroactive polymer program of the Naval Research Laboratory (NRL) is directed towards the development of synthetic, non-metallic polymers with properties superior to those of the currently available electrical and electronic materials, whose utility is often limited by such factors as weight, mechanical fragility, fabrication problems, corrosion, scarcity and high cost. These limiting properties of current electronic materials closely match the superior properties of non-metallic polymeric materials, i.e. (1) high strength to weight ratio; (2) unlimited availability; <div style="text-align: right;">(Abstract continues)</div>		

DD FORM 1 JAN 73 1473

EDITION OF 1 NOV 68 IS OBSOLETE
S/N 0102-LF-014-6601

SECURITY CLASSIFICATION OF THIS PAGE (When Data Entered)

20110

500

20. Abstract (Continued)

(3) low cost; (4) simplified fabrication; and (5) variability in molecular design and properties. The thrust of this program is therefore to determine those chemical combinations of molecules that have high electrical conductivity and then by chemical synthesis or modification incorporate them into polymers that combine the required electrical and electromagnetic properties with the desired material characteristics. This summary report contains thirteen contributions in four interrelated areas: theory, synthesis, characterization, and application.

Accession	
NTIS GR&I	<input checked="checked" type="checkbox"/>
DDC TAB	<input type="checkbox"/>
Unannounced	<input type="checkbox"/>
Justification	
By _____	
Dist _____	
Av _____	
Dist	OR
<i>P</i>	1

CONTENTS

	Page
Introduction	
N. L. Jarvis.	1
Searching for S-P Analogues of (SN) _x	
F. L. Carter.	3
Semi-Empirical Calculations on Electroactive Polymers	
J. A. Hashmall, L. C. W. Baker, F. L. Carter, P. Brant, and D. C. Weber.	11
Some Effects of Internal Coordinates on the Properties of Nonsimple Metals and Semiconductors	
C. T. White	24
Further Considerations on "Molecular" Electronic Devices	
F. L. Carter.	35
Ion Implantation Studies on (CH)	
D. C. Weber, P. Brant, and C. Carosella.	53
Characterization of Halogen-Doped (CH) and (SN). Part II	
J. R. Holtzclaw, D. C. Weber, F. E. Saalfeld, J. R. Wyatt, and J. J. DeCorpo	59
Pressure Effects on the Resistivity of Pure and Doped (CH)	
D. C. Weber, J. P. Ferraris, P. Brant, W. B. Fox, A. W. Webb, and E. R. Carpenter, Jr..	72
Progress Notes on Studies of (SN), (CH) _x , and Related Materials	
P. Brant, D. C. Weber, C. T. Ewing, and J. A. Hashmall.	83
Characterization of (SN) _x Paste Electrodes in Nonaqueous Media	
R. J. Nowak, C. L. Joyal, D. C. Weber, and D. L. Venezky	97
Electrical Conductivity of TCNQ Salts Dispersed in Poly(vinylacetals) As Matrix Polymers	
O.-K. Kim and R. B. Fox	103
Electrical Conductivity of Conjugated Organic Polymers	
T. M. Keller and J. R. Griffith	116
Electrical Conductivity of Networks Derived from Acetylene-Terminated Dianil Prepolymers	
T. R. Walton.	124
¹⁹ F NMR Spectroscopic and Relaxation Studies of SbF ₅ , AsF ₅ , and Other Intercalants in Graphite, Graphite Fibers, and Polyacetylene	
H. A. Resing.	130

THE NRL PROGRAM ON ELECTROACTIVE POLYMERS

SECOND ANNUAL REPORT

Introduction

N. L. Jarvis
Surface Chemistry Branch
Chemistry Division

The electroactive polymer program of the Naval Research Laboratory (NRL) is directed towards the development of synthetic, non-metallic polymers with properties superior to those of the currently available electrical and electronic materials, whose utility is often limited by such factors as weight, mechanical fragility, fabrication problems, corrosion, scarcity and high cost. These limiting properties of current electronic materials closely match the superior properties of non-metallic polymeric materials, i.e. (1) high strength to weight ratio; (2) unlimited availability; (3) low cost; (4) simplified fabrication; and (5) variability in molecular design and properties. The thrust of this program is therefore to determine those chemical combinations of molecules that have high electrical conductivity and then by chemical synthesis or modification incorporate them into polymers that combine the required electrical and electromagnetic properties with the desired material characteristics.

The NRL program of research on electroactive polymers has four inter-related tasks - Theory, Synthesis, Characterization, and Application.

Theoretical studies relating electrical properties to molecular structure are an important part of the NRL program. Such studies provide direction for the synthesis of new materials, give guidance for the modification of new and existing materials, and describe the electronic behavior of the conducting materials, which is necessary before they can be utilized in electronic devices. The theoretical effort involves a number of mathematical approaches to determine electronic properties, including semi-empirical molecular orbital methods, tight binding calculations, and polyhedral atomic volume determinations. As a part of this effort, electronic energy levels and other molecular parameters derived from photoelectron spectroscopy (XPS), carbon-13 nuclear magnetic resonance spectroscopy and electrical conductivity measurements are being compared with theoretically derived values.

The synthesis of new conducting polymers is primarily directed to preparing derivatives of polyconjugated linear and network polymers. The linear polyconjugated systems include polyacetylene and polydiacetylene derivatives, while the synthesis of new network polymers is directed primarily to the

Manuscript submitted July 14, 1980

dianil-linked polyphthalocyanines. The earlier effort to synthesize analogues of $(SN)_x$, specifically the sulfur-phosphorus compounds, has been discontinued based on the theoretical determination that they will not have a high conductivity. A different approach to preparing electrically conducting polymers was shown to be promising. That was the dispersion of charge transfer materials, such as salts of TCNQ, in poly(vinylacetal) as the matrix polymer. Only a few percent of the neutral TCNQ added to the TCNQ complex salt dispersed poly(vinylacetal) system increased the conductivity dramatically.

In addition to synthesizing new electrically conducting materials, efforts have continued to modify existing conducting and material properties. Ion implantation is one promising technique being investigated. It has been demonstrated that ion implantation of certain halogens into $(CH)_x$ will increase conductivity without damaging the polymer, and in fact may help stabilize the polymer to oxidative degradation. Halogens are also being studied as chemical dopants for both $(SN)_x$ and $(CH)_x$, and the results are being compared with the ion implanted materials.

Another modification technique studied was based on the observation that $(CH)_x$ as prepared is a very low density material. It was suggested that under high pressure the density of the polymer, and perhaps its ordering, would increase and thus increase its conductivity. Initial results were not conclusive. For example with an acceptor doped sample there was an initial decrease in resistivity with increasing pressure, but with further pressure increases the resistivity subsequently increased.

A variety of physicochemical and spectroscopic measurements is being used to determine the electrical properties, mechanical properties and molecular structures of materials. Techniques include X-ray induced photoelectron spectroscopy to study the electronic energy levels, mass spectroscopy and carbon-13 and fluorine-19 to characterize some of the interactions between the chemical dopants and the polymer matrix.

The NMR technique is being used to study "intercalated" or doped graphite and graphite fibers, as well as $(CH)_x$. The graphite fibers also have high electrical conductivity, combined with their very high tensile strength, and are potentially useful to the Navy as light weight electrical conductors, or when used as reinforcing fibers to produce highly conducting reinforced polymeric structural materials.

As promising new electroactive polymeric materials evolve from the program, applications which exploit their unique properties will be examined. Two such studies are now beginning. $(SN)_x$ is being studied as a paste electrode and a more theoretical effort is now underway to consider the use of these materials as "molecular" electronic devices. In addition to specific applications it is anticipated that these studies will lead to the discovery of important new phenomena and exciting new technologies.

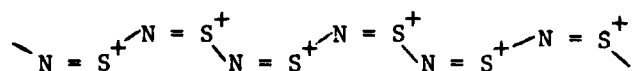
SEARCHING FOR S-P ANALOGUES OF $(\text{SN})_x$

Forrest L. Carter
Theoretical Chemistry Section
Surface Chemistry Branch

In the search for analogues of the metallically conducting polysulfur nitride, $(\text{SN})_x$, one is attracted to the isomorphous replacement of nitrogen by phosphorus. In such a case one might hope to improve upon the poor thermal stability of $(\text{SN})_x$ as well as to enhance the metallic conductivity by some d orbital participation in the bonding of the phosphorus analogues. At the same time, however, the isomorphous replacement of P for N should not upset the sensitive charge balance, approximately indicated by $(\text{S}^{+.5}\text{N}^{-.5})_x$, and which results from the sharing or delocalization of a conducting electron between both N and S in an antibonding π^* molecular orbital.

Rather than investing a large amount of time in a possible futile attempt to synthesize a metallically conducting $(\text{SP})_x$, the approach used here is to compare known S-N compounds with related S-P compounds in terms of the atomic volume of sulfur. If the sulfur volume is approximately the same in both series then the sulfur charges will probably be similar and a metallically conducting $(\text{SP})_x$ is feasible. On the other hand a much larger sulfur in the S-P compounds would suggest that sulfur is neutral or negative, and attempts to prepare a metallically conducting $(\text{SP})_x$ would be futile. Before describing the method of calculating the atomic volume, it will be desirable to discuss in greater detail the origin of the atomic charges and their importance to conduction in $(\text{SN})_x$.

The basic bond structure in the chain of $(\text{SN})_x$ can be considered to be one in which one electron per S-N unit is missing:



Note that by ionizing sulfur to the +1 charge state sulfur can be trivalent. (An alternative view would be to have each sulfur as a trivalent d-state radical.) The electron to be added (per S-N group) goes into a delocalized anti-bonding π^* orbital to which both nitrogen and sulfur contribute approximately equally. This means that the nitrogen is charged ~ -0.5 and sulfur $\sim +0.5$. If the electron is added entirely to sulfur then the sulfur is forced to be divalent and each nitrogen is left with an unpaired unshared electron, a very unstable situation. Accordingly not only does the conductivity, but even the existence of the $(\text{SN})_x$ chain, depends on the sulfur having

a fractional positive charge. The replacement of nitrogen by phosphorus does not change this structural argument.

The effective charges on the sulfur atoms in both the S-N and S-P compounds are correlated with their polyhedral atomic volumes (PAVs) which are calculated as the volumes of Voronoi (or Wigner-Seitz) cells except that the different sizes of the atoms are taken into account [1,2]. The classic construction of the Voronoi cell of a point in an aggregate involves selecting the smallest cell formed by planes perpendicularly bisecting all the point to neighbor vectors. Such a cell must contain the point of interest and the collection of all such cells for an aggregate fills all space [1]. In constructing PAV cells the plane perpendicular to the interatomic vector is located nearer the smaller atom by bisecting the distance between the surfaces of spheres whose radii are Pauling's single bond radii. In such a case one is approximately dividing in half the bonding electron cloud [2]. Accordingly the PAV cells are reasonably described as an atomic volume. Further details of the bonding in $(\text{SN})_x$ and the construction of PAV cells may be found in the first annual EAP report [3].

RESULTS

Calculations of PAVs were based on the known crystal structures of $(\text{SN})_2$, $(\text{SN})_4$, $(\text{SN})_x$, P_4S_3 , P_4S_4 , P_4S_5 , P_4S_7 , P_4S_{10} , and $\text{P}_4\text{S}_3\text{I}_2$. In the nitrogen compounds sulfur is always in a bridging position between two nitrogens whereas in the phosphorus series sulfur is either bridging between two phosphorus atoms or in a terminal position on a pentavalent phosphorus. The PAV results for sulfur in these compounds are shown in Figure 1 as a function of a generalized coordination number that recognizes fractional bonds [4]. It is seen that there is a clear distinction among sulfur bridging between nitrogens, between phosphorus atoms, and in a terminal position on a phosphorus atom. The corresponding average PAVs are 22.0, 26.0, and 31.2 \AA^3 . Since ESCA results [5] and molecular orbital calculations using the MNDO [6] and SCF-X α [7] methods, indicate that the sulfur charge in the nitrogen compounds is between +0.3 and +0.5, the higher sulfur PAVs for the S-P compounds strongly indicate that the sulfur charges are neutral or negative.

Some of the PAV cells for the phosphorus compounds are indicated in Figure 2 where the number 1 in the face centers correspond to a bonded interaction with sulfur and a number 2 to a bonded interaction of the central atom with a phosphorus neighbor. Near the center of the cells are two symbols:

$+$ gives the position of the atom, while \times shows the geometric center of the cell. The distance between them, the first moment, provides a measure of the symmetry or the evenness of the bonding about the central atom, a property Gorter [8] coined as "isonomicity".

Our attempt to quantify the concept of isonomicity using a scheme based on spherical harmonics was not particularly successful for these compounds. However, the results using the first and second moments of the cell shape were similar and promising. Figure 3 illustrates the results for phosphorous. Not only is there a clear separation between tri- and pentavalent phosphorous, but trivalent phosphorus shows a clear PAV increase with the first moment. A

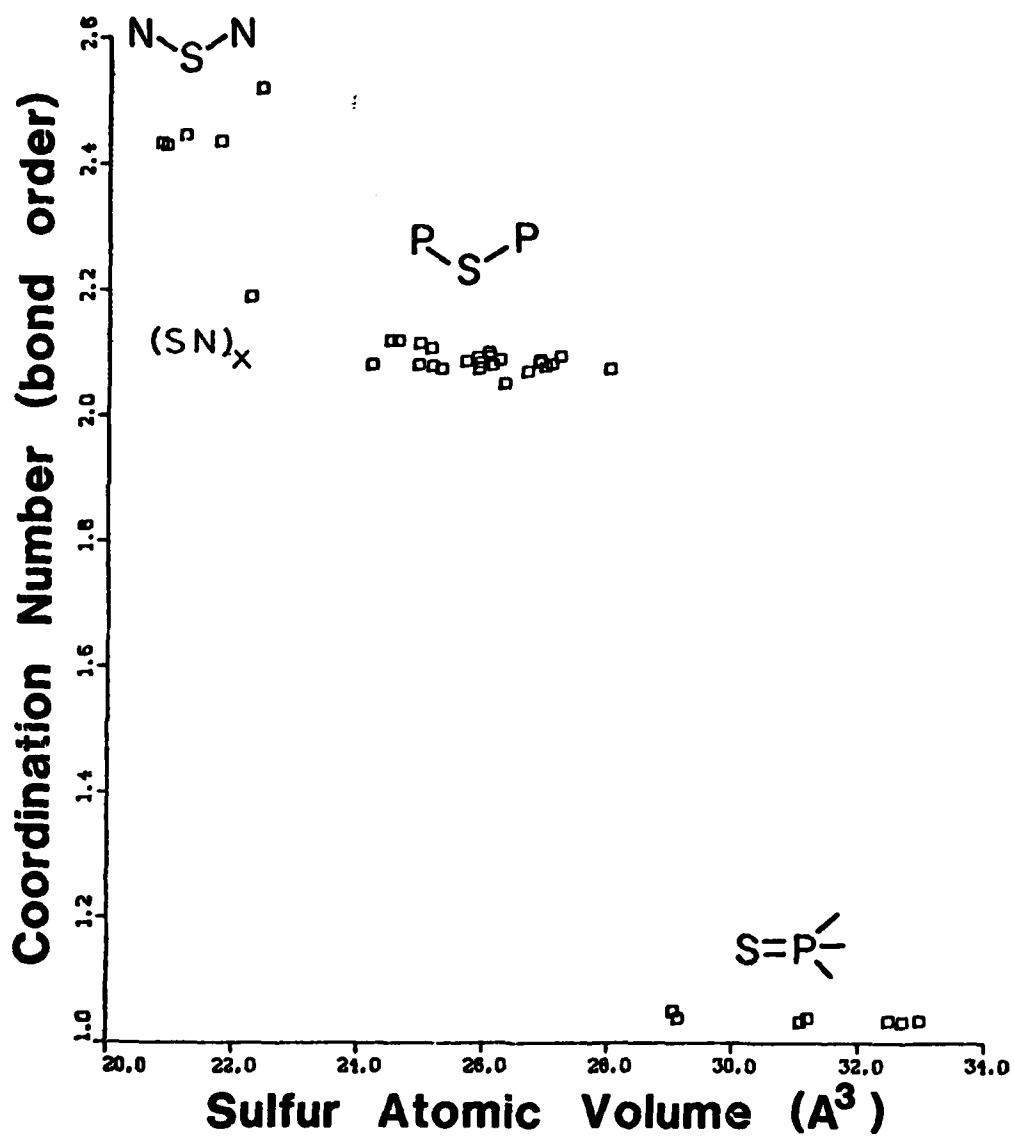


Fig. 1. This figure shows the clear separation of sulfur PAV according to the kind and number of its neighbors. Even though sulfur in $(\text{SN})_x$ has a similar CN to sulfur in the P_4S_{4n} series its volume is significantly smaller.

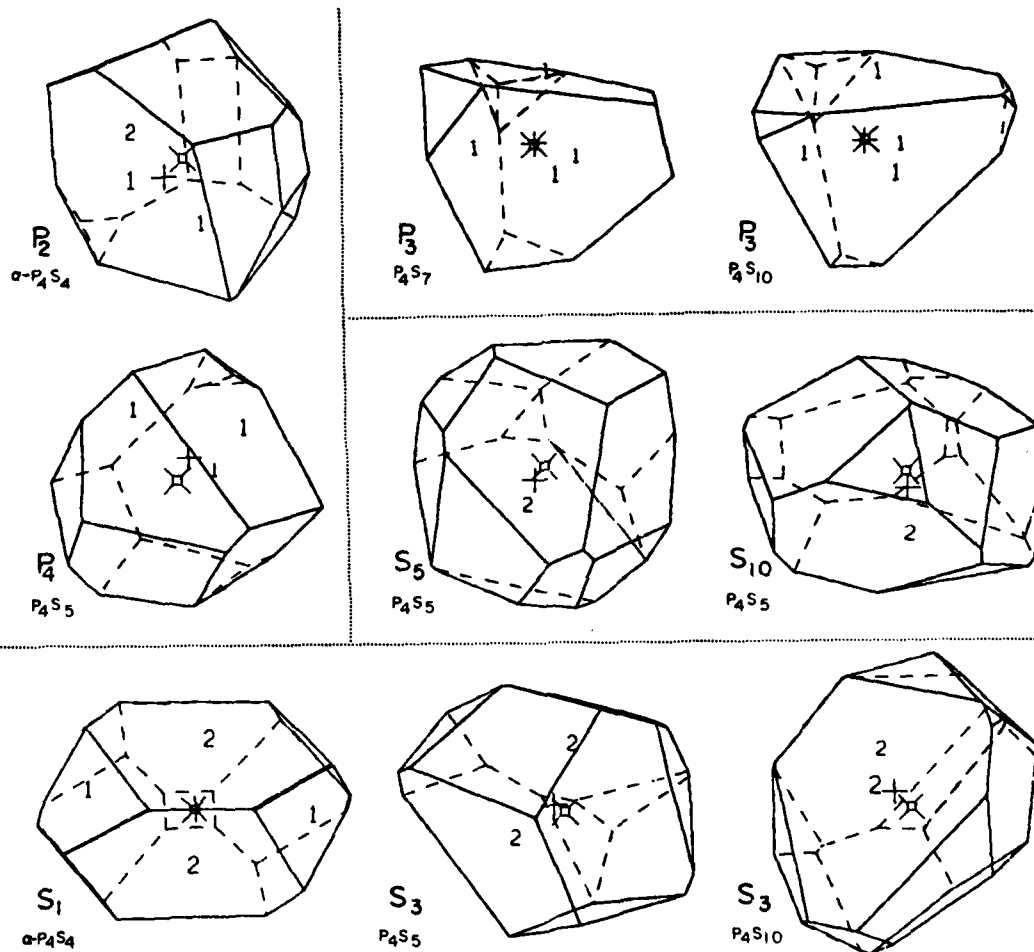


Fig. 2. The wide variety of PAV cells for sulfur and phosphorus are shown for the P_4S_n series. On the upper left are seen two trivalent phosphorus atoms, while the upper right shows two pentavalent phosphorus atoms. Terminal sulfurs are on the middle right, while bridging sulfurs are on the bottom. The PAV cells for the S-N compounds are found in Reference 3.

very similar figure (not shown) is obtained when the cell second moment (radius of gyration) is used. These results are in agreement with Gorter's observations that anionic volumes increase with their anisonomicity [8].

Table 1 indicates the average PAVs for the phosphorus compounds as a function of bond type. The large difference between the bridging and terminal sulfur volumes is expected since the latter have more van der Waal's contacts. We also note that both the trivalent and pentavalent phosphorus PAVs can be arranged in descending order by bond type or $\sum \Delta x_{ij} n_{ij}$ where Δx_{ij} is the electronegativity difference of the bonded atoms i and j , and the bond order is n_{ij} .

The internal consistency obtained above (Table 1) for the six P-S compounds suggests that, for these closely related compounds of sulfur, nitrogen, and phosphorus, the PAV calculations yield meaningful and chemically significant results even for molecular crystals. The added beauty of this approach is that these results depend almost wholly and simply upon known crystal structures and not upon a protracted semi-empirical molecular orbital or ab initio calculation.

SUMMARY

The application of the PAV calculations to the primarily molecular crystals $(\text{SN})_2$, $(\text{SN})_4$, P_4S_n , and $\text{P}_4\text{S}_3\text{I}_2$ not only clearly distinguishes between bridging and terminal sulfurs and between tri- and pentavalent phosphorus atoms, but shows understandable volume variations according to kind and number of neighbors. While such a result is expected for non-molecular crystalline materials, it is not a priori obviously correct for molecular crystal types. The comparison of sulfur PAVs in the nitrogen compounds with those in the phosphorus compounds clearly suggests that in the latter compounds, the sulfur is no longer positively charged. This leads to the conclusion that metallically conducting phosphorus analogues of $(\text{SN})_x$ will not be forthcoming and any attempt to prepare them will be futile. Finally, we note that the moment analysis of PAV cell shape is a promising method for the quantification of Gorter's isonomicity concept.

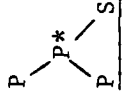
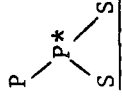
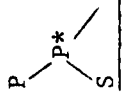
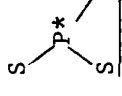
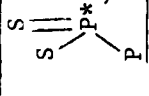
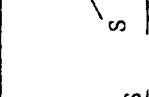
ACKNOWLEDGEMENTS

I want to express my appreciation for the interest shown by my colleagues, D. C. Weber and P. Brant, in PAV calculations and to acknowledge many useful discussions with them concerning the contents of this manuscript.

REFERENCES

1. G. Voronoi, J. Reine Angew. Math. 134, 198 (1908).
2. F. L. Carter, J. Less-Common Metals 47, 157 (1976).
3. F. L. Carter, in "The NRL Program on Electroactive Polymers," Ed. by L. B. Lockhart, Jr., NRL Memo. Report 3960, March 30, 1979, p. 121.
4. F. L. Carter, Acta Cryst. B34, 2962 (1978).

Table 1
Polyhedral Atomic Volumes vs. Bond Type

	Sulfur		Phosphorus					
	P-S*-P	S*=P						
$\Sigma \Delta x_{ij}^n$	0.8	0.8	-0.4	-0.8	-0.8	-1.2	-1.6	-2.0
Cpd.								
P ₄ S ₃	26.19		24.75			21.97		
α -P ₄ S ₄	24.69		22.65					
β -P ₄ S ₃ I ₂	25.41		21.52		22.79	21.15		
P ₄ S ₅	25.83	29.14	22.47	24.39		22.10	16.03	
P ₄ S ₇	25.48	30.07		22.60				14.94
P ₄ S ₁₀	27.05	32.35						15.23
Ave.	25.95	31.24	23.65	22.88	22.79	21.74	16.03	15.13

* atom in cell center

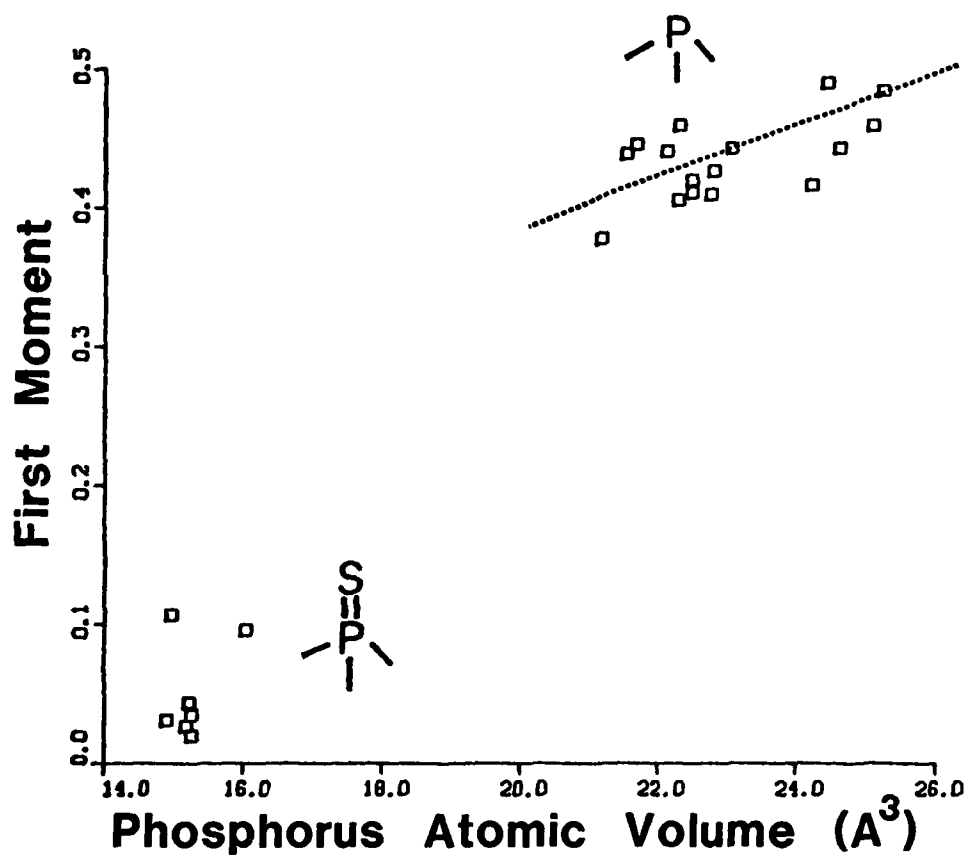


Fig. 3. The displacement of the PAV cell center from the atomic position is plotted against the phosphorus volume. The trivalent P volume is seen to increase with increasing anisotropy (the dashed line was placed to guide the eye).

5. P. Brant, D. C. Weber, C. T. Ewing, F. L. Carter, and J. A. Hashmall, submitted to J. Synthetic Metals.
6. J. Hashmall and F. L. Carter, this annual report.
7. D. R. Salahub and R. P. Messmer, J. Chem. Phys. 64, 2039 (1976).
8. E. W. Gorter, J. Solid State Chem., 1, 279 (1970).

SEMI-EMPIRICAL CALCULATIONS ON ELECTROACTIVE POLYMERS

J. A. Hashmall, L. C. W. Baker, F. L. Carter, P. Brant, and D. C. Weber

INTRODUCTION

Development of methods to predict the band gaps of polymers would be of enormous utility to experimental chemists seeking to synthesize polymers with specific electrical properties. Such a method, to be maximally useful, should display the following properties:

- (1) It should predict the band structure (or at least the band gap) of polymers accurately.
- (2) It should be applicable to a wide variety of polymers, and for each polymer to different configurations of the polymer.
- (3) It should be computationally simple enough so that the cost of predicting a polymer band structure is much less than the cost of synthesizing the polymer itself.
- (4) It should be able to treat anomalies within the polymer structure, such as kinks, anomalous substitution (doping sites), etc.

We have developed a method that comes close to satisfying these criteria; it is based on the Modified Neglect of Differential Overlap (MNDO) (1) semi-empirical molecular orbital method. We have tested this method on known electroactive polymers, and have used it to predict the band gap of a number of postulated electroactive polymers. In addition, we have attempted to ascertain the source of the regular errors in our method in order to compensate for them. The results indicate three new polymers as extremely promising candidates for highly conducting materials.

Our method consists of performing MNDO calculations on monomers, dimers, trimers, etc. of the repeat unit of a polymer, and extrapolating the highest occupied molecular orbital (HOMO) energy level and the lowest unoccupied molecular orbital (LUMO) energy level to infinite chain length, thus obtaining an estimate of the energies of the top of the filled band and the bottom of the conduction band, and thereby the band gap. We have performed these calculations on $(\text{SN})_x$, $\text{H}-(\text{CH})_x-\text{H}$, $\text{H}-(\text{CH})_x-\text{Y}$ (where the substituent Y is F, NH_2 , BH_2 , BeH , Cl, S^x or O^-), and on the polymer that would be obtained by copolymerization of acetylene with methyl isocyanide with one nitrogen introduced into each chain of polyacetylene as well as on the protonated form of this copolymer.

The band gap estimates, calculated for the above polymers, had relative magnitudes that were in excellent agreement with all experimental evidence on these systems. The absolute magnitudes of the estimated band gaps were, however, considerably larger than experimental values. To aid in evaluating the reason for this discrepancy we performed calculations on the first excited singlet and triplet states of short-chain molecules of $(CH)_x$. The results of these calculations indicated that the overestimate of the band gap was probably due to the assumption that the first excited state could be represented as a product function of ground state electron wavefunctions.

THEORY

In a simple one dimensional polymer, if non-nearest neighbor interactions are ignored, theory predicts the j th energy level in any band obtained by interaction of n orbitals to be given (2) by:

$$E_j = 2\beta \cos j\pi/(n+1) \quad (1)$$

In such one dimensional polymers the net energy is minimized if alternating units distort (geometrically or by spin flipping) so that the interactions between each unit and its two neighbors are not equal. This inequality affects the energy of the levels in the band by causing a gap in which no energy levels exist. For the case with one electron on each atomic orbital which combine to form the band, for example the π band in polyacetylene, the gap is in the middle of the band and the energies of the top of the filled half band and bottom of the empty half band are given by:

$$E_t = A_t + B_t \cos \frac{n\pi}{2(n+1)} \quad (2)$$

$$E_b = A_b + B_b \cos \frac{(n/2+1)\pi}{(n+1)} \quad (3)$$

The terms A and B are parameters which indicate the magnitude of the perturbation leading to band splitting and the magnitude of the nearest neighbor interactions. Since

$$\cos\left(\frac{n/2}{n+1} \pi\right) = \cos\left(\frac{\pi}{2} - \frac{1}{n+1} \frac{\pi}{2}\right)$$

$$\text{and } \cos\left(\frac{\pi}{2} - x\right) = \sin x$$

$$E_t = A_t + B_t \sin\left(\frac{1}{n+1} \frac{\pi}{2}\right). \quad (4)$$

Similarly

$$\cos \frac{n/2+1}{n+1} \pi = \cos\left(\frac{\pi}{2} + \frac{1}{n+1} \frac{\pi}{2}\right), \cos(\pi - x) = -\cos x,$$

and

$$\begin{aligned} \cos \frac{n/2+1}{n+1} \pi &= \cos \left[\pi - \left(\frac{\pi}{2} - \frac{1}{n+1} \frac{\pi}{2} \right) \right] \\ &= \cos \left(\frac{\pi}{2} - \frac{1}{n+1} \frac{\pi}{2} \right) \\ &= -\sin \left(\frac{1}{n+1} \frac{\pi}{2} \right) \end{aligned}$$

so

$$E_b = A_b - B_b \sin \left(\frac{1}{n+1} \pi/2 \right). \quad (5)$$

Both equations 4 and 5 are of the same form and can be linearized by the transformation:

$$f(n) = \sin \left(\frac{1}{n+1} \frac{\pi}{2} \right) \quad (6)$$

This transformation produces a linear relation between the energy of an orbital (the top of the occupied split halfband or the bottom of the vacant split halfband) and the function f , which is a known function of the degree of polymerization, n . A least squares fit of E calculated as the HOMO or LUMO in MNDO calculations on oligomers to the values of n for these oligomers to the equation

$$E = A + Bf(n) \quad (7)$$

provides values of A and B . Because $f(n)$ goes to zero as n becomes large, A is simply the infinite degree of polymerization limit of the band edge: E_∞ . Small deviation from exactly half-filled splitbands will affect the form of the functions 3 and 4 only slightly for high degrees of polymerization, and therefore these equations should be useful even for polymers with splitbands that are not exactly half-filled.

RESULTS

Before calculations on $(SN)_x$ were performed, calculations on several simple SN containing compounds were performed to evaluate the accuracy of the MNDO method for molecules containing the SN unit. The sparse experimental data for these compounds were compared with calculated values. Geometries, ionization potentials and, where possible, thermodynamic data were evaluated.

MNDO calculations including geometry optimization were performed on S_2N_2 , S_4N_4 (both in cyclic configurations similar to the known stable forms), S_2N_2 in an acyclic form in both cis and trans conformations, and the series $(SN)_x$ for $x = 4, 6, 8$ in conformations similar to that known for polymeric $(SN)_x$. In addition, calculations along the reaction path for ring opening of S_2N_2 and along the reaction path for twisting of the acyclic S_2N_2 from cis to trans configurations were performed.

The enthalpies of formation and HOMO and LUMO energies of the calculated species are summarized in Table 1.

The calculated geometries of S_2N_2 and S_4N_4 are similar to measured geometries. The calculated geometry parameters (with experimental values (3,4) in parentheses) are:

$$S_2N_2: R_{SN} = 1.621\text{\AA} (1.654\text{\AA}), \angle SNS = 85.0^\circ (89.0^\circ) \angle SNS = 95.0^\circ (91.0^\circ)$$

$$S_4N_4: R_{SN} = 1.581\text{\AA} (1.616\text{\AA}), \angle NSN = 108.2^\circ (104.5^\circ)$$

The calculated S-S non-bonded distance in S_4N_4 is considerably larger than the experimental value; 2.951 Å calc vs. 2.580 Å exptl. The calculated charges on sulfur and nitrogen are ± 0.40 in S_2N_2 , and ± 0.53 in S_4N_4 which are in good agreement with X-ray photoelectron spectroscopic data (5).

Calculations on the ring opening of S_2N_2 show that the reaction proceeds with an activation energy of 43.4 kcal/mole at a geometry with one S-N bond stretched to about 2.1 Å and the ring twisted about 20° out of planarity. This twisting allows mixing of the σ and π orbitals. Acyclic S_2N_2 has a σ HOMO. The energy of the triplet diradical is only slightly above that of the ground state ($\Delta E = 4.6$ kcal/mole) in agreement with the observation of unpaired spins in the course of the polymerization of S_2N_2 to $(SN)_x$ (7).

Rotation about the central bond in acyclic S_2N_2 has a transition state at 90° with an energy only 1.3 kcal/mole above that of the cis isomer.

MNDO calculations are sufficiently reliable for hydrocarbons and their simple derivatives (8) that no calculations were performed to examine the reliability of MNDO for these systems. MNDO calculations were performed on short-chain molecules of $H-(CH)_x-H$ for $x = 2, 4, 5, 6$ and 10, on all possible monofluoro-derivatives of these x compounds and on derivatives with substituents: NH_2- , BH_2- , $BeH-$, $Cl-$, $O-$, and $-S-$. All of these calculations were performed with the carbon chain in its all-trans conformation and all of the substituents were in the cis-terminal position (see Figure 1) except that in the case of the fluoro-derivative, both cis and trans isomers were calculated. In addition, calculations were performed on oligomeric molecules of a polymer which has been postulated as the product of copolymerization of acetylene with methyl isocyanide (9). To model this copolymer, protons were used instead of methyl groups and the substituent was placed in a terminal position on the oligomer chain. The resulting compounds are identical to the compounds that would be obtained by replacing a terminal methylene group (CH_2) in the polyacetylene oligomers with an imide group (NH). In addition, MNDO calculations on the N protonated cations of each of these copolymer oligomers were performed. All geometry parameters were optimized in the hydrocarbon calculations, but in the calculations on derivatives it was determined that optimization was required only for the parameters local to the substituent and those local to the carbon directly bonded to the substituent. The HOMO and LUMO energies of these molecules are presented in Table 2.

The values obtained were extrapolated using a least squares fit to equation (7) with f as defined in equation (6). The resulting calculated band limit energies, the correlation coefficient of the fit (r^2), and the band gap calculated from the difference between the HOMO band and the LUMO band limit, are presented in Table 3.

Calculation of band gap energies as equal to the difference between calculated HOMO and LUMO energies involves the implicit assumption that the two states involved can be well represented as products of different members of the same set of one electron functions, with only the one electron wavefunction representing the excited electron changing. The assumption is also made that the one electron function representing the electron in the conduction band can be well represented by the first virtual orbital calculated for the ground state electronic distribution. To test these approximations

and to determine the source of errors resulting from these approximations, calculations were performed on the anions, cations, singlet excited states and triplet excited states of the polyacetylene oligomeric molecules for which the neutral ground state energies had previously been calculated. The energy differences between the appropriate species are reported in Table 4 as the singlet excitation energy, the triplet excitation energy, the ionization potential and the electron affinity. In addition, excitation energies obtained by summing the ionization potential and electron affinity are also reported. These values were extrapolated to infinite chain length as above and the extrapolated energies are also presented in this table.

Similar calculations were performed for the vertical processes - those in which the geometry of the excited state or ion was not changed from that of the ground state molecule. Results of these calculations are included in Table 4.

DISCUSSION

The agreement between experimental and calculated geometries of S_2N_2 and of S_4N_4 indicates that the MNDO method treats compounds with the SN unit accurately, except that S-S non-bonded attractions are underestimated. This conclusion is supported by the few thermodynamic data available. When $(SN)_x$ is heated, an acyclic form of S_4N_4 vapor is evolved. The enthalpy of this x vaporization has been determined to be 29 kcal/mole from mass spectra (10) and 32.49 kcal/mole by the direct Knudsen method (11). For the reaction $S_8N_8 \rightarrow 2S_4N_4$ as a model for this reaction, a MNDO calculation gives an enthalpy of vaporization of 31.1 kcal/mole.

The consistently high values of correlation coefficients for the least squares fits, indicates that the extrapolation method is consistent with the data. The resulting calculated band gaps, 3.49 eV for $(SN)_x$ and 6.05 eV for trans $(CH)_x$, are considerably larger than experimental values; ≤ 0.0 eV for $(SN)_x$ and 1.5-2.0 eV for $(CH)_x$.

Much of this error results from the Koopmans' theorem-like frozen orbital approximation. The ground state polymer is represented as an antisymmetrized product function of restricted, paired one electron wavefunctions. The use of the variation method to obtain these functions produces virtual functions in addition to occupied functions. The energy necessary to excite an electron to the conduction band is taken as the difference between the one electron energy of the highest energy one electron occupied wavefunction and the energy of the lowest virtual one electron wavefunction. There are several inherent sources of error in this procedure:

- (1) The one electron energy of virtual orbitals are not well represented by any variation method-based MO technique because the minimized total electronic energy is insensitive to these functions.

- (2) The change in the remaining occupied orbitals, especially the spin-pair of the electron which has been excited, is ignored.

- (3) Changes in repulsion energy due to the excitation are not included.

All of the above sources of error can be seen to have a large effect by comparing the data in Table 4 to that in Table 3. The additional error due to spin correlation is known to be small for MNDO calculations on small systems but may be significant in polymeric systems.

In an infinitely long polymer chain, the dominant effect on the re-arrangement of electrons on excitation is the extent of the polymer rather than the nature of the monomer units. For a perturbed free electron model one would expect all of the above sources of error to be similar for polymers which are similar. In fact, if one assumes that the total error in the calculated band gap is the difference between the maximum experimental band gap for (SN)_x (0 eV) and the calculated band gap, one obtains a correlation factor, which when applied to (CH)_x yields a corrected estimate of the band gap as being no greater than 2.56 eV. This value is only slightly higher than the experimental value of between 1.5 and 2 eV. Comparisons of band gaps of (CH)_x and derivatives of this polymer should yield even more accurate band gap differences.

CONCLUSIONS

The method developed, calculation of HOMO and LUMO energies of monomers and small oligomers by the MNDO method, followed by extrapolation to infinite polymer length, yields band gap estimates which are higher than experimental values. Differences between these estimates are, however, consistent with experiment.

Simple substituents on polyacetylene seem unlikely to alter the band gap substantially. On the other hand, substituents such as -O⁻, S⁻, or -CH=NH₂⁺ which can donate or remove charge from the pi system of the chain by a pi resonance effect (as opposed to an inductive effect) show enormous promise of radically decreasing the band gap of this polymer.

REFERENCES

1. M. J. S. Dewar and W. Theil, J. Am. Chem. Soc., 99, 4899 (1977).
2. C. A. Coulson and J. Streitwieser, Jr., "Dictionary of π -Electron Calculations," W. H. Freeman and Co., San Francisco, 1965, p. xxix; C. A. Coulson and G. S. Rushbrooke, Proc. Cambridge Phil. Soc., 36, 193 (1940); E. Heilbronner and H. Bock, "The HMO Model and Its Application," John Wiley and Sons, London, p. 131-135.
3. A. G. MacDiarmid, C. M. Mikulski, P. J. Russo, M. S. Saran, A. F. Garito, and A. J. Heeger, J. C. S. Chem. Comm., 1975, 476; C. M. Mikulski, P. J. Russo, M. S. Saran, A. G. MacDiarmid, A. F. Garito, and A. J. Heeger, J. Am. Chem. Soc., 1975, 97, 6358; M. J. Cohen, A. F. Garito, A. J. Heeger, A. G. MacDiarmid, C. M. Mikulski, M. S. Saran and J. Kleppinger, J. Am. Chem. Soc., 1976, 98, 3844.
4. P. B. Zeeman, Can. J. Phys., 1951, 29, 179.
5. P. Brant, D. C. Weber, C. T. Ewing, F. L. Carter, and J. A. Hashmall, Inorg. Chem., to appear August, 1980.

6. R. H. Findlay, M. H. Palmer, A. J. Downs, R. G. Egdeil, and R. Evans, Inorg. Chem., to appear Autumn 1979.
7. M. J. S. Dewar and W. Theil, J. Am. Chem. Soc., 1977, 99, 4907.
8. C. M. Mikulski, A. J. Russo, M. S. Saran, A. G. MacDiarmid, A. F. Garito, and A. J. Heeger, J. Am. Chem. Soc., 1975, 97, 6358.
9. P. Brant, unpublished work.
10. R. D. Smith, J. R. Wyatt, J. J. DeCorpo, F. E. Saalfeld, M. J. Moran, and A. G. MacDiarmid, J. Am. Chem. Soc., 1977, 99, 1726.
11. D. C. Weber and C. T. Ewing, Inorg. Chem., 16, 3025 (1977).

Table 1

Results of MNDO Calculations

	ΔH_f (kcal/mole)	HOMO energy (eV)	LUMO energy (eV)
S_2N_2 (cyclic) ^a	117.5	-10.95 π	-2.14 π
S_2N_2 (cisoid) ^b	139.6	- 9.38 σ	-2.01 π
S_2N_2 (transoid)	140.4	- 9.57 σ	-2.13 π
S_4N_4 (open)	236.3	- 9.55 π	-2.57 π
S_6N_6 (open)	338.8	- 8.70 π	-2.74 π
S_8N_8 (open)	441.5	- 8.32 π	-2.82 π
S_4N_4 (cyclic) ^c	246.8	- 9.48	-3.58 π

^aDifferences between calculated cation or anion energies and the calculated molecular energy yield values for the ionization potential and electron affinities of 10.68 adiabatic IP, 10.71 vertical IP (10.56 eV exptl)⁶ and -2.42 EA.

^bCalculated singlet energy = 155.0 kcal/mole and triplet energy = 144.2 kcal/mole. Highest occupied π M.O. energy = -12.86 eV.

^c ΔH_f of S_4N_4 in its experimental geometry is calculated as 267.2 kcal/mole (exptl IP = 9.36 eV).⁶

Table 2

Calculated HOMO and LUMO Energies (eV) for Trans-Polyacetylene and Derivatives

Polymer	Orbital	Degree of Polymerization (x in H-(CH) _x -H)				
		2	4	6	8	10
H-(CH) _x -H unsubstituted	HOMO	-10.18	-9.14	-8.64	-8.34	-8.17
	LUMO	1.32	0.39	-0.10	-0.42	-0.61
Cis-1-F-	HOMO	-10.18	-9.19	-8.71	-8.41	-8.23
	LUMO	0.67	-0.03	-0.38	-0.62	-0.76
Trans-1-F-	HOMO	-10.18	-9.22	-8.76	-8.46	-8.28
	LUMO	0.67	-0.06	-0.42	-0.67	-0.81
2-F-	HOMO	-	-9.39	-8.92	-8.59	-8.38
	LUMO	-	-0.01	-0.40	-0.66	-0.82
3-F-	HOMO	-	-	-8.78	-8.43	-8.24
	LUMO	-	-	-0.41	-0.65	-0.79
4-F-	HOMO	-	-	-	-8.52	-8.36
	LUMO	-	-	-	-0.67	-0.83
5-F-	HOMO	-	-	-	-	-8.29
	LUMO	-	-	-	-	-0.82
1-NH ₂ -	HOMO	-10.05	-9.22	-8.75	-8.45	-8.27
	LUMO	1.08	0.10	-0.32	-0.60	-0.76
1-BH ₂ -	HOMO	-10.66	-9.53	-8.97	-8.61	-8.40
	LUMO	-0.12	-0.60	-0.82	-0.98	-1.06
1-BeH-	HOMO	-10.16	-9.17	-8.71	-8.41	-8.23
	LUMO	0.79	0.08	-0.31	-0.58	-0.73
1-Cl-	HOMO	-10.28	-9.32	-8.81	-8.48	-8.29
	LUMO	0.64	-0.06	-0.43	-0.67	-0.81

Table 2 (Continued)

Calculated HOMO and LUMO Energies (eV) for Trans-Polyacetylene and Derivatives

Polymer	Orbital	Degree of Polymerization (x in $\text{H}-(\text{CH})_x-\text{H}$)				
		2	4	6	8	10
$1-\text{O}^-$	HOMO	- 1.68	-2.19	-2.56	-2.82	-3.00
	LUMO	8.38	6.22	4.69	3.63	2.82
$1-\text{S}^-$	HOMO	- 2.59	-2.95	-3.20	-3.37	-3.48
	LUMO	6.77	5.07	3.88	3.00	2.23
$\text{H}-(\text{CH})_{x-1}\text{NH}$	HOMO	-11.19	-10.05	-9.20	-8.71	-8.47
	LUMO	1.17	0.16	-0.33	-0.64	-0.81
$\text{H}-(\text{CH})_{x-1}\text{NH}_2^+$	HOMO	-20.18	-15.65	-13.67	-12.46	-11.61
	LUMO	- 6.71	- 6.31	- 5.99	- 5.78	- 5.64

Table 3

Values of Extrapolated Energies (eV)

$$E_n = E_\infty + B \sin \frac{1}{n+1} \frac{\pi}{2}$$

	E_∞ HOMO	r^2	E_∞ LUMO	r^2	Band Gap
(SN) _x	-6.69 ^a	0.9955 ^a	-3.20	0.9973	3.49 eV
Trans (CH) _x	-7.38	0.9996	-1.33	0.9964	6.05 eV
Cis-1-F-(CH) _x	-7.48	0.9990	-1.30	0.9970	6.18 eV
Trans-1-F-(CH) _x	-7.55	0.9987	-1.37	0.9973	6.18 eV
2-F-(CH) _x	-7.54 ^b	0.9966	-1.50	0.9984 ^b	6.03 eV
1-NH ₂ -(CH) _x	-7.61	0.9944	-1.48	0.9997	6.13 eV
1-BH ₂ -(CH) _x	-7.53	0.9984	-1.42	0.9985	6.11 eV
1-BeH-(CH) _x	-7.49	0.9992	-1.29	0.9939	6.20 eV
1-Cl-(CH) _x	-7.54	0.9965	-1.36	0.9966	6.18 eV
1-O ⁻ -(CH) _x	-3.43	0.9730	1.07	0.9733	4.48 eV
1-S ⁻ -(CH) _x	-3.78	0.9797	0.89	0.9649	4.67 eV
(CH) _{x-1} NH	-7.45	0.9850	-1.58	0.9991	5.88 eV
(CH) _{x-1} NH ₂ ⁺	-8.30	0.9997	-5.29	0.9703	3.01 eV

^aS₂N₂ not used because HOMO was σ .

^b_x = 2 not used.

Table 4

Calculated Energies (eV) of Electron Transfer Processes in Trans-(CH)_x

x	Adiabatic Process		Band Gap		
	Singlet Excitation	Triplet Excitation	I.P.	E.A.	I.P. - E.A.
2	5.54	1.73	9.67	-1.02	10.69
4	5.25	1.43	8.66	-0.00	8.66
6	4.64	1.31	8.12	0.58	7.54
8	4.40	1.13	7.76	0.97	6.79
10	4.24	1.08	7.55	1.21	6.34
E_{∞}	3.81	0.85	6.76	2.02	4.74
r^2	0.9085	0.9771	0.9956	0.9924	0.9941
x	Vertical Process		Band Gap		
	Singlet Excitation	Triplet Excitation	I.P.	E.A.	I.P. - E.A.
2	5.80	2.21	9.96	-1.12	11.08
4	5.36	2.13	8.87	-0.13	9.00
6	4.77	1.96	8.32	0.43	7.89
8	4.49	1.87	7.97	0.80	7.17
10	4.32	1.89	7.74	1.01	6.77
E_{∞}	3.82	1.74	6.94	1.80	5.14
r^2	0.9434	0.8966	0.9984	0.9939	0.9965

Conformations of calculated polyacetylene derivatives

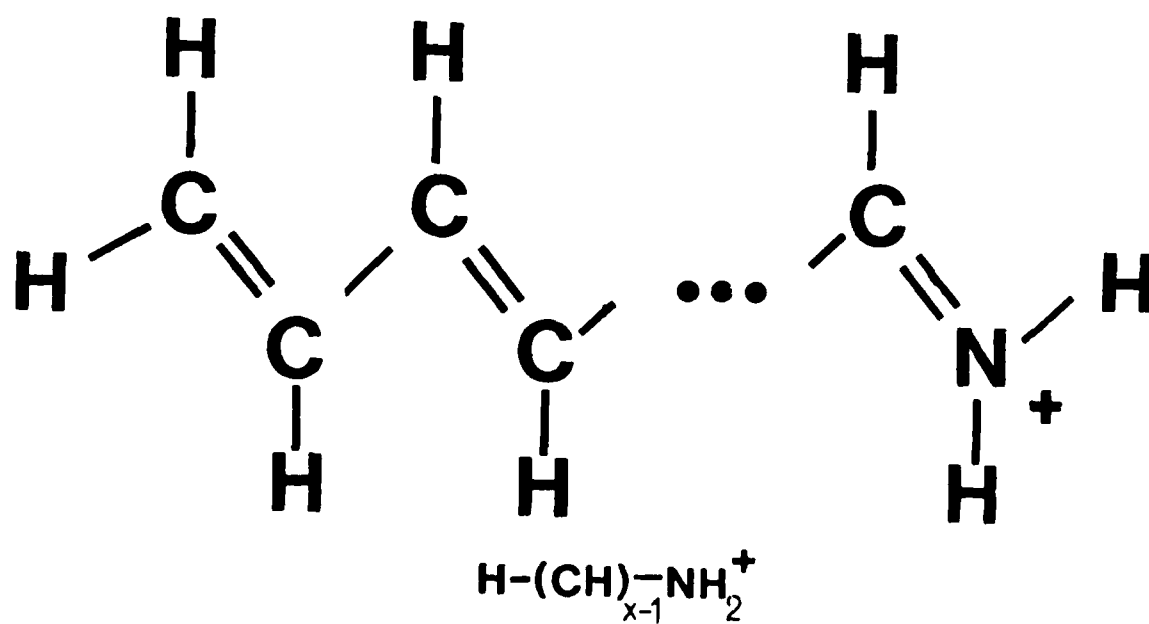
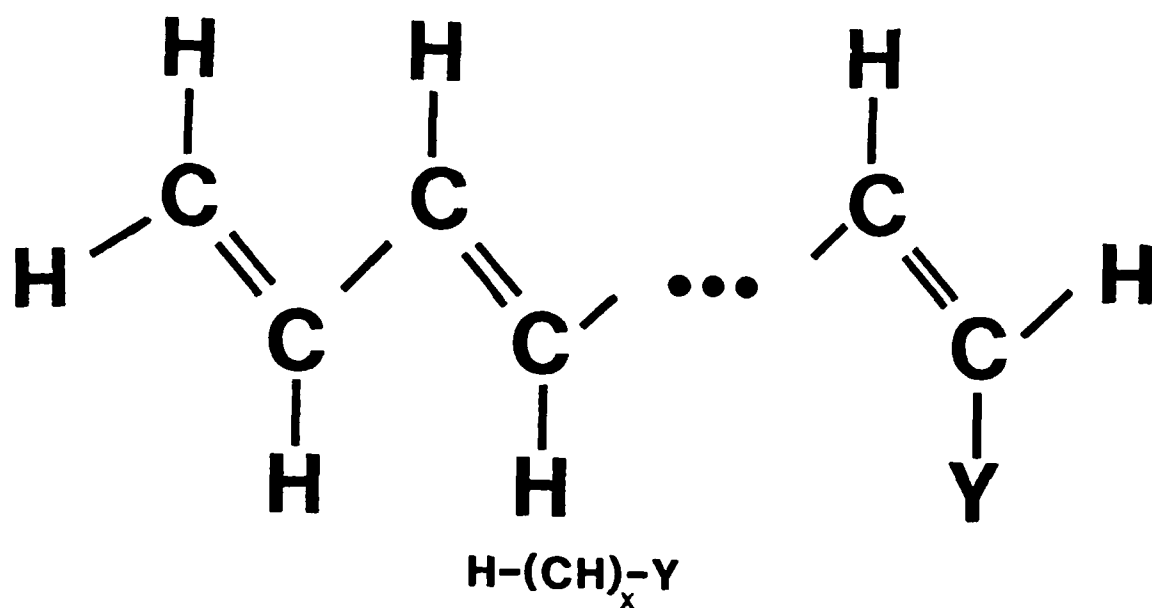


Figure 1

SOME EFFECTS OF INTERNAL COORDINATES ON THE PROPERTIES OF
NONSIMPLE METALS AND SEMICONDUCTORS

C. T. White
Surface Chemistry Branch
Chemistry Division

INTRODUCTION

In recent years there has been a continued and developing interest in the electronic properties of novel polymeric metals and semiconductors due to their potential technological usefulness. For example, the successful doping (1) of the quasi-one-dimensional polymer $(CH)_x$ and its subsequent use in the fabrication of such photovoltaic devices (2) as Schottky (metal-semiconductor) barriers and p-n junctions has stimulated much additional research into the nature of this and related conjugated polymeric systems. Additional examples along these lines are provided by the charge transfer salts (3) such as TTF-TCNQ and NMP-TCNQ as well as the "semimetallic" polymer $(SN)_x$ (4).

It is noteworthy that the aforementioned examples are not only interesting for purely technological reasons but are also important from a fundamental viewpoint. More specifically, these and related systems may well represent prototypes for studying the effects of correlations in reduced dimensions and how they may manifest themselves through such collective effects as a superconducting state, ferromagnetism, antiferromagnetism (and consequent novel excitations such as spin polarons (5)) and charge density waves (and consequent novel excitations such as solitons (6)).

The physical structure as well as the chemical bonding of such polymeric metals and semiconductors can be quite complex in comparison to the corresponding simple metals and crystalline semiconductors. As we shall see, this can introduce into the description of these systems important complicating factors associated with what we will term internal coordinates. For example, in the nonsimple metallic systems, bonding between the constituents of course occurs but it is not the usual metallic bonding and can involve hybridization to one degree or another. In addition, these systems are certainly more disordered and nonstoichiometric than the traditional simple metals and semiconductors and hence contain many more imperfections, impurity defects, vacancies and the like, all of which can give rise to internal coordinates associated with e.g. abnormal bonding configurations, etc. Furthermore, many of these nonsimple metals and semiconductors represent reduced dimensional systems and this aspect of their structure will enhance the effects of internal coordinates over what would be expected in the corresponding fully three-dimensional materials.

Here I will discuss some of the aspects of these internal coordinates which are expected to be important in the description of nonsimple metals and semiconductors and make some qualitative comparison of the resultant pictures to experiment. It is noteworthy that although the ensuing discussion will be largely confined to systems which one usually thinks of as polymers and/or organic conductors, many of the concepts mentioned here may be found applicable to the study of other nonsimple metals such as the A-15s (V_3Si , Nb_3Ge), the transition metal dichalcogenides (TaS_2 , $WbSe_2$, etc.), the carbides and nitrides (NbC , etc.), the chevril phases ($PbMg_{6-x}S_8$, etc.) and the tungsten bronzes (Na_xWO_3) as well as some of the less "exotic" semiconductors such as hydrogenated amorphous Si and Ge, etc.

BASIC CONCEPTS WITH SOME APPLICATIONS

As pointed out above, the reduced dimensional nature of many of the polymeric metals and semiconductors can enhance the importance of internal coordinates in their description. In order to develop this aspect of the picture further as well as make other points, let us consider the quasi-one-dimensional semiconductor trans-(CH)_x. A single infinite strand of this polymer is assumed to have either of the energetically degenerate structures shown in Fig. 1 where the usage of the carbon single and double bond symbols indicates only that the two carbons participating in the "double bond" (C=C) are closer together than the two carbons participating in the "single bond" (C-C).

Perhaps the simplest model (7) of this system that allows for an understanding of its behavior is partially generated by treating the carbon π -electrons within a nearest neighbor tight-binding scheme so that the Hamiltonian describing these electrons is

$$H = \sum_{i\sigma} \epsilon_{i\sigma} n_{i\sigma} + \sum_{ij\sigma} V_{ij} a_{i\sigma}^\dagger a_{j\sigma}, \quad (1)$$

where $a_{i\sigma}^\dagger$, $a_{i\sigma}$ are the usual creation and annihilation operators, respectively, for electrons of spin σ in the Wannier state centered at the site i and the hopping integrals, V_{ij} , are taken for simplicity as zero unless $i||j\rangle$ and the nearest neighbors. Experimentally, trans-(CH)_x is found to be semiconducting. This observation can be explained within the context of Eq. (1) by viewing (CH)_x as a Peierls distorted system (8) in which case the chain is dimerized along the x-direction of Fig. 1, and the nearest neighbor hopping integrals entering Eq. (1) will take on two values V_2 , V_1 (with $V_2 > V_1$) corresponding to the carbon double and single bonds, respectively. In this case the density of states (DOS) per site associated with Eq. (1) can be expressed as

$$\rho_o(E) = -\frac{1}{\pi} \lim_{\epsilon \rightarrow 0} \text{Im}(Z - \epsilon_o) / (\sqrt{[(Z - \epsilon_o)^2 + V_1^2 - V_2^2]^2 - 4V_1^2(Z - \epsilon_o)^2}) \quad (2)$$

where $Z \equiv E + i\epsilon$ and E is the energy. A graph of this DOS is shown in Fig. 2. It is seen that the DOS exhibits a gap [$E_g = 2(V_2 - V_1)$] at the Fermi-energy E_F (separating occupied from unoccupied states) consistent with the observed semiconducting behavior. The physical basis for expecting such a Peierls distortion leading to $V_1 \neq V_2$ can be understood from Fig. 2 as well, since it is

seen to lower the energy of the π -electron system from what is obtained if one supposes $V_1 = V_2$, which leaves no gap in the DOS. This distortion and the consequent π -electron energy lowering of course occurs at the expense of the σ -electron system, etc. which serves to stabilize it. However, it will always occur (9) in one dimensional nonpathological models at low temperatures due to the square root singularity that develops due to the distortion. More explicitly for the present example, if we expand V_{ij} as $V_{ij} = V_0 + \alpha(u_i - u_j)$ where u_n represents the displacement of the n th CH group relative to where it would sit in the undimerized case and model the elastic energy of the system as $K \sum_i (u_i - u_{i+1})^2$, then the dimerization will always be energetically favorable for any $\alpha \neq 0$. This however is not the case if we introduce some three-dimensional character into the system associated with crosslinking between chains, etc., which should smooth the square root singularities shown in Fig. 2 and introduce a critical value of α below which the distortion will no longer occur. Thus, we already see how the importance of internal coordinates (in this example associated with nearest neighbor carbon-carbon distances along the molecular symmetry direction of the chain) in describing the electronic structure of a system can increase purely because of decreasing dimensionality.

Consider now the role of internal coordinates associated with defects in $(CH)_x$. Perhaps the simplest intrinsic defects that will exist in samples of $(CH)_x$ are strained carbon-carbon bonds that arise because of mechanical constraints associated with the disordered nonstoichiometric nature of the system. One can show that the DOS for a $(CH)_x$ chain described by Eq. (1) with a single strained bond between the carbon atoms located at the sites i, j is given by

$$\rho(E) = \rho_0(E) - \frac{2}{\pi} \lim_{\epsilon \rightarrow 0} \text{Im} \left\{ \frac{V^2 G_{ii} G'_{ii} + V(1 - V G_{ij}) G'_{ij}}{(V G_{ii})^2 - (1 - V G_{ij})^2} \right\}, \quad (3)$$

where $V \equiv V_s - V_{ij}$ with V_{ij} the unperturbed hopping integral (either V_1 or V_2 depending on the position of sites i, j), $G_{ij} = \langle i | [Z-H]^{-1} | j \rangle$ with H given by 1, the primes denote differentiation with respect to energy and $\rho_0(E)$ is given by Eq. (2). Localized states in the gap of Fig. 2 introduced by this strained bond occur at energies where the real part of $[(V G_{ii})^2 - (1 - V G_{ij})^2]$ vanishes.

If the strained bond is located where a double (single) carbon-carbon bond would exist in the ideal system corresponding to a hopping integral V_2 (V_1) and is weaker than the ideal bond, i.e., $V < V_2$ (i.e. $V < V_1$), then this condition is always (never) satisfied. This result has a number of important consequences. First of all, as an aside, it can explain why one does not observe experimentally a large number of states in the gap of $(CH)_x$ close to either the valence or conduction band edges associated with weakened single bonds which are expected to exist in appreciable numbers in the system and connect chain segments together so to produce pathways of macroscopic dimensions. Secondly, and important to our present development, is the result that an arbitrarily weakened (strengthened) double (single) bond will generate two states (four if we include spin) in the gap located at $\epsilon_0 \pm E_p$ with $E_p = \frac{1}{2V_s} \{V_s^2 + V_{ij}^2 - \sqrt{(V_s^2 - V_{ij}^2) + 4V_s^2 V_{ij}^2}\}$. This result is a consequence of the one-dimensional nature of the system and related to the divergences in the DOS that occur at $\pm(V_2 - V_1)$ in the unperturbed system. In fact, introduction of some three-dimensional character into the problem will smear out these divergences and introduce a lower bound in the magnitude of the strains capable

of generating such gap states. Of course this bound will still be appreciably lower than what would be appropriate for a strictly three-dimensional system. The fact that such gap states are localized will enhance the effect of the internal coordinates associated with them. Consider, e.g. a weakened carbon-carbon double bond. As an approximation, we may consider the gap states introduced by such a bond and located at $\epsilon_0 \pm E_p$, as simply the bonding and antibonding levels associated with this weakened double bond. Now, as the two carbon atoms participating in this bond are moved further apart they interact less, i.e., V_s decreases and the splitting between the two levels is decreased. In the limit $V \rightarrow 0$ no $pp\pi$ bond is formed at all and the two states approach the nonbonding p_π energy ϵ_0 .

The above properties of weakened double bonds in $(CH)_x$ can have many important consequences. First of all such a weakened double bond is expected to act in $(CH)_x$ as an efficient electron-hole recombination center exhibiting a large non-radiative component and hence could account partially (10) for the small photoluminescence efficiency in this system. How this can occur is outlined schematically in Fig. 3. In panel (a) the DOS corresponding to the ground state of the system in the presence of one weakened carbon double bond is shown. Panel (b) shows the system immediately after an electron-hole pair is created by the absorption of a photon of energy $h\nu > E_{gap}$. Panel (c) illustrates the achievement of quasi-equilibrium in the system through the thermalization of the electron and hole to the antibonding and bonding states associated with the strained bond. Next, panel (d) illustrates the spontaneous weakening of the strained double bond accompanied by moving the two carbon atoms participating in the bond apart so to reduce the energy of the electron-hole pair. This process is accompanied by the emission of many phonons. It is reasonable to expect that such a distortion can occur before the radiative recombination of the electron-hole pair since a typical time scale for it should be of the order of a lattice time, 10^{-13} sec, while a typical time before radiative recombination would occur should be of the order of 10^{-8} sec. Panel (e) represents the recombination of the electron-hole pair accompanied by the emission of a photon with energy much less than that of the initially absorbed photon. Finally, panel (f) represents the return of the system to its ground state accompanied by the emission of many phonons. It is noteworthy that the above assumes in effect that the electron and hole are captured before any distortion occurs which would follow if they are already bound together as an exciton. On the other hand if they were not already bound together as an exciton one expects that first one particle (either the electron or hole) would be captured. Then a distortion to lower the energy of this particle before the other particle is captured (this distortion would in fact make the capture of the remaining particles even more likely) and then another distortion to arrive at the situation of Fig. 3d. The present and related processes may also account for the relatively low quantum efficiency of $(CH)_x$ photovoltaic devices for excitation energy within 1 eV or so of E_{gap} , since such self-trapping effects can generate efficient electron-hole recombination centers when the concentration of carriers is high as well as produce an enhanced electron-hole binding. Furthermore, one would not expect in general that all electrons and holes were captured in pairs and this could lead to a host of residual metastable effects after the light is removed. For example, the electron can be captured at one location and the hole at another and because of the distortion effects involved become severely localized at these sites and hence only recombine after long times. Such a picture is consistent with the rather persistent changes

observed (11) in subsequent photoresponse of $(CH)_x$ heterojunctions after their exposure to band gap radiation.

Actually most of the effects detailed above can be expected in $(CH)_x$ without the postulating of the pre-existence of strained bonds. For example, because of the one-dimensional nature of this system the ideally Peierls distorted system is the presence of an excited electron hole pair would be expected to be unstable toward the spontaneous production of e.g. a weakened carbon double bond. Concomitantly with the generation of this weakened double bond phonons will be emitted associated with the self-trapping of the electron-hole pair by/through the creation of the weakened bond.

These self-trapping ideas in the present system associated with internal coordinates are not restricted to electron-hole pairs but will apply as well to carriers introduced by doping. For example, in this vein a single electron (hole) in the conduction (valence) band is expected to be unstable toward the formation of a small polaron accompanied by a splitting off of states from the continuum into the gap. Moreover, if the energy shift accompanying this splitting is large enough to offset the Coulomb repulsion between electrons (holes), these carriers should condense into bipolarons as opposed to small polarons. Such a picture seems consistent with what is known experimentally about the behavior of carriers introduced into $(CH)_x$ through doping. First of all, localized bipolarons are diamagnetic in agreement with experimental results (12). Secondly, at low carrier densities bipolaron transport would be expected to occur through diffusive hopping as experimentally implied (13). Moreover, for a fixed impurity concentration the number of such bipolarons should be independent of temperature as is indicated (13) experimentally. Further, bipolaron formation would be expected (14) to give rise to an activated conductivity with an activation energy that decreases with increasing carrier density, and this also is observed experimentally. Finally, at low carrier densities bipolarons can be associated with essentially any carbon-carbon double bond consistent with the relatively large thermopower experimentally observed (13) in this limit. One should note that the formation of small polarons as opposed to bipolarons would also be consistent with the above experimental results if it were not for the lack of any observed new local moments introduced by light doping. Further note that the solitons suggested (7) by Su et al., are also consistent with the data discussed above and may well represent lower-lying quasi-particles than bipolarons or polarons. If this is the case, however, one might still expect bipolaron or polaron formation as an initial step in the formation of solitons.

So far we have confined our discussion of the effects of internal coordinates on nonsimple semiconductors to $(CH)_x$. It should by now be clear that the concepts we have developed in this context should be applicable with little alteration to other reduced dimensional semiconductors. In addition, these concepts are expected to be applicable to systems such as amorphous carbon. In this instance one will not expect e.g. spontaneous self-trapping of low energy electron-hole pairs in the pristine system, diamond. One would, however, expect such effects in the corresponding disordered system because of the presence of strained carbon-carbon bonds that introduce states already localized in the energy gap which can shift due to distortions according to their occupancy. Actually in this system there are many additional interesting possibilities arising from self-consistent distortions

(15) that can produce important metastabilities. Indeed, such effects may account for the fact that some samples of amorphous carbon exhibit (16) memory switching behavior. As an aside, because of the importance of internal coordination in nonsimple semiconductors, one should always be alert to the possibility of memory switching effects in these systems.

Up to this point we have only focused our attention on effects associated with internal coordinates in nonsimple semiconductors. Let us now generalize the discussion to nonsimple metals and semimetals. As discussed above, in the context of bipolarons, internal coordinates associated with distortions, e.g. at defects can give rise to an effective attractive (neg. U) interaction between electrons in the vicinity of this defect. Such negative U centers, when they exist, are expected to affect the normal state transport properties. In collaboration with K. L. Ngai and C. S. Ting, I have studied this problem in some detail and since the particulars will appear elsewhere (17), I will simply quote the significant results here. In particular, we find that such negative U centers when in contact with a Fermi-sea will produce a temperature squared contribution to the normal state resistivity. This result may apply to the polymeric metal $(\text{SN})^x$ which exhibits (18) a resistivity, ρ , with a T^2 component over a significant temperature range. It may also apply to the electroactive charge transfer salts which are found (19) to have a T^n contribution to ρ with $(2 \leq n \leq 2.3)$. One should note though that in the case of the organic transfer salts and $(\text{SN})^x$, alternative explanations have been proposed (18,19). Other nonsimple x metals show a T^2 contribution to ρ as well but we will not go into these here but rather refer the reader to Ref. 17 for the details.

Another important result of our investigation of the effects of negative U centers in nonsimple metals is the observation that the introduction of such negative U centers can actually induce a superconducting state at low temperature or enhance the transition temperature of an already superconducting material. A possible candidate for this effect is Pd which is not in the stoichiometric form superconducting at temperatures as low as several millidegrees Kelvin but becomes superconducting at temperatures up to 3°K after being bombarded by helium atoms (20).

CONCLUDING REMARKS

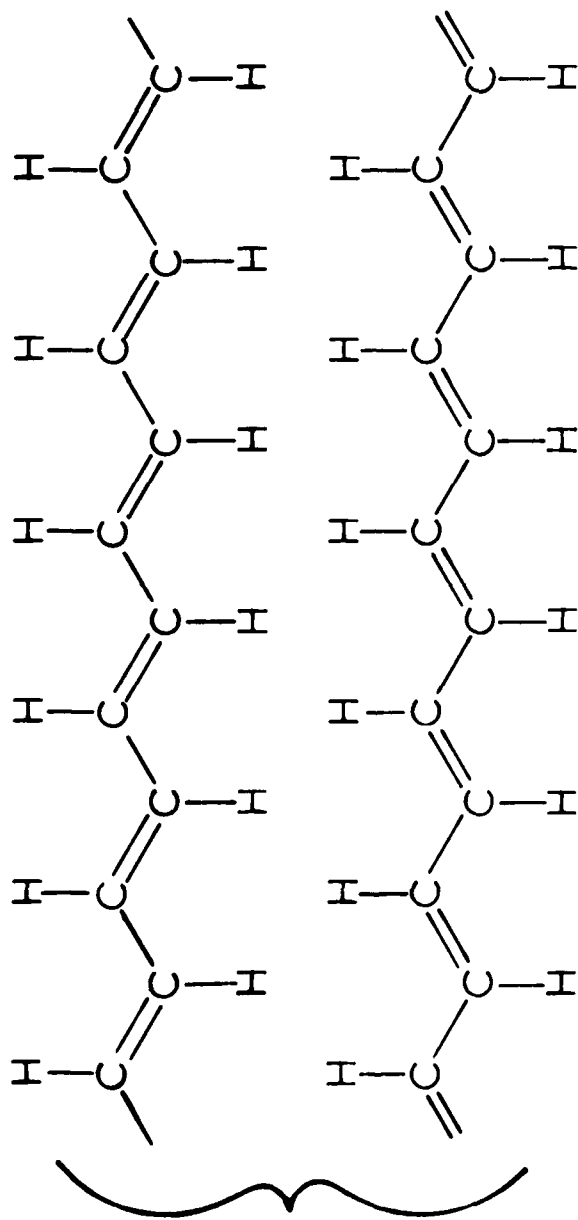
Here I have pointed out why internal coordinates are expected to be important ingredients in the description of nonsimple metals and semiconductors for essentially three interconnected reasons. They are: (1) Many of these systems are reduced dimensionally so that the effects of any fluctuations associated with internal coordinates can be enhanced over what one would expect in three-dimensional systems. (2) These systems are by and large less crystalline than the more usual metals and semiconductors and hence one would expect internal coordinates associated with strained bonds etc. to be important in their description. (3) On the whole electrons and holes in these systems would be expected to occupy states quite sensitive to changes in the local environment of the electron or hole. Also, I have explored how such internal coordinates can lead to, e.g. important effects in $\text{trans}-(\text{CH})^x$ associated with self-trapping as well as produce anomalous temperature dependencies in the resistivity of nonsimple metals.

In conclusion, it should be noted that there are many other important effects associated with the present class of internal coordinates not detailed in this paper such as changes in the vibrational spectral after photostimulation, etc.

REFERENCES

1. C. K. Chiang, C. R. Fincher, Jr., Y. W. Park, A. J. Heeger, H. Shirakawa, E. J. Louis, S. C. Gau, and A. G. MacDiarmid, Phys. Rev. Lett. 39, 1098 (1977).
2. C. K. Chiang, S. C. Gau, C. R. Fincher, Jr., Y. W. Park, A. G. MacDiarmid and A. J. Heeger, Appl. Phys. Lett. 33, 181 (1978).
3. See e.g., I. F. Shehegolev, Phys. Stat. Solidi (a) 12, 9 (1972).
4. See e.g., V. V. Walatka, M. M. Laber, and J. H. Perlstein, Phys. Rev. Lett. 31, 1139 (1973).
5. A spin polaron is formed by improperly joining two long antiferromagnetic chains (see C. T. White and E. N. Economou, Phys. Rev. B 18, 3959 (1978)).
6. In analogy to a spin polaron a soliton is essentially formed by improperly joining two alternating double-single bond chains (see Ref. 7).
7. W. P. Su., J. R. Schrieffer and A. J. Heeger, Phys. Rev. Lett. 42, 1698 (1979).
8. This view has been questioned by Ovchinnikov et al. in Sov. Phys. Usp. 15, 575 (1973).
9. See e.g., H. R. Zeller, Advances in Solid State Physics, Vol. 12, Editor H. J. Queisser, Pergamon Press, New York, 1973, p. 31.
10. Other inelastic processes such as Auger can, of course, also lead to nonradiative recombination of electrons and holes.
11. M. Ozaki, D. Peebles, B. R. Weinberger, C. K. Chiang, S. C. Gau, A. J. Heeger and A. G. MacDiarmid, Appl. Phys. Lett. 35, 83 (1979).
12. B. R. Weinberger, J. Kalufer, A. J. Heeger, A. Pran and A. G. MacDiarmid, Phys. Rev. B 20, 223 (1979).
13. Y. W. Park, A. Denenstein, C. K. Chiang, A. J. Heeger and A. G. MacDiarmid, Sol. State Commun. 29, 747 (1979).
14. See e. g., C. T. White and K. L. Ngai, Surf. Sci. 73, 116 (1978).
15. C. T. White and K. L. Ngai, Journal Vac. Sci. and Technol. (in press).
16. K. Antonowicz, A. Jesmanowicz and J. Wiecezorek, Carbon 10, 81 (1971).
17. C. S. Ting, K. L. Ngai and C. T. White Phys. Rev. B (in press).

18. C. K. Chiang, M. J. Cohen, A. F. Garito, A. J. Heedger, C. M. Milulski and A. G. MacDiarmid, Sol. State Commun. 18, 1451 (1976).
19. See e.g., M. Wager and H. Gutfreund, Comments Sol. St. Sci. 8, 135 (1978).
20. B. Stritzker, Phys. Rev. Lett. 42, 1769 (1979).



TRANS

Fig. 1: Illustrates the two equivalent forms of trans-(CH)_x .

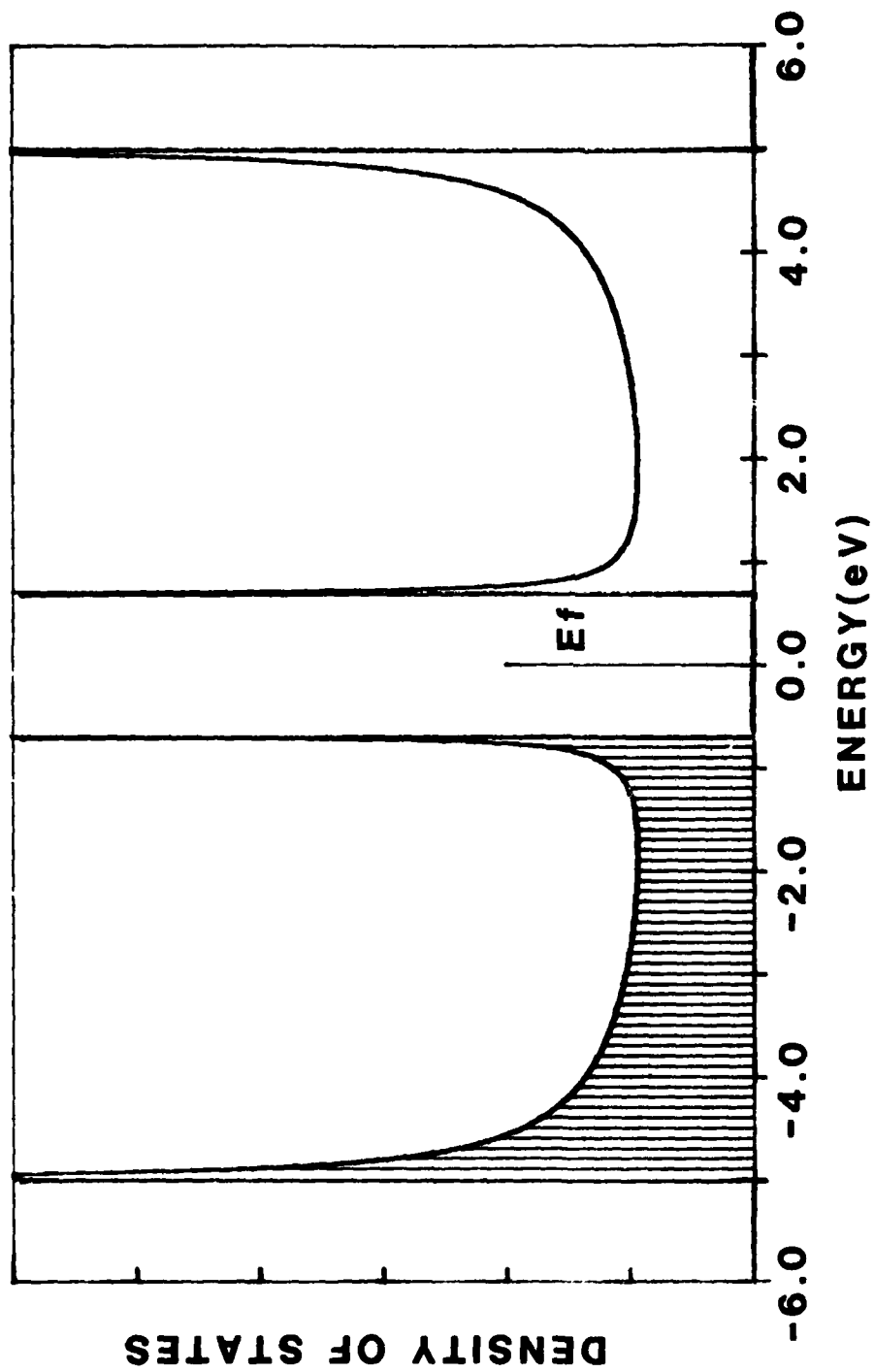


Fig. 2: The density of states for p_r electrons in dimerized $(CH)_x$ implied by the model Hamiltonian (1) of the text

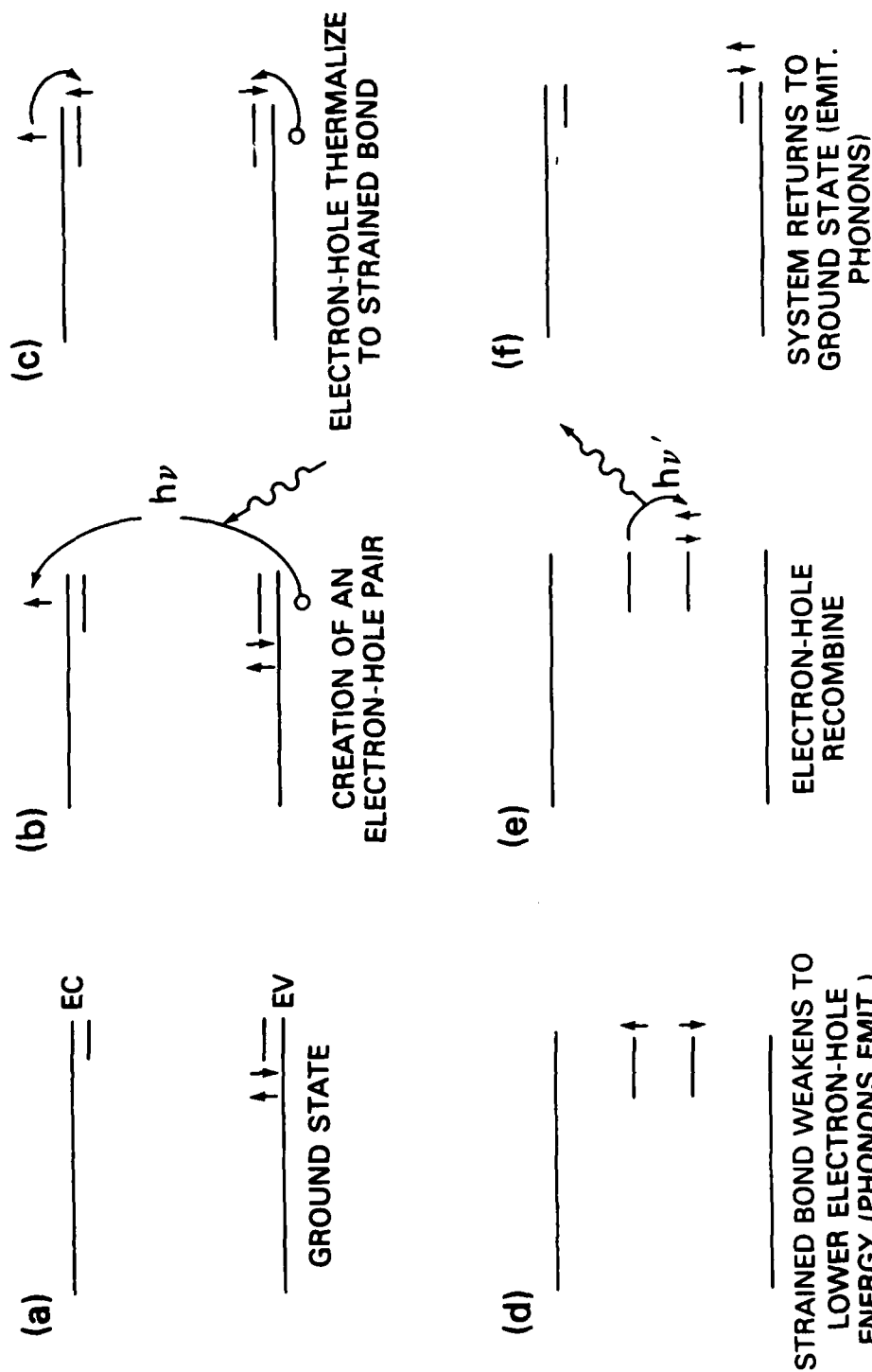


Fig. 3: Schematic of how a weakened carbon-carbon double bond in $(\text{CH})_x$ can behave as a recombination center for electrons and holes

FURTHER CONSIDERATIONS ON "MOLECULAR" ELECTRONIC DEVICES

Forrest L. Carter
Surface Chemistry Branch
Chemistry Division

INTRODUCTION

In looking ahead at problems and prospects of the NRL Electroactive Polymer Program the possibility of the development of a "chemical" computer was envisioned (1). As conceived, this computer would be based on components (diodes, gates, etc.) with molecular dimensions, i.e., 50 Å to 500 Å, and would be constructed along a three- rather than the current two-dimensional architecture. Such a computer could provide a quantum jump advance, in terms of both speed and switch element density (e.g. 10^{15} per cm^3), over both existing systems and those planned as extensions of current semiconductor practice (2).

It is worth noting here that the technology of both fabricating and operating such a "chemical" computer was sketched (1) as significantly different from current approaches. For example, one method of fabricating the computer might be through a series of computer-controlled chemical reactions in which chemical functional groups are added on a substrate one set at a time. Such a scheme is kin to the synthesis of long chain polypeptides by the Merrifield technique (3). Recognition of the difficulty of communicating with molecules suggests that input-output functions of a chemical computer might be accomplished through a relatively few surface-modified metal leads and a larger number of optical receptors and highly oriented micro lasers (1).

While such a chemical computer and its adjuncts are in the conceptual development stage, it is now clear that such a high density of switches would have an enormous impact on much of technology. However, interest based on a molecular device technology is justified not only as a way to leapfrog the current VLSI semiconductor based approach but also for the stimulus such an effort would give to numerous areas of chemistry, physics and biology.

To provide a suitable starting point for considering the concept of 'molecular' electronic devices, the next section of this paper will present an updated listing of various signal-transport mechanisms operating at the molecular level. Succeeding sections will discuss in turn: Cooperative Particle Transfer; Control Groups for Periodic Electron Tunnelling; Soliton Transport and 'Molecular' Adders;

Insulating Layers and Molecular Spaghetti; and Chemical Memories.

Signal Transport Mechanisms

The flow of information or energy between molecules can occur by a wide variety of ways, some of which are indicated in Table I, updated from Table III of reference (1). The nature of the signal (or the particle), the distance travelled, and the principle phenomena involved are also suggested in Table I. The right most column further indicates a method by which the signal flow can be switched off. Items 1, 3, 4, 5, and 7 have been previously treated in the first EAP Annual Report (1). Item 2 is an example of cooperative particle transfer and will be treated next; to be followed by discussions of electron tunnelling in periodic structures and the soliton phenomena, items 6 and 8.

Cooperative Particle Transfer

This new concept of signal transport depends on the collective action of several molecules with the net result that a small particle is "absorbed" at one site and a second particle is released some distance away, 50 Å or greater. In the example to be given both particles are hydrogen atoms; schemes involving protons or hydride ions are also plausible.

The plausibility of such an effect is suggested by the observation (4) that 7-azaindole exists as a hydrogen bonded dimer in moderately dilute solutions in hexane and when excited at $\lambda = 260\text{nm}$ apparently undergoes a double proton transfer as indicated below:

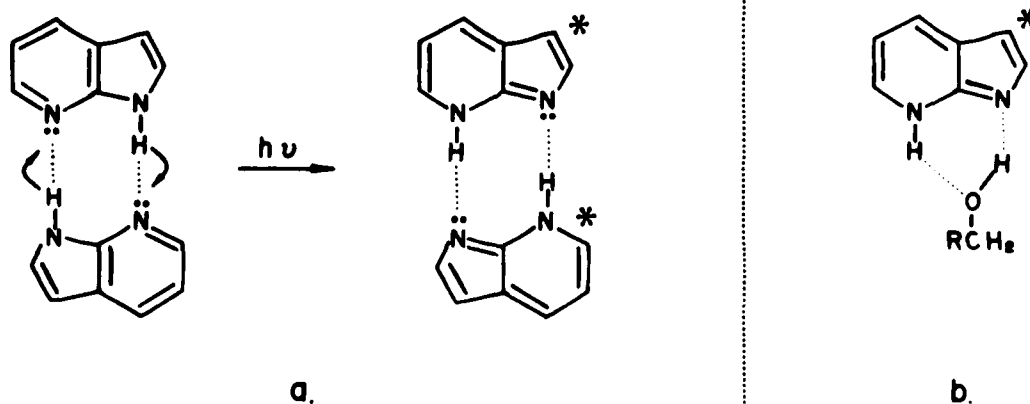
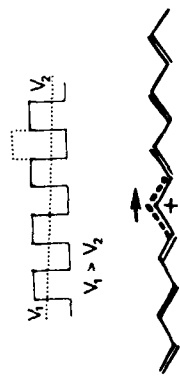


Table I. Transport of Signal (Within Device)

<u>Particle</u>	<u>Distance</u>	<u>Structure</u>	<u>Phenomena</u>	<u>Switch</u>
1. H^-, H^+	3 A	Asy. Hydrogen Bond	Particle Tunnelling "Molecular Diode"	Reverse Potential
2. H atom	50 A	Hydrogen Bonded Chain	Double Proton Transfer	Electric Field + $h\nu$
3. Photon	35 A	Dipole-Dipole	Excimer	Rotate Dipole
4. Exciton	50 A	1,2,3-d Structure	Collective Electronic Excitation	Alternate Trap
5. Phonon	100 A	Polymer Chain	Vibration	Disconnect Chain
6. Soliton -vib.	700 A	Chain of α -Helix	Solitary Vibrational Wave	Vibrational Trapping
7. Electron	300 A		Periodic Tunnelling	Well - Barrier
8. Soliton $\pm Q$	600 A		Solitary Charged Wave	Charge Transfer Trap

COOPERATIVE PARTICLE TRANSFER

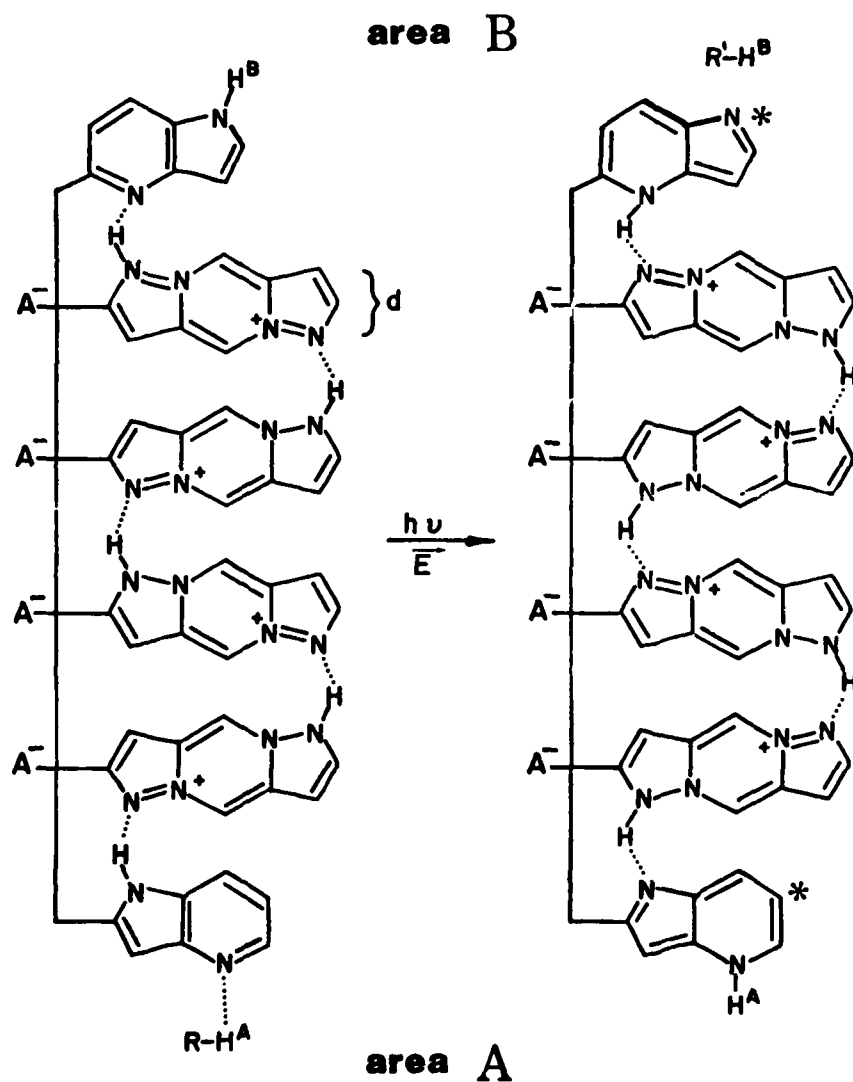
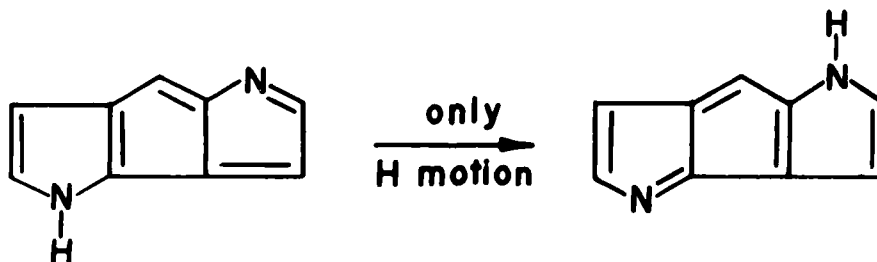


Figure 1. In this proposed photostimulated cooperative mechanism, a hydrogen is transferred from area A to area B via a series of intermediate transfers which are primarily energy independent. However, note that the end members 4-azaindoles are left in an excited state (*).

Streak camera studies (5) of the fluorescence spectra of the excited states (*) on the right (a) indicate that the double proton transfer takes place in less than five picoseconds. Apparently a similar effect occurs when 7-azaindole is dissolved in alcohols for which the corresponding state is illustrated above in (b).

Cooperative particle transfer can be illustrated as an extension of the double proton transfer via the use of a special oligomer. In Figure 1 we wish to transfer a hydrogen atom (proton) from area A at the bottom to area B at the top. This is achieved upon photo-absorption by the hydrogen transfer of the H^A hydrogen to the nitrogen in 4-azaindole (I) at the bottom while hydrogens are cooperatively transferred by the intervening tetra-azaindacene derivatives (II) to the moieties above. As the top 4-azaindole moieties receive a hydrogen from the moiety below it can give up its amine hydrogen, H^B , in the 5-member ring to a proton receiver in area B at the top. There are several points to note in this example: (1) The 4 azaindoles on the right side of the equation are both in an excited state (indicated by *) and normally would decay rapidly. (2) The tetraazaindacene moieties (II) on both sides of Figure 1 are in a ground state in the absence of an electric field, i.e., the proton transfer agent is bimodal with respect to hydrogen coordinate. (3) Note also that the + charge in each II moiety, which is balanced by the anion A^- attached to the chain, has shifted by a distance d parallel to the net proton transfer direction. The net charge motion per H is then d^* times the number of II moieties. This suggests that the entire process could be controlled by the presence and strength of an electric field as well as by the photon energy. (4) By proper choice of molecules it is possible to both make the end members I and the intervening H transfer molecules II very nearly bimodal and free of major charge transfer; for example consider the three member ring system below in two tautomeric states having a similar valence resonance form.



(5) Finally, we note that this system (Figure 1) transfers one H atom that must be restored before it can transfer an H atom again; i.e., there is no net material flow.

There are of course several interesting theoretical questions, e.g., (1) in this cooperative particle transfer are all the H atoms transferred simultaneously; or (2) how many members are necessary before the particles are not transferred simultaneously; and (3) is this a fast multiple particle tunnel or is it strongly mediated by phonon processes?

Control Groups for Periodic Electron Tunnelling

In the first EAP Review (1) it was emphasized that an important effect to be considered in the area of molecular electronics is the tunnelling of electrons through periodic barriers. In a quasi-classical approach, Pschenichnov (6) indicated that the transmission coefficient for an electron through a set of periodic barriers was very close to 1.0 when the electron energy matched that of the pseudo-stationary (or resonant) states in the wells (see Figure 2 and Figure 16 of Reference 1). However, the transmission probability very sharply declined if it failed to match one of those energies. Based on this idea, we then suggested molecular analogues to the transistor-based NAND and NOR gates (Figure 17 of Reference 1).

In Figure 2 (top) we schematically indicate the transmission of an electron through a series of four identical barriers. In the bottom of Figure 2 we denote the molecular device as a body with three Control Groups (CGi) that regulate the depth of the potential wells and hence the pseudo-stationary state energies. In this case the Body is a semi-conducting molecule with four built in potential barriers. Attached to the opposite ends of the Body are the conducting molecular leads indicated here by $-(SN)_x^-$.

What we want to emphasize here is the enormous variability that is permitted by the concept of control groups based on molecular structure. Four possibilities are indicated in Figure 3.

In the first, entitled "Charge Flow," the quaternary charged nitrogen of the control group provides a potential well at the point of attachment to the Body of the gate. If this + charged nitrogen is neutralized by charge flow up the $(SN)_x^-$ chain then the pseudo-stationary levels at that well would be dramatically altered and the switch would be turned off, i.e., electron tunnelling through the Body would be stopped.

In the second case the effect is of a smaller magnitude and arises from the tautomerism associated with an enol-keto system. One method of changing the dipole direction would be the application of an electric field. If a tunnel Body contained several such enol-keto control groups, the normal state of the switch would be "off" in the absence of an electric field. This is because the rapid equilibration between the two alternatives would quickly result in a randomization of dipole directions along the Body. In fact, however, the direction of the dipole can be controlled by using carbon rings of different sizes. In Figure 2, part 2, both rings have six carbons. If the ring furthest from the Body had only five atoms, the enol-keto configuration to the right would be preferred. Hence, this control group can be readily made with a built-in bias.

The third example of a control group is intermediate between the charge flow case and the enol-keto tautomerism of case 2 in terms of the

ELECTRON PERIODIC TUNNELLING and CONTROL GROUPS

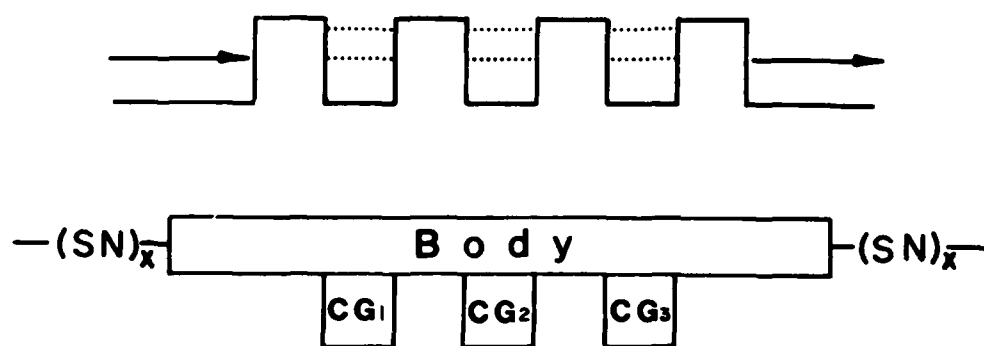
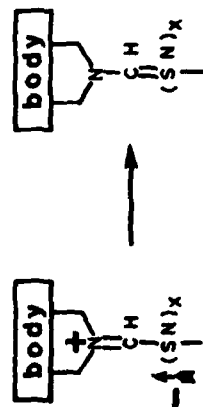


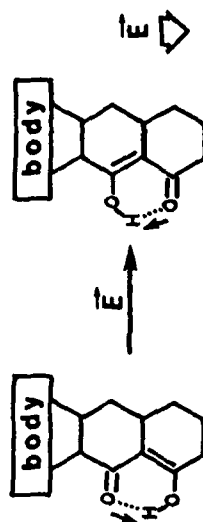
Figure 2. If the energy of the incoming particle matches precisely that of the pseudo states then Pschenichnov (6) showed that the transmission coefficient is 1.0. These pseudo-states, however, can be changed by the Control Groups (CG) that are attached to the body of the molecular device; such a change would turn off the device (i.e. stop electron tunnelling).

PERIODIC TUNNELLING CONTROL GROUPS

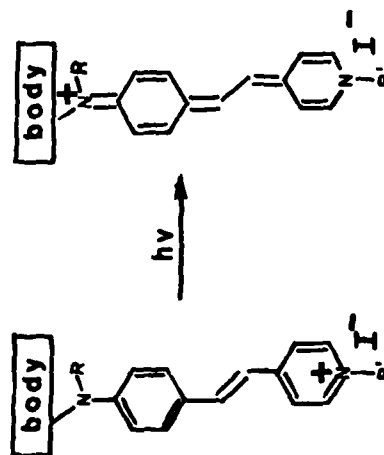
1. Charge Flow



2. Electric Field



3. Photochromic Groups



4. Electron Shift

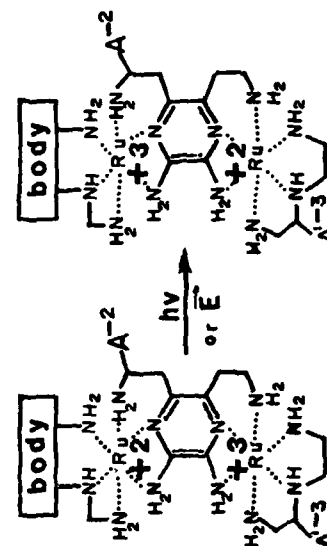


Figure 3. This figure indicates four of the many possible kinds of control for device based on periodic tunnelling.

distance the charge moves. In this case, photo-absorption shifts the plus charge of the quaternary nitrogen by ten atoms closer to tunnel Body. The control group indicated here is modeled after the photochromic probe 4-[p-(dipentylamino)styryl]-1-methylpyridinium iodide which has been used by Loew, Scully, Simpson, and Waggoner (7) to detect membrane formation. In this work (7) the probe functions by imbedding its dipentylamino group in the hydrophobic portion of the membrane, etc.; so situated, its absorption spectra becomes sensitive to the electric field across the membrane.

For this case (3) many different zwitterionic or dye molecules could have been used as examples of photo-activated control groups, however, the one chosen is useful in that it also clearly indicates bond distances change significantly during photo-stimulation.

Electron shift between metal atoms is offered as the fourth example of a control group for a periodic tunnel body. This example is of interest because it represents a very large class of possible control groups. By the proper choice of metal atoms and ligands, it is possible to develop either a bimodal ground state or a ground state and an excited state as indicated in the fourth example. Further, the separation between cations can be easily adjusted by the size of the common ligand, here a 5,6 derivative of 2,3-diaminopyrazine. Such a control group can be photo-activated or possibly driven by an electric field. The final point is that the electron transfer rate involved in the relaxation process can be varied by many orders of magnitude by the proper choice of the common ligand. These complexes are an area of considerable current interest; for further details the reader is referred to the work of T. J. Meyer and H. Taube and their respective co-workers (see references 8 and 9).

By the above four examples, we hope to have illustrated the enormous variability possible in periodic tunnelling switches.

Soliton Transport and Molecular Adders

Soliton transport is a topic that is of interest to many theoretical physicists and may make important contributions to signal transport in biological systems. A soliton can be described as a solitary wave that propagates without change of form or energy in a medium that is normally dissipative. As such, a soliton is like a pseudo-particle having an effective mass, an energy, and velocity. In developing the theory of the concept for a polypeptide chain, Davydov and Kislukha (10) related local distortions between groups and the electric dipole moment of the peptide linkage parallel to the chain direction. The high stability of the soliton has encouraged Davydov (11) to use it in explaining the high efficiency with which the bond breaking energy of ATP in living systems is transported along the α -helix. It is especially interesting that this energy is only about four times that of thermal background.

SOLITON TRANSPORT

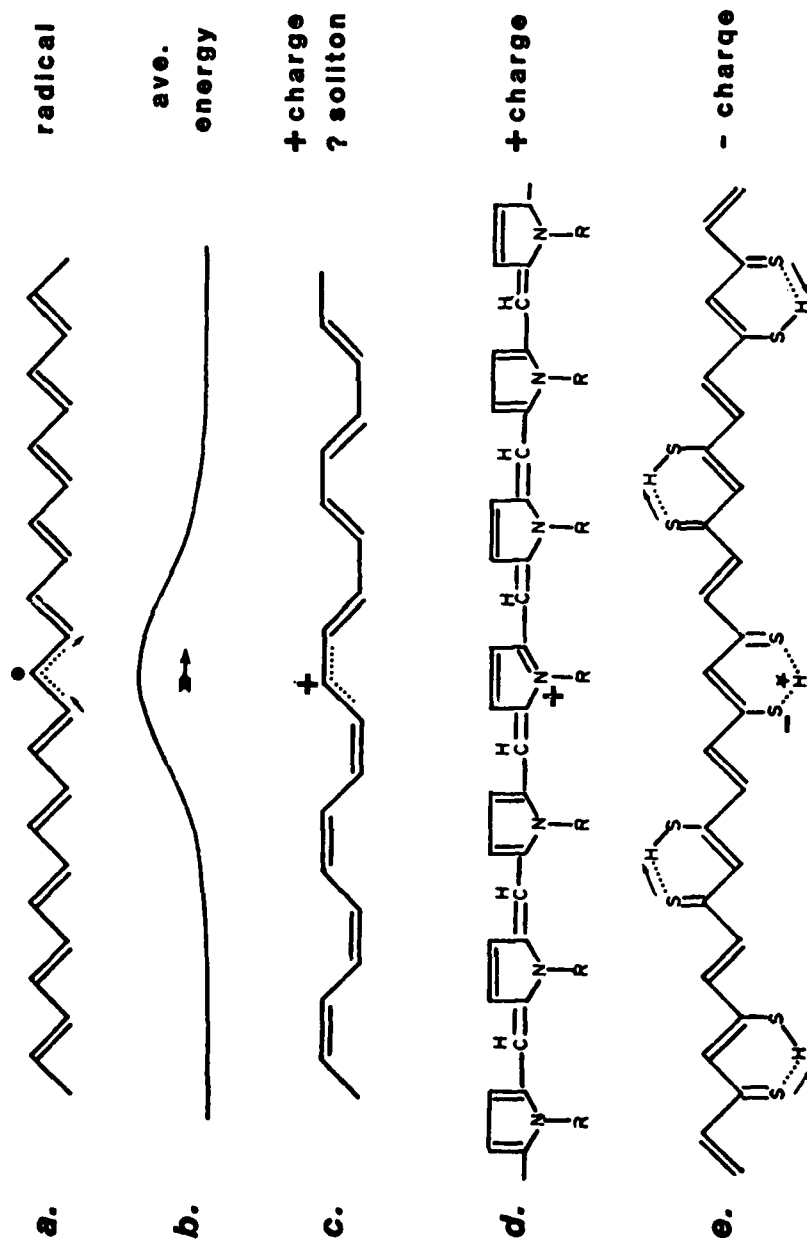


Figure 4. Energy or signal transport by means of solitons or solitary waves can take many different forms. In cases a - d the molecular distortion and velocity remain unchanged as the wave progresses. In case e the soliton energy might change by increments.

Radical as well as charged solitons are illustrated in Figure 4. It should be noted that not only are solitons of a finite width, i.e., of a few monomer units, but that also a change of bonding often occurs near the center of the soliton. In Figure 4a we see this in the radical soliton in trans-polyacetylene where the dotted line indicates a bonding intermediate between a single and double bond. This bonding disturbance may involve more atoms than are indicated and is expected to have a distributed impaired electron character. Note also that a phase change in the single bond, double bond relationship occurs at the soliton. This phase change or "kink" is characteristic of solitons.

A stylized version of the soliton is suggested in Figure 4b. The object is to suggest not only the motion of the soliton as a solitary wave but also that the local disturbance and energy is maximized at the soliton center.

A possible positively charged soliton in cis-polyacetylene is suggested in Figure 4c. To the left we note that the double bonds are in the horizontal plane while to the right of soliton or phase kink the double bonds have a large vertical components. If there is any finite energy difference associated with this change in the double bond position, then it is likely that a soliton will not exist in such a case as the total energy associated with the soliton would be very large, i.e., a small energy at the soliton center, and a very large amount distributed over the right half of the molecule (i.e., over a long distance).

The difficulty in Figure 4c is however obviated in Figure 4d. Here double bonding on both sides of the soliton occurs in both the horizontal and the vertical plane so that there is no net configurational energy difference between the left and the right sides of the chain. In this positively charged soliton the figure is drawn as if the charge were associated with the quaternary nitrogen only, which is unlikely. The distribution of the positive charge between the nitrogen and the carbon atoms as the soliton moves is an interesting theoretical question beyond the scope of this brief survey.

Figure 4e illustrates a negatively charged soliton in a conjugated system containing a periodic array of thio-enol-keto groups. Note that the central thio-enol-keto group contains a negative sulfur and an excited H bonded to both neighboring sulfurs. As illustrated, not all the enol-keto groups are similarly oriented (note the arrow directions). This kind of situation suggests the possibility that a soliton transport mechanism can be used as a counter or adder sensitive to the orientations of the dipoles along its path. While a soliton moves at a velocity less than the velocity of sound in the chain, its velocity is dependent upon its energy (10).

Since the soliton couples strongly with polymer dipoles that are parallel to the propagation direction, it is conceivable that some dipole directions might be reversed and the energy, hence velocity, of the soliton would reflect this transformation. Generally, of course,

dipole reversibility is not an expected phenomenon; however, in situations as in the enol-keto group it is not an unusual event at all. If a soliton propagating down a linear polymer chain as in Figure 4e can reverse the thio-enol-keto bonding arrangement in a reliable manner, then by monitoring the soliton velocity or energy change one has a measure of the dipoles reversed. In short, one has the essence of a molecular adder.

As an example of a more near term soliton application, we note that the motion of a soliton is less than the velocity of sound and hence might be used as a delay line on the molecular scale.

Insulating Layers and Molecular Spaghetti

In a very interesting and instructive article entitled "Molecular Recognition and Self-Organization in Fluorinated Hydrocarbons," F. H. Stillinger and Z. Wasserman (12) demonstrated a principle that should play an important role in the design and fabrication of the chemical computer. The principle is that the various chemical components should be so designed and assembled that the computer is largely self-organizing.

The authors demonstrated the self-organizing concept by looking at the pair potentials for a family of saturated partially fluorinated fused-ring hydrocarbons. For example, in Figure 5a we indicate schematically perhydrocoronene which has twelve hydrogens on each side which project normal to the general plane of the molecule. For each side there are a total of 1376 different patterns that can result if these twelve hydrogens are replaced by fluorine (i.e., by 0 to 12 F's). One such possibility is indicated in Figure 5b while Figure 5c shows what Stillinger and Wasserman call its "conjugate". If the pattern of Figure 5b is indicated by A and is the top of one fluorinated perhydrocoronene (FPHC) and Figure 5c is symbolized by \bar{A} and is the bottom of another FPHC, then the two can fit together perfectly. Such a pair has a deep well in terms of its pair potential while face A with any other FPHC has a very shallow pair potential curve, if a minimum even exists. Now, since each FPHC has two sides one could develop a crystallized series like (F/A) (\bar{A}/B) (\bar{B}/C) (\bar{C}/D) etc., where each face A, B, or C is attracted only by its conjugate face, \bar{A} , \bar{B} , or \bar{C} .

Consider now a substrate surface (either organic or inorganic) that was very similar to A, call it A', and hence, a surface on which \bar{A} would be strongly attracted. Then by using a single solution containing the mixed FPHC species (\bar{A}/B), (\bar{B}/C), (\bar{C}/D), and (D/E) one could put down an insulating layer on the A' substrate which was in this case exactly four FPHC molecules thick and having a top surface specified by E. Such a solution as we have just described might be termed a "pre-organized" solution.

This possibility of engineering with relative weak pair potentials while paying close attention to packing considerations provides a useful step of fabrication beyond the Merrifield approach of molecule by molecule buildup.

Conjugate Pairs for Perhydrocoronene

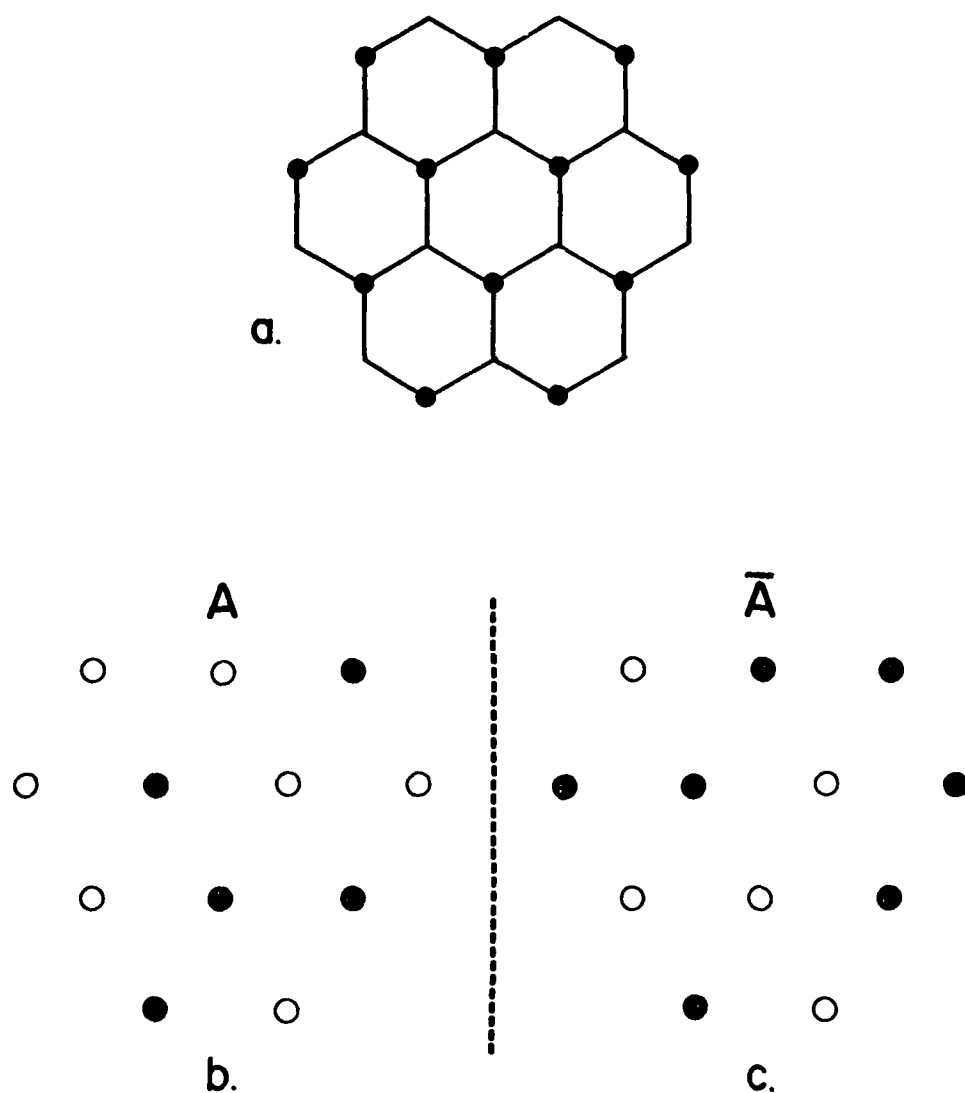
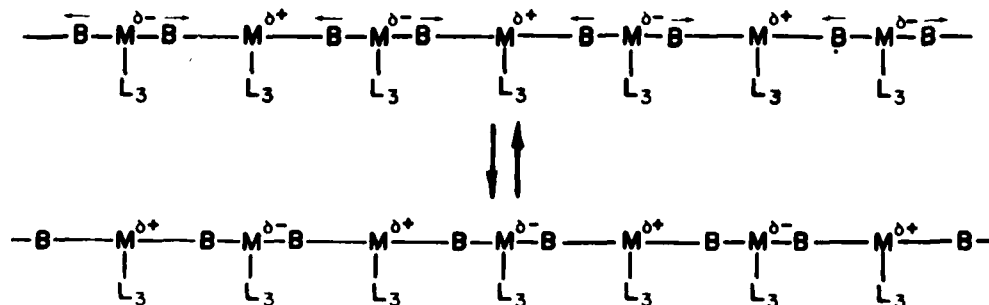


Figure 5. The carbons in fully saturated perhydrocoronene have a pleated sheet structure such that 12 C-H bonds project up, 12 C-H bonds project down and the remaining 12 C-H bonds are horizontal. Figure 5b indicates a possible replacement pattern of five fluorines for hydrogens that project up from the molecular plane. Figure 5c is the corresponding conjugate (12).

Chemical Memories

In Figure 7 we propose such a bimodal memory which is based on the premise that a chain system similar to the one below is possible:



48

MOLECULAR SPAGHETTI

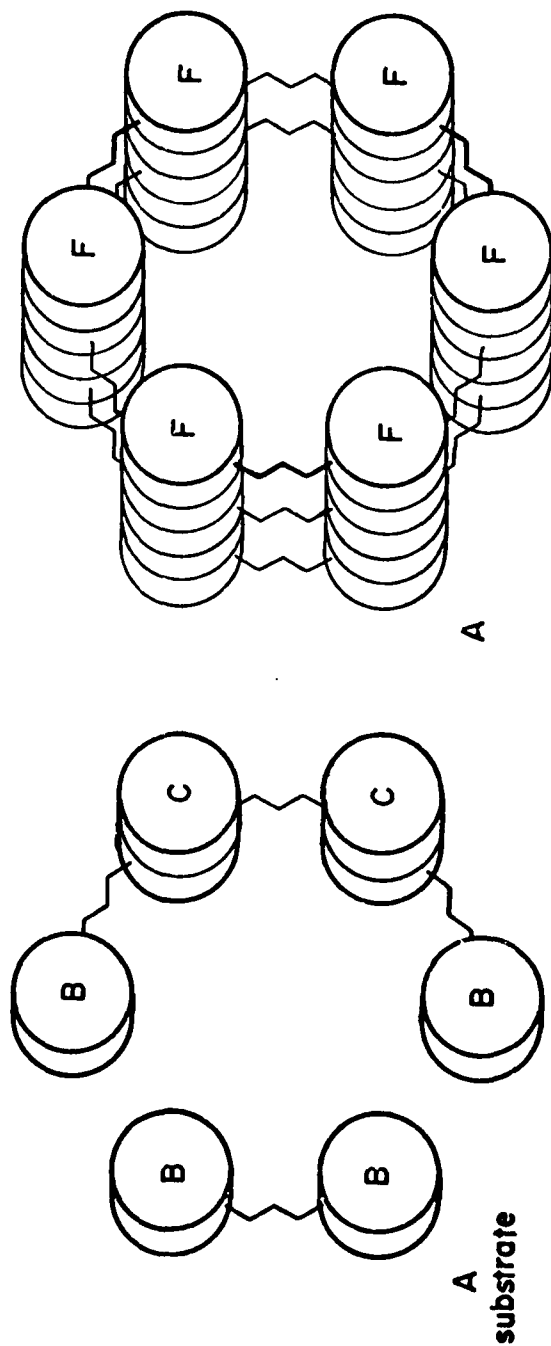


Figure 6. This figure symbolizes the formation of molecular spaghetti using bridged fluorinated perhydrocoronene pairs. Figures 5 and 6 were adapted from the work of Stillinger and Wasserman (12).

BISTABLE CHEMICAL MEMORY

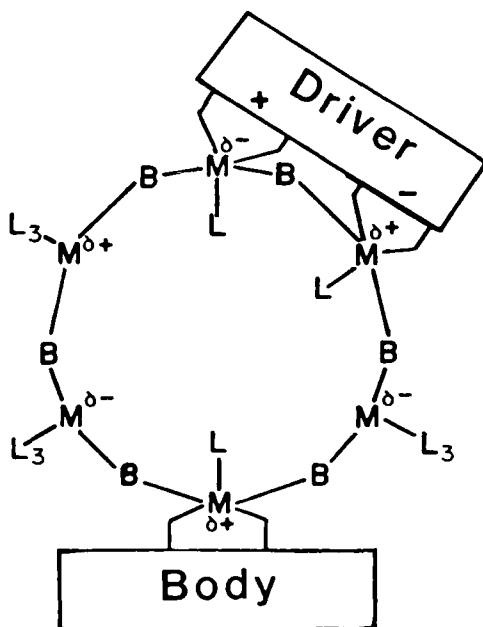


Figure 7. This proposed chemical memory element has two stationary states determined by the Driver. In state changes, the bridging ligands move away from the $M^{\delta-}$ atoms toward the $M^{\delta+}$ atoms causing a valence switching between them. The memory is read here by an electron periodic tunnelling device.

the M^{δ^-} and M^{δ^+} can be interchanged throughout the chain. That is, the valences and effective charges of the metal atoms M can be changed by a relatively small adjustment of metal ligand M - B distances. This valence change may involve an electron movement from one metal to its neighbors or an internal electron shift from a valence bond orbital to a localized state and vice versa.

In Figure 7 we show a chemical memory element which consists of (1) a section of the chain just discussed formed into a ring; (2) a Driver which is capable of interchanging the valence states of all the metals M in the ring by controlling the valences of the two metals adjacent to and joined to the driver; and (3) a Body of a periodic tunnelling switch, which can readily read the valence state of the metal atom joined to it. Note that the Driver is pictured as stabilizing the valences of the two attached metal atoms, M^{δ^-} and M^{δ^+} , by its + and - charge. If these charges of the Driver were to be reversed, the adjacent metal atoms would presumably respond by becoming M^{δ^+} and M^{δ^-} and this change would be propagated completely around the ring. In such a system reading the memory element should not destroy the memory contents of the ring. It is also conceivable that a short section of linear chain could be used instead of the ring: the ring, however, would appear to be more stable and hence desirable.

SUMMARY

In this report we have continued the conceptual development of the "chemical" computer based on "molecular" electronic devices. In particular, we have (1) extended the concept of proton tunnelling in hydrogen bond formations to the concept of cooperative particle transfer via the experimental observation of a fast double proton transfer; (2) provided a variety of control groups for periodic barrier tunnelling; (3) explored some of the implications of soliton signal transport and indicated how it could be used as an adder; (4) emphasized the importance of self-organization in chemical computer fabrication; and (5) suggested a molecular memory element which can be independently set and read.

In so doing we hope that we have shown that the opportunity for the use of the chemists' and physicists' imagination in the concept of the chemical computer is virtually unlimited, as well as extremely stimulating.

REFERENCES

1. F. L. Carter, Problems and Prospects of Future Electroactive Polymers and "Molecular" Electronic Devices, in The NRL Program on Electroactive Polymers, First Annual Report, Ed. by L. B. Lockhart, Jr., NRL Memorandum Report 3960, March 30, 1979, p. 121 ff.
2. J. A. Krumhansi and Y-H. Pao, Physics Today, 32, 25 (1978); A. N. Broers, *ibid.*, 38; and J. L. Moll and D. Hammond, *ibid.*, 46.

3. C. Birr, Aspects of the Merrifield Peptide Synthesis, Springer-Verlag, Berlin, Heidelberg, New York, 1978.
4. C. A. Taylor, M. A. El-Bayoumi, and M. Kasha, Proc. Nat'l. Acad. Sci. U.S., 63, 253 (1969).
5. K. B. Eisenthal, K. Gnadig, W. Hetherington, M. Crawford, and R. Micheels, "Picosecond Laser Studies of Electron-Hole Interactions and Double Proton Transfer" in Picosecond Phenomena, Proc. of First International Conference on Picosecond Phenomena, Eds., C. V. Shank, E. P. Ippen, and S. L. Shapiro, Springer-Verlag, Berlin, Heidelberg, New York, 1978, p. 34.
6. E. A. Pschenichnov, Soviet Physics - Solid State, 4, 819 (1962).
7. L. M. Loew, S. Scully, L. Simpon, and A. S. Waggoner, Nature, 281, 497 (1979).
8. T. J. Meyer, Accounts of Chem. Res., 11, 94 (1978); M. J. Powers and T. J. Meyer, Inorganic Chem. 17, 1785 (1978).
9. A. Von Kameke, G. M. Tom, and H. Taube, Inorganic Chem., 17, 1790 (1978).
10. A. S. Davydov and N. I. Kislukha, Phys. Stat. Sol. (b) 59, 465 (1973); Sov. Phys. JETP, 44, 571 (1976).
11. A. S. Davydov, "Vibrational Solitons as Energy Carriers in Biological Systems," Preprint ITP-76-12E, Kiev (1976).
12. F. H. Stillinger and Z. Wasserman, J. Phys. Chem., 82, 929 (1978).

ION IMPLANTATION STUDIES ON $(CH)_x$

D. C. Weber and P. Brant
Inorganic and Electrochemistry Branch
Chemistry Division

C. Carosella
Materials Modification Branch
Radiation Technology Division

INTRODUCTION

We have shown previously (1,2) that ion implantation can be used to introduce dopant species into $(CH)_x$. In one case it appeared that the dopant could be incorporated into the polymer film with little or no observable damage to the $(CH)_x$. The samples exhibited increases in conductivity but the exact reasons for these increases were not clearly understood. Since that time, we have investigated the technique in greater detail in an attempt to answer some of the questions raised in the initial work. We present here the results of that study as well as new possible uses for materials obtained. The work was primarily centered on the effects of halogen implantation and also the possible effects of the ion beam damage.

EXPERIMENTAL

The experimental setup has been described elsewhere (2) for the implantation apparatus. During this past year, a new implanter has become operational which is capable of much higher flux rates, enabling a faster sample throughput.

After implanting, the samples are analyzed via XPS for damage and the conductivities measured by the 4-probe technique. Conductivities are expressed as a ratio of the unimplanted vs. the implanted portion of each film to minimize differences due to slightly different sample preparation and sample handling. Table I gives the data obtained for the implanted samples.

RESULTS AND DISCUSSION

Halogen Implantation

The halogens (F, Cl, Br, I) were implanted into $(CH)_x$ films at low energies (~ 25 keV) to keep the implanted layer close to the surface for XPS investigation. When comparing the conductivities of the implanted materials with the conductivities of the corresponding vapor-doped films, the results are quite interesting. Opposing trends were observed in conductivity of the halogen series for the chemically doped vs. the ion implanted films. What is significant in these trends is that for the ion implanted samples, the conductivity tracks with the oxidation strength of the halogen atom used for

TABLE I

Dopant	Core Level Binding Energy C(1s)	X^a	Conductivity Ratio $\sigma_{\text{doped}}/\sigma_{\text{pure}}$
25 Kev F^+	284.6 (2.2) ^b	686.1 (2.1)	2.3×10^3
F_2	286.0 (1.8)	686.8 (2.6)	$10^{-1} - 10^{-2}$
Cl^+	284 (2.2)	199.8	3.4×10^2
Cl_2	286.5 (1.7) 284.5 (1.7)	200.0 (1.7)	$10 - 10^3$
Br^+	284.5 (2.3)	69.3	7.8
Br_2	284.8 (1.9)	69.4	10^4
I^+	284.3 (1.8)	619.8 (1.5)	$3.8 - 100$
I_2	284.4 (2.0)	619.6	$\sim 10^5 - 10^7$
Ar^+	283.3 (3.5)		~ 1

^a X is F 1s, Cl 2p_{3/2}, Br 3d, I 3d_{3/2}.

^b Values in parentheses are peak full width at half maxim (FWHM), in eV.

implantation; whereas in the chemically doped species the property which follows the conductivity most closely is the ability of the halogen to form large polarizable counter ions of the oxidized polymer backbone. These observations, we believe, can be used to gain insight into the conduction processes in the polymers. Considering that the conductivity of a material is directly proportional to the number of charge carriers and the mobility of these carriers, one can relate the chemistry directly to these properties. In the implanted materials, it appears that the major effect of the implanted ions is to generate charge carriers in the polymer backbone by oxidation of the chain. This would then give rise to an increase in conductivity based solely on increased charge carriers.

In looking at the chemically doped materials, there is also present the ability for oxidation of the chain giving rise to charge carriers but in this system there exists the second ability of the halogens to form large easily polarized counter ions. We believe that it is the presence of these ions that aid in the mobility of the charge carriers by acting as low energy alternatives to the inter chain hopping, which appears to limit the conductivity. This increase in mobility seems to be the more important of the two conditions for increasing the conductivity, since when looking at the magnitude of the increases with respect to the undoped polymer the chemical doping technique leads to the larger increases.

XPS analysis of the implanted films shows that the halogens appear to be bound to the polymer backbone in a form resembling a normal covalent C-X bond. There appears to be no evidence for the presence of the large poly-halogen anions of the type observed (3) for the corresponding chemically doped species.

One possible caveat to the above reasoning is that the conductivity increases are based on a bulk measurement that does not reflect the fact that the implanted layer is a small fraction of the sample thickness and therefore the actual increase may in fact be larger than we are measuring.

In the investigation of the halogen series, one unexpected result was obtained with the Br^+ implanted samples. Previous to this work $(\text{CH})_x$ films have been observed to lose the shiny luster, characteristic of the freshly prepared films, when exposed to air for a few weeks. However, the $(\text{CH})_x$ films which had been implanted with Br^+ ions have retained their high metallic luster over the area of the film exposed to the ion beam. Portions of the same film that had been masked from the beam showed the normal loss of luster and embrittlement.

Damage Studies

When evaluating ion implantation, it is important to separate the effects of the ions one is implanting from the possible consequences of the ion beam itself. In other words, is one dealing with a change caused by the presence of the new ion in the material or is the observed alteration of the substrate material's properties strictly a damage related phenomenon? Methods devised for sorting out these effects include implantation with the ion that makes up the substrate or implanting with an ion that one would expect to be inert with respect to the substrate material. Since in this case we are dealing with a covalent molecular species, the first method is not applicable. We then chose to implant the films with Ar^+ ions under similar conditions as the

halogens were implanted. The films obtained showed no real increase in conductivity which indicated that the increases observed with the halogens were a result of the halogen-polymer interaction and not a damage related effect. A second check of this was obtained from the XPS data for the C(1s) spectra of the Ar implanted films compared with the halogen implanted films. The FWHM of the C(1s) peak in the halogen implanted cases is comparable to those of the chemically doped species. The Ar⁺ implanted samples showed a very broadened C(1s) signal with the formation of a second peak in the spectrum (Figures 1 and 2). This result indicated that damage had occurred on the polymer backbone. Although some damage induced charge carriers might be generated, one would also expect a shortening of the chains; therefore, reduced mobility and consequently little or no increase in conductivity would be expected, a fact borne out by the data.

FUTURE WORK

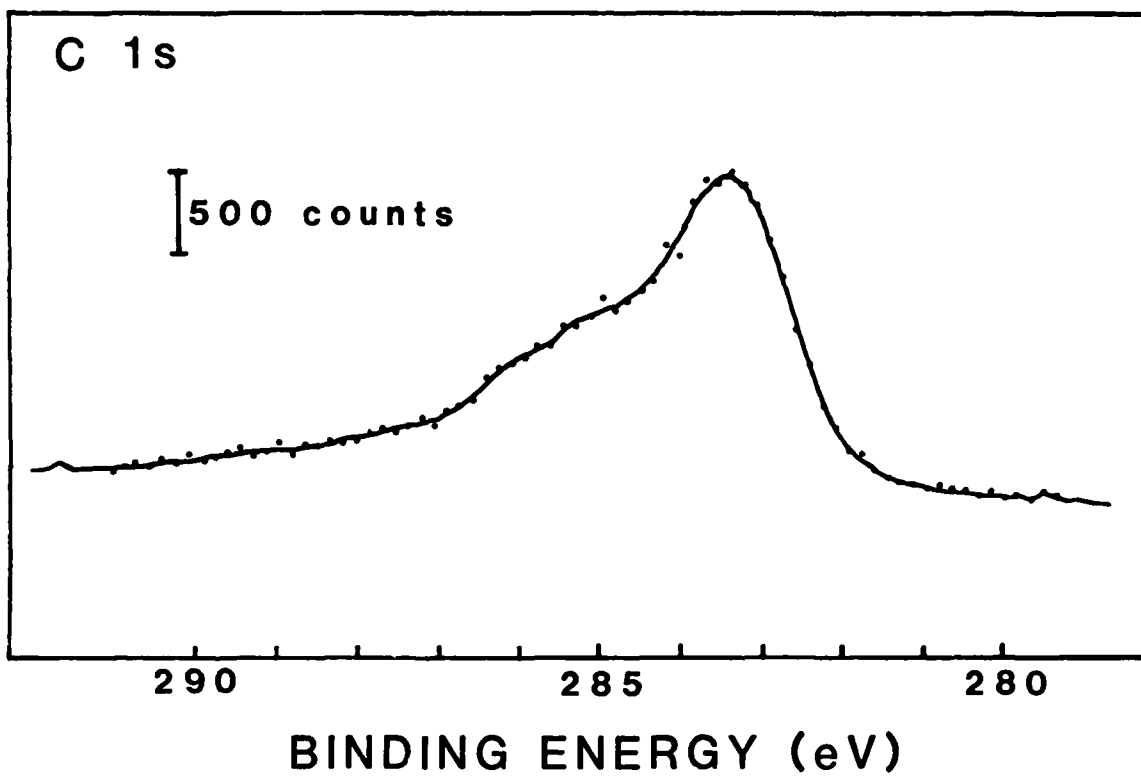
At this stage we feel that the ion implantation technique should be utilized to its full potential in the modification of the electrical properties of the conducting polymers. For example, the highly reproducible control over doping levels as well as the spatial resolution characteristics should be tested with the hope of device fabrication from the polymers. A further look at the stabilization of the films should be undertaken since poor air stability of the materials to date has been a drawback to their application. It is in these areas that the utilization of the present materials will come.

SUMMARY

The work has shown that ion implantation appears to be a viable technique in the modification of the electrical properties of (CH)_x. It has been shown that the effects observed are real manifestations of chemical reactions as opposed to damage induced phenomena. Insight has been given to understanding the role of the dopant in increasing the electrical conductivity. This information used properly by the synthetic chemist may lead to new materials with enhanced conductivity. New directions of work have been suggested with practical payoffs possible.

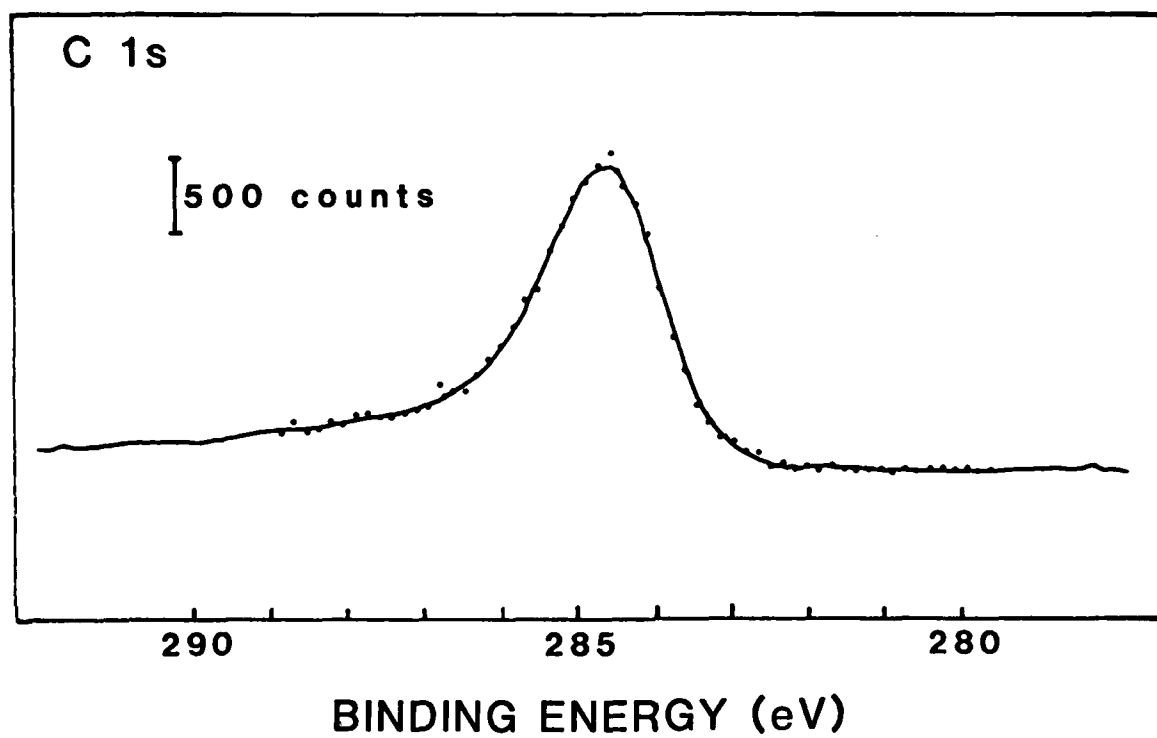
REFERENCES

1. P. Brant, D. C. Weber, and C. T. Ewing, "X-ray Photoelectron Spectroscopic Investigations of (SN)_x and (CH)_x and Related Materials and ESR Studies of (CH)_x" in NRL Memorandum Report 3960, L. Lockhart, Jr., ed. (1979).
2. W. N. Allen, P. Brant, C. A. Carosella, J. J. DeCorpo, C. T. Ewing, F. E. Saalfeld and D. C. Weber, J. Syn. Metals 1, (2), 151-159 (1980).
3. S. L. Hsu, A. J. Signorelli, G. P. Pez, and R. H. Baughman, J. Chem. Phys. 69, (1), 106 (1978).



Ar Implanted $(CH)_x$

Figure 1



F Implanted (CH)_x

Figure 2

CHARACTERIZATION OF HALOGEN-DOPED $(CH)_x$ AND $(SN)_x$, PART II

J. R. Holtzclaw, D. C. Weber, F. E. Saalfeld,
J. R. Wyatt and J. J. DeCorpo
Chemistry Division

INTRODUCTION

Electroactive polymers have become the subject of considerable research effort because of their potential application in the electronics and semiconductor industry with some of the most extensively studied polymers being poly(sulfur nitride); $(SN)_x$, polyacetylene; $(CH)_x$, and their doped derivatives.

In previous communications^{1,2,3} we have described mass spectral studies on brominated $(SN)_x$ and halogenated $(CH)_x$. We present in this report the results of additional work on brominated $(SN)_x$, iodinated polyacetylene, as well as on arsenic pentafluoride (AsF_5) doped $(SN)_x$ polyacetylene and report the characterization of some of the interactions between the chemical dopant and the polymer matrix.

EXPERIMENTAL

Polyacetylene was prepared by the method of Shirakawa et al.⁴ and doped by exposing the film to vapors of either iodine⁵ or distilled AsF_5 .⁶ Samples of brominated $(SN)_x$ were prepared and analyzed by the method described earlier.² The AsF_5 doped samples were cryogenically pumped for 15 hours, sealed under vacuum and stored at $-196^\circ C$. Mass spectra of the AsF_5 doped $(CH)_x$ were recorded with a Bendix TOF instrument. Samples were attached to a Monel gas inlet manifold and the manifold passivated with distilled AsF_5 vapor. Complete passivation was assured by analyzing the residual manifold vapor with the mass-spectrometer. Once the manifold was passivated, the breakseal on the sample vial was cracked and spectra of the volatiles recorded while the sample warmed to room temperature. The sample vials could also be heated in an oil bath while attached to the inlet manifold. Quantitative analyses were carried out on a modulated, molecular beam mass spectrometer equipped with the previously described manifold system.

Iodinated $(CH)_x$ and brominated $(SN)_x$ sample manipulation was carried out in a dry box to minimize exposure to air. Mass spectral data were acquired on a Hewlett-Packard 5985A Mass Spectrometer with a direct insertion probe as described previously.

RESULTS AND DISCUSSION

Brominated $(SN)_x$

Previous studies^{1,2} have shown that a hydride impurity associated with crystalline $(SN)_x$ is converted to HBr upon $(SN)_x$ bromination. In an attempt

to determine the relationship between HBr and single crystal conductivity, the conductivity of a sample of brominated (SN)_x was measured before the removal of the HBr. Electrodeless conductivity measurements showed the crystal's conductivity to decrease by a factor of ~2 after removal of HBr. However, the decrease in conductivity was probably due to loss of Br₂ from the crystal and not a result of HBr removal.

The results of new experiments in which the conductivity was measured after re-exposing the HBr-free crystal to Br₂ indicate that the conductivity of (SN)_x is not affected by the presence of HBr or the hydride impurity. A sample of (SN)_x containing the hydride impurity was brominated to produce (SN Br_{0.4})_x, and the conductivity and vapor species of this new material analyzed. The crystal was then heated at 60°C in a vacuum system for 24 hours to remove HBr and produce (SN Br_{0.25})_x which was similarly analyzed. The (SN Br_{0.25})_x was then rebrominated and again analyzed. This procedure was repeated several times, and the averaged experimental results are presented in Table 1. In the left-hand column of Table 1 the treatment to produce various species is shown. In the next column the conductivity of the (SN Br_y)_x relative to the conductivity of (SN)_x is shown. The last two columns report whether or not a (SN)_x hydride species or HBr evolves from the material when it is heated after bromination or de-bromination. Initially, a (SN)_x hydride species is detected. After bromination the material's electrical conductivity increases and the (SN)_x hydride species vanishes but HBr is observed. These results suggest that the hydride in the (SN)_x reacted to form hydrogen bromide. However, after some of the bromine is removed by evacuation and heating, the electrical conductivity decreases to approximately that of (SN)_x, and neither (SN)_x hydride nor HBr is observed. Upon rebromination to (SN Br_{0.4})_x the material's electrical conductivity returns to the value originally found after the first bromination of (SN)_x. Again, neither the (SN)_x hydride nor the HBr is observed. Therefore, we conclude that the hydride impurity does not influence the conductivity of (SN)_x.

I₂ Doped Polyacetylene

Preliminary mass spectral studies of iodinated polyacetylene indicated the presence of two different iodine species in the polyacetylene crystal. This is in agreement with optical spectroscopic evidence presented earlier by Baughman, et al.^{9,10}

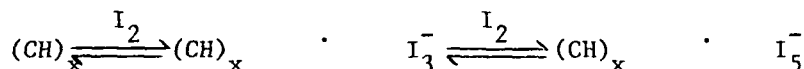
To further investigate the nature of the I₂ evolution from doped (CH)_x and to examine more carefully the observed double peaking in I₂ ion intensity, mass spectral data were taken on freshly prepared samples as well as redoped specimens. The double peaking of the I₂ intensity vs. temperature is clearly visible in Figure 1 which was obtained from freshly prepared specimens. The lower temperature I₂ peak occurs at 60°C. More dramatically, after heat treating the sample at 60°C for five minutes the low temperature peak was effectively removed (Figure 2). Thus iodine-doped polyacetylene has more than one I₂ species, one of which can be removed by heat treatment. The post-heating I₂ temperature profile in Figure 2 shows no evidence of the first I₂ peak. The low temperature peak will reappear after a sample which had been heat treated is subsequently redoped with iodine (Figure 3).

The amount of I₂ in polyacetylene was also varied. Shown in Figure 4 are I₂ temperature profiles for three different doping concentrations. The lightly doped sample, with a composition of approximately (CH I_{0.7})_x, shows only a single peak while two peaks emerge at the higher doping concentrations.

The HI temperature profile, Figure 1, shows that there is no low temperature (<90°C) evolution of HI as in the case of I₂. It is believed that the 100 - 240°C evolution of HI is due to HI absorbed on the surface during the synthesis process and/or I₂ reacting as it is heated and released into the gas phase since on reheating there is no evolution of HI in this temperature range. The increase in HI intensity in Figure 1 at about 300°C is probably from dehydrohalogenation of the polymer chain.

The double peaking in the iodine doped systems is a clear indication that I₂ is associated with the polymer in at least two forms. There are two reasonable explanations for the presence of the two species. One possibility is that one of the observed peaks was due to absorbed I₂ on two specific sites on the polymer chain; thus, Figure 4 shows that the higher temperature peak occurs only on heavy doping of the polymer and is dominant in older samples. But once present, the higher temperature peak cannot be removed by heat treating. The lower temperature peak is present at higher dopant concentrations in freshly prepared samples and can be easily removed by heat treatment. This suggests that its precursor is present in a weakly bound manner to the polymer chain and may be slowly diffusing deeper in the matrix.

A second explanation was given by Baughman et al. who have presented spectroscopic data indicating the presence of I₃⁻ and I₅⁻ in the polymer matrix. Our data are also consistent with this model. The production of the two different I₂ species, observed mass spectrometrically, from the I₃⁻ species would be expected to require different amounts of thermal energy due to the different stabilities of the two species. If one considers the possible equilibrium below



it is obvious that with more I₂ present, the further to the right the equilibrium will be. Conversely as one drives off I₂ the equilibrium will shift to the left. Such an equilibrium is consistent with Baughman's observation that one species, probably I₅⁻, decreased in concentration relative to the other (a priori I₃⁻) upon thermal annealing or under high mechanical stress. Applying Baughman's identification of the interactive iodine species, the lower temperature peak observed in our study is attributable to I₅⁻ and the higher temperature peak to I₃⁻. This assignment is consistent with the proposed equilibrium. The same observations of two I₂ peaks were made on examination of the temperature dependence of the mass spectra of iodinated Al and Ga fluorine bridged phthalocyanines.¹¹ In these cases, Raman spectra run on the samples showed a correspondence of the I₅⁻ species with the lower temperature I₂ peak. The data also are consistent with the proposed equilibrium. It is our belief that the data should be interpreted along the lines of the second explanation and work is being carried out to relate the two peaks to I₃⁻ and I₅⁻ which can be independently identified by other techniques.

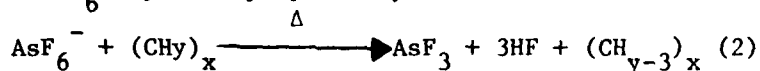
AsF₅ Doped Polyacetylene

The nature of the chemical interaction between AsF₅ and polyacetylene is incompletely understood despite the great body of information that has been collected on the AsF₅ - (CH)_x system. In fact, there is even disagreement on the form of the AsF₅^x species in the doped polyacetylene film. A detailed mass spectral study of AsF₅ doped polyacetylene was undertaken in an effort to shed some light on the nature of the AsF₅ - polyacetylene interaction.

Mass spectra of the volatiles evolved from the sample as it was warmed from -196°C to room temperature show AsF_5 and HF to be the predominant species (see Figure 5,6). When the sample is warmed to higher temperatures the total amount of gas increases with AsF_5 and HF remaining the predominant species at temperatures below 50°C , while above 50°C , the concentration of AsF_3 and HF increase relative to that of AsF_5 (Figure 6). In addition, if the sample is heated to temperatures above 60°C for an extended period of time, the AsF_5 species can be completely removed and upon cooling and re-heating of this sample, the only observed materials are AsF_3 and HF.

The relative concentrations of AsF_3 and HF remain essentially constant over the $120^{\circ} - 160^{\circ}\text{C}$ temperature range, as shown in Figure 7, and a HF to AsF_3 ratio of 3:1 has been measured. At higher temperatures, the HF to AsF_3 ratio increases, which may indicate that AsF_3 is reacting with the hot glass of the sample vial.

These results indicate that the AsF_5 /HF species observed at temperatures below 50°C are due to unreacted AsF_5 and HF absorbed onto or into the polymer, whereas the AsF_3 and HF species produced at temperatures above $\sim 110^{\circ}\text{C}$ originate from the same As_2F_6 material and are not independently diffusing out of the polymer. The AsF_3 /HF species are probably thermal decomposition products of the AsF_6^- species proposed by Clarks et al.^{12,14}



Further experiments to characterize the species involved in AsF_5 doped polyacetylene are underway.

REFERENCES

1. R. D. Smith, J. R. Wyatt, J. J. DeCorpo, F. E. Saalfeld, M. J. Moran, and A. G. MacDiarmid, J. Am. Chem. Soc., **99**, 1727 (1977).
2. W. N. Allen, J. J. DeCorpo, F. E. Saalfeld, and J. R. Wyatt, Chem. Phys. Lett., **54**, 524 (1978).
3. W. N. Allen, J. J. DeCorpo, F. E. Saalfeld, J. R. Wyatt, and D. C. Weber, NRL Memorandum Report 3960, L. B. Lockhart, ed., March 30, 1979.
4. H. Shirakawa and S. Ikeda, Polymer J., **2**, 231 (1971).
5. H. Shirakawa, E. J. Louis, A. G. MacDiarmid, C. K. Chiang and A. J. Heeger, J. Chem. Soc., 578 (1977).
6. C. K. Chiang et al., Phys. Rev. Lett., **39**, 1089 (1977).
7. W. N. Allen, J. J. DeCorpo, F. E. Saalfeld, J. R. Wyatt, and D. C. Weber, submitted to J. Syn. Met.
8. J. S. Lass and A. P. Pippard, J. Phys. E., **3**, 137 (1970).
9. R. H. Baughman, S. L. Hsu, and A. J. Signorelli, Fifth Intl. Symp. of Chem. of Org. Solid State, Brandeis Univ., Waltham, Mass., 13-16 June 1978.

10. S. L. Hsu, A. J. Signorelli, G. P. Pez, and R. H. Baughman, J. Chem. Phys., 69, 106 (1978).
11. P. M. Kuznesof, K. J. Wynne, R. S. Nohr, and M. E. Kenney, Accepted for publication, J. Chem. Soc., Chem. Comm.
12. T. C. Clarke et al., Chem. Comm., 332 (1979).
13. J. G. Wooley, Carbon, 11, 225 (1973).
14. T. C. Clarke, R. H. Geiss, W. D. Gill, P. M. Grant, H. Morawitz, O. B. Street, and D. W. Sayers, Synthetic Metals, 2, 21 (1979).

Table 1

Summary of Experimental Results for Brominated $(SN)_x$

	$\sigma_{\text{sample}}/\sigma_{(SN)_x}$	S, N, H_k	HBr
$(SN)_x$	1	yes	no
$\downarrow Br_2$ $(SNBr_4)_x$	10	no	yes
$\downarrow 60^\circ C, vac$ $24\ hr$ $(SNBr_{25})_x$	5	no	no
$\downarrow Br_2$ $(SNBr_4)_x$	10	no	no

**POLYACETYLENE
I₂ DOPED**

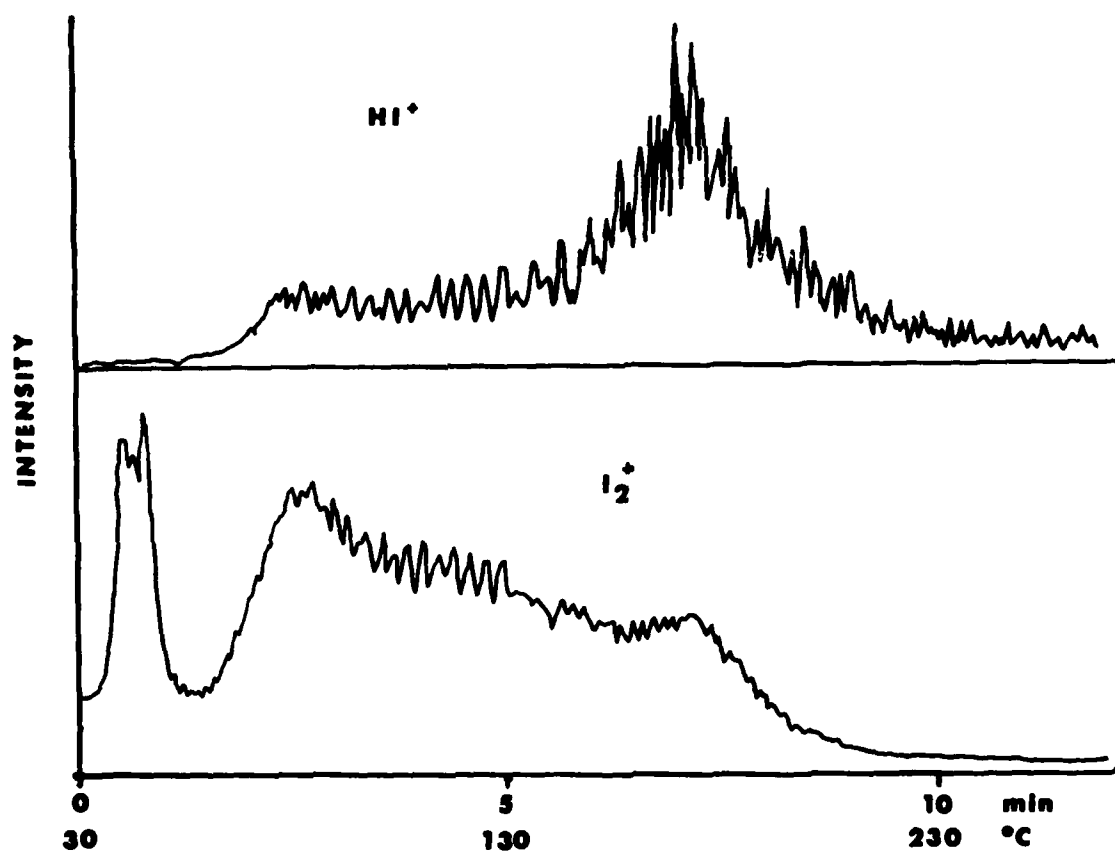


Fig. 1 - Profiles of HI and I₂ intensities vs. temperature on freshly prepared, heavily I₂ doped (CH)_x

POLYACETLYENE IODINE-DOPED

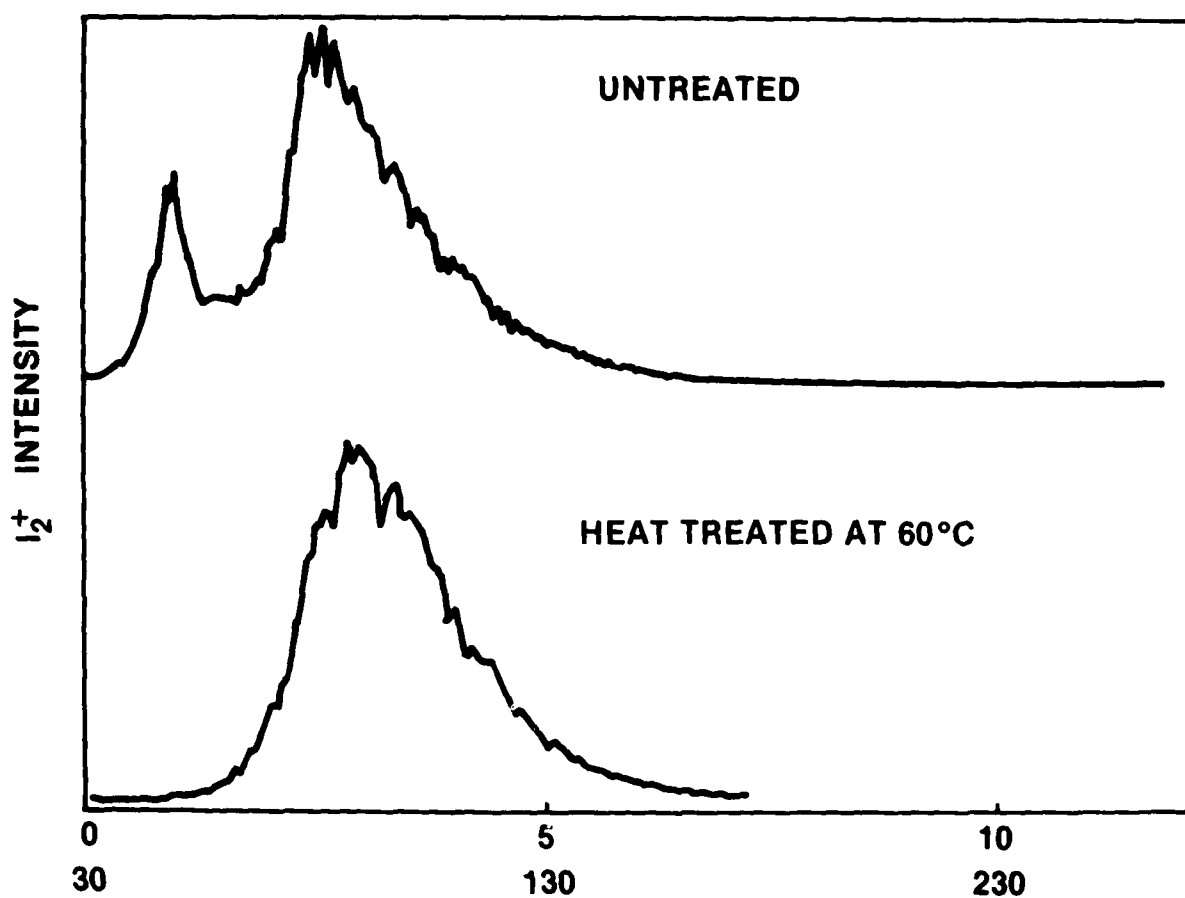


Fig. 2 - Profile of I_2^+ intensity vs. temperature of heavily I_2 doped $(CH)_x$ before and after heat treatment

**POLYACETYLENE
I₂ DOPED**

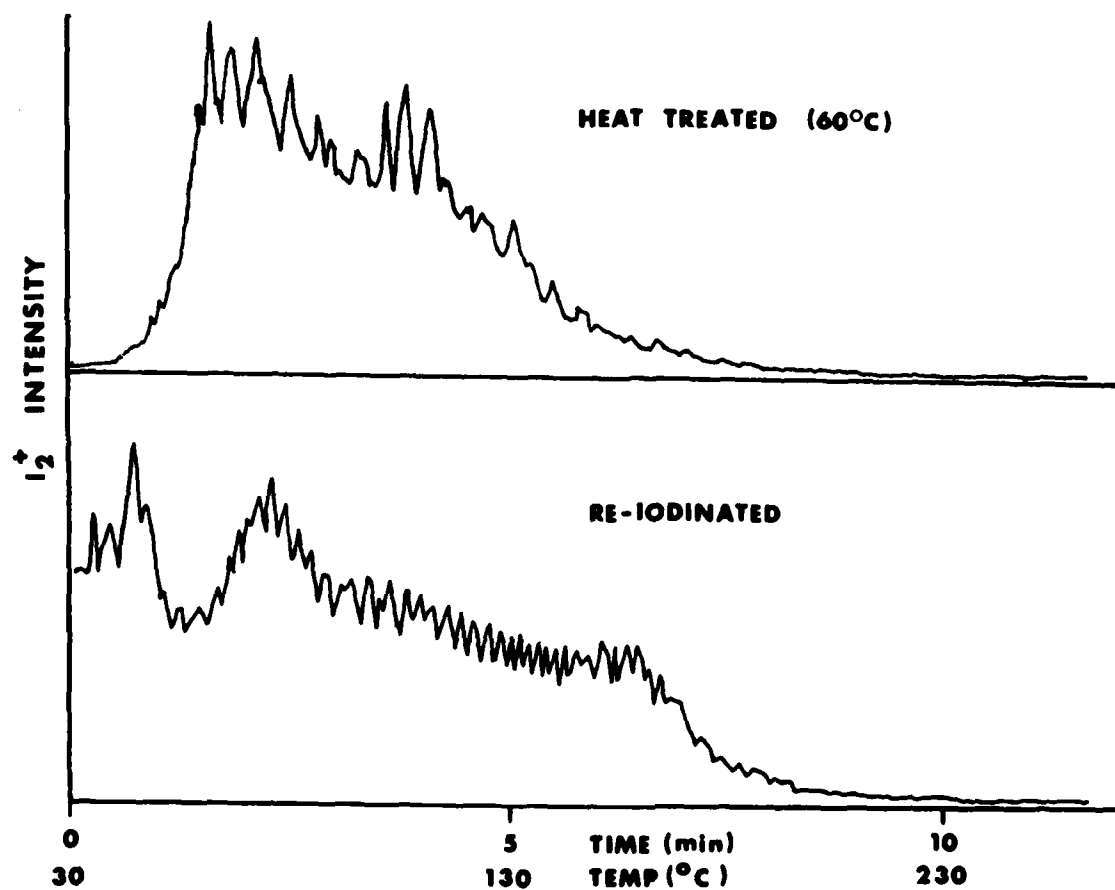


Fig. 3 - Profile of I₂ intensity vs. temperature of heat treated and reiodinated (CH)_x

POLYACETYLENE I₂ DOPED

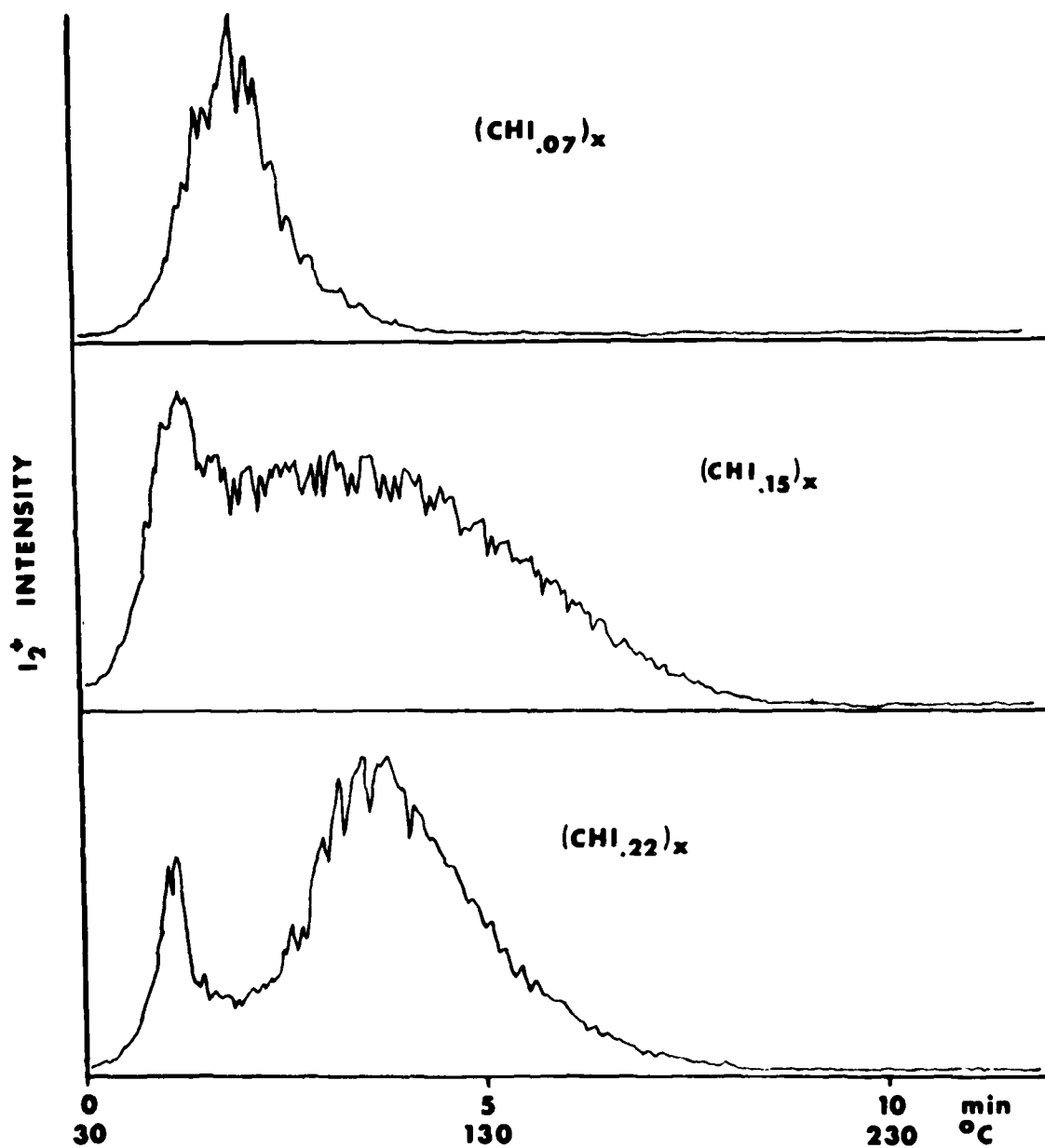


Fig. 4 - Profile of I₂ intensity vs. temperature of (CH)_x with different doping levels of I₂

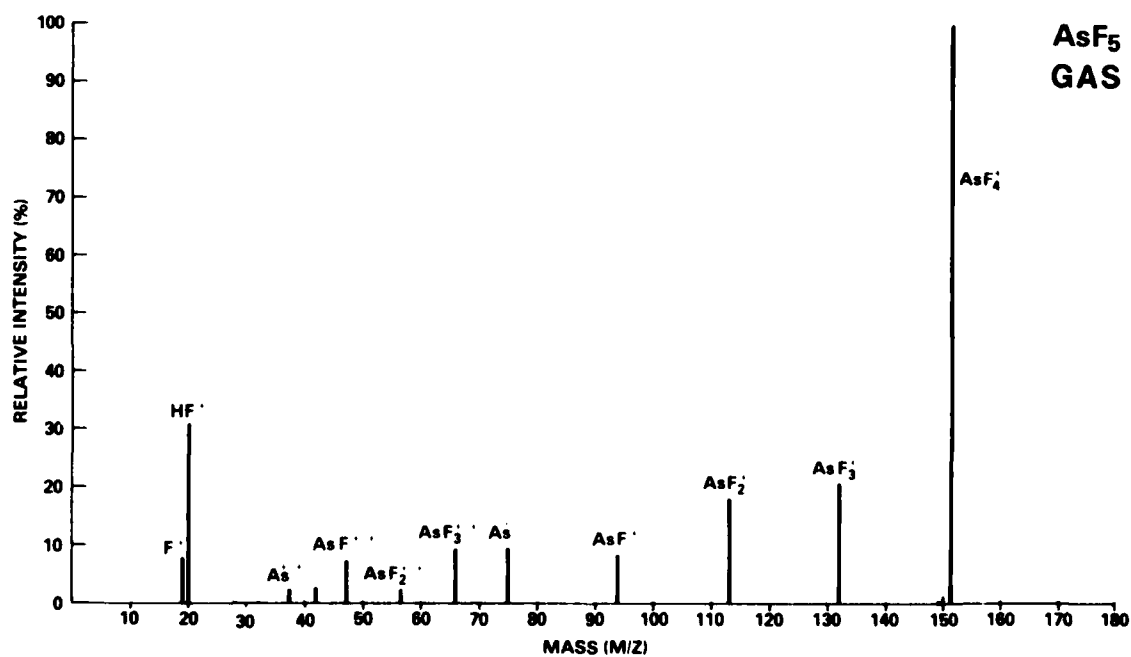
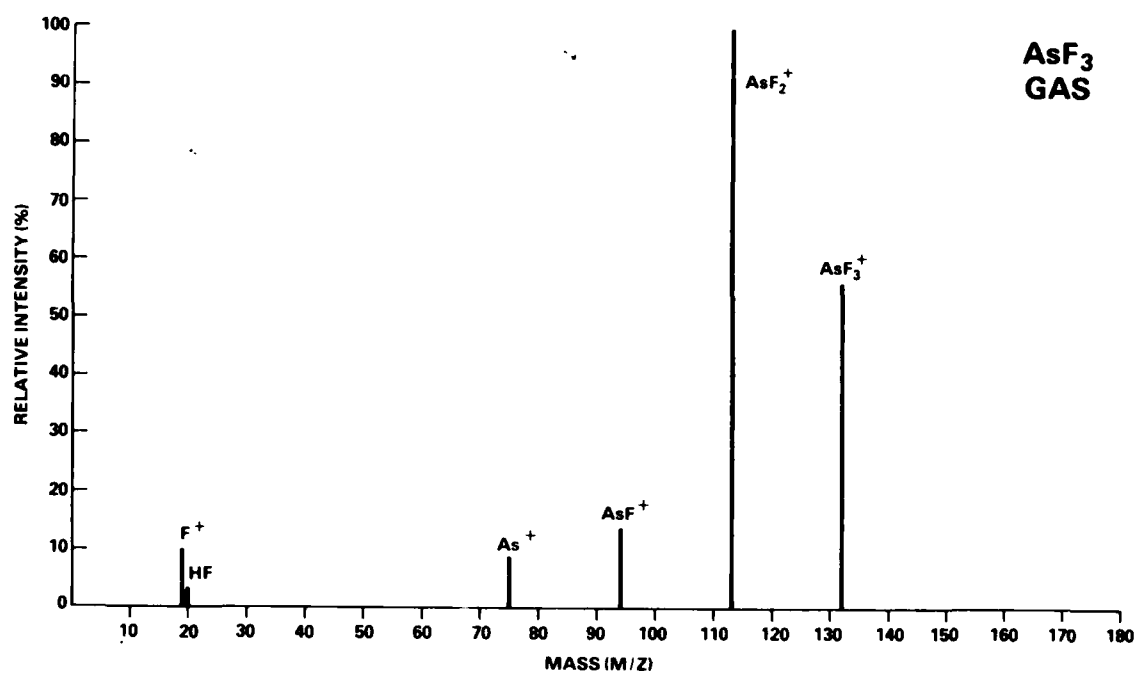


Fig. 5 - Mass spectra of AsF₅ and AsF₃ vapor

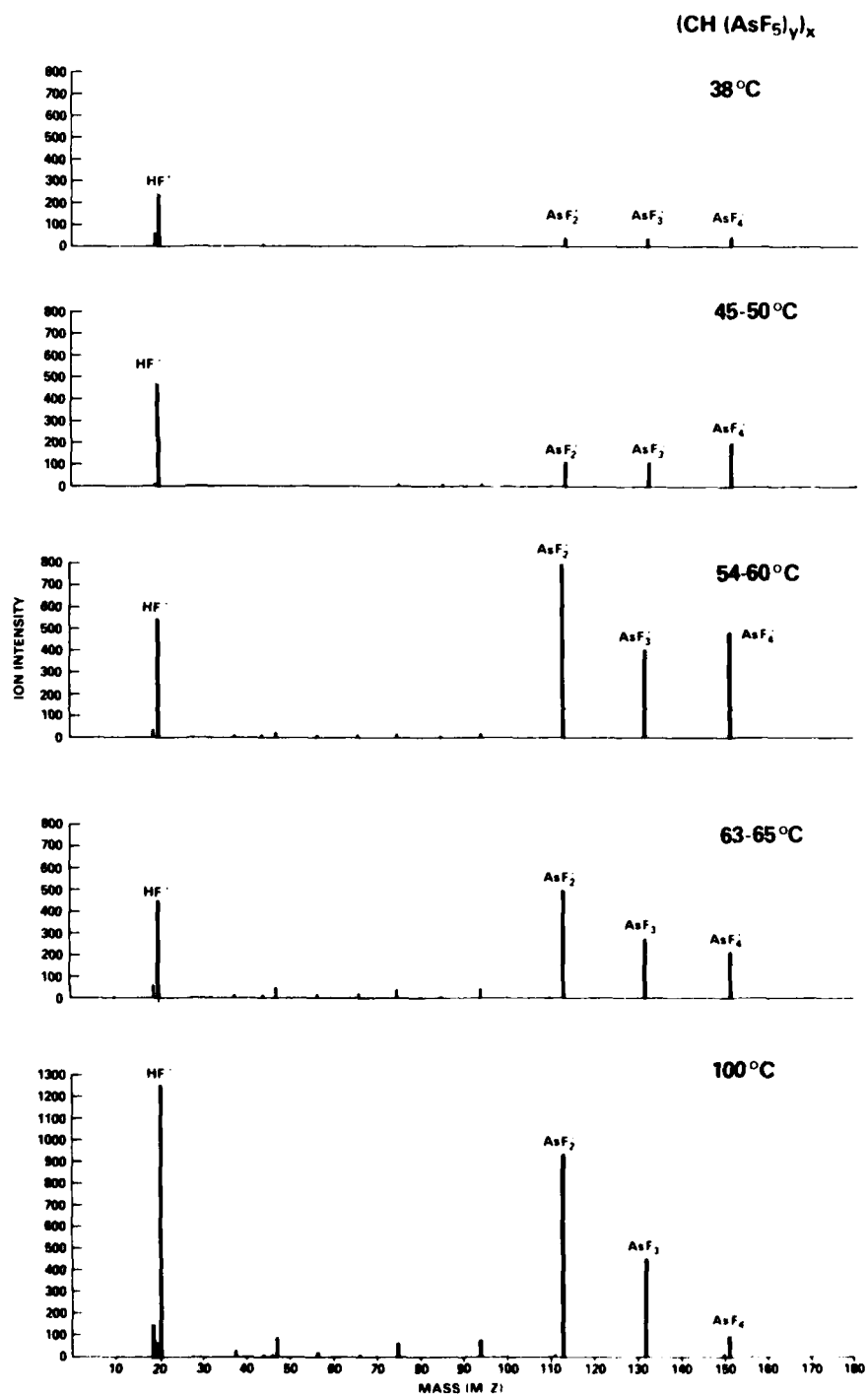


Fig. 6 - Mass spectra of vapor evolved from heated, AsF_5 doped $(CH)_x$

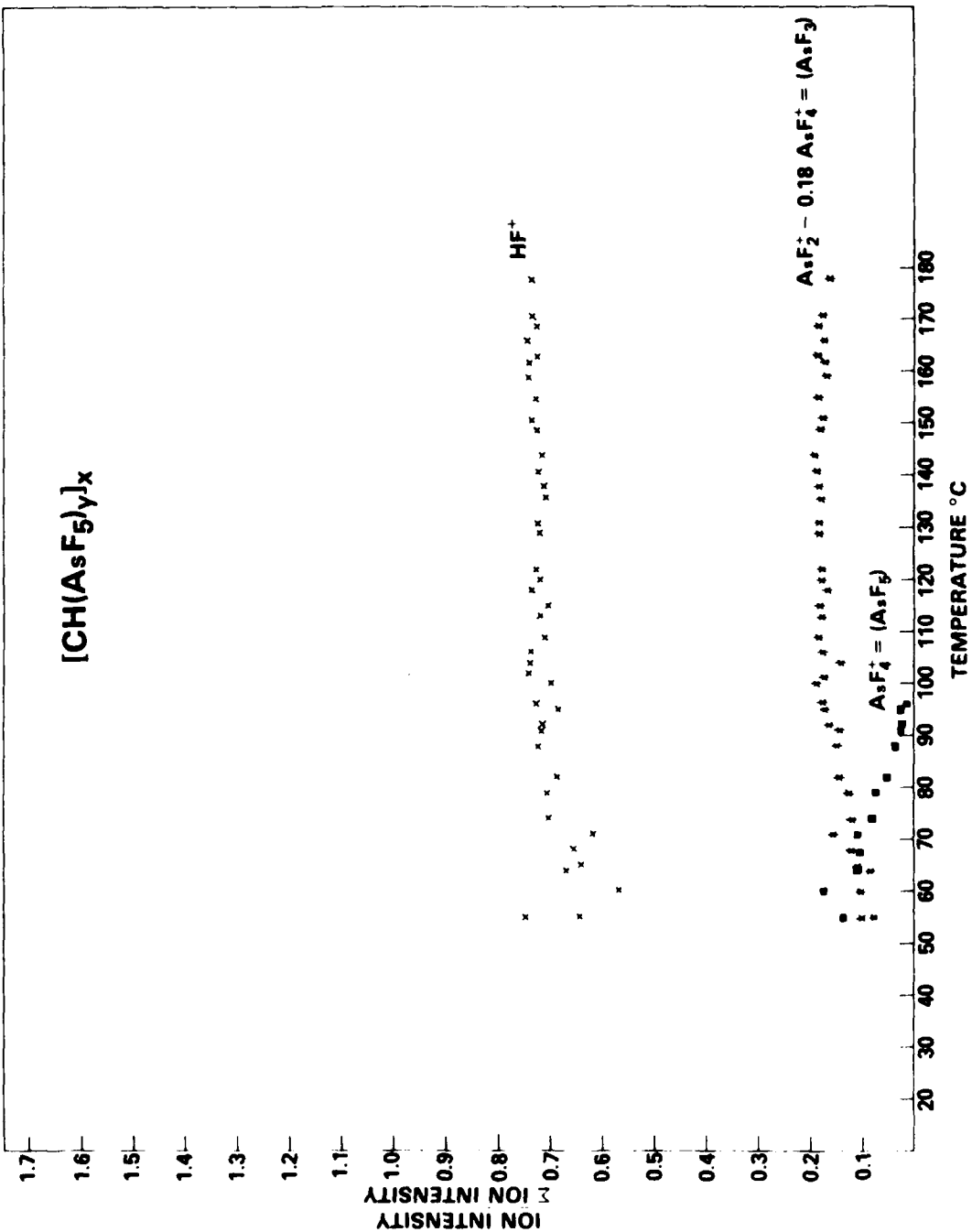


Fig. 7 - Plot of relative ion intensities vs. sample temperature for AsF_5 , AsF_3 , and HF evolved from AsF_5 doped $(CH)_x$

PRESSURE EFFECTS ON THE
RESISTIVITY OF PURE AND DOPED $(CH)_x$

D. C. WEBER, J. P. FERRARIS^{*}, P. BRANT, W. B. FOX
INORGANIC & ELECTROCHEMISTRY BRANCH

A. W. WEBB AND E. R. CARPENTER, JR.
MATERIALS SCIENCE & TECHNOLOGY DIVISION

The investigation of conduction processes in molecular crystals and macromolecules has nearly a century long history,¹ but it is only recently that organic materials displaying metal-like properties have yielded to the synthetic chemist's ingenuity. The potential application of these materials as lightweight, inexpensive and readily available alternatives to traditional conductors and semiconductors has led to a resurgence of activity in the area. Systems based on charge transfer salts of tetracyanoquinodimethane and a variety of heterocycles² have been subjected to myriad physical measurements and chemical modification but difficulties with their stability and fabrication detract from their useful applicability. The wealth of polymer processing technology, however, has inspired the development of highly conducting macromolecular systems. The inorganic polymer $(SN)_x$ couples improved processibility with metallic conductivity³ but its limited⁴ chemistry allows only minor variation in its electrical properties. Polyacetylene, $(CH)_x$, on the other hand, although hampered by only moderate stability and modest processibility, enjoys (via doping) an eleven order of magnitude variability in its electrical properties⁵ with maximum conductivities extending into the metallic regime. Silvery films of $(CH)_x$ appear as masses of intertwined fibrils under microscopic investigation⁶ and density measurements show the material is about two-thirds void. This allows rapid uptake of intercalants but ultimately limits the magnitude of the conductivity because of interfibril resistance and reduced chains/cross section. We now report our efforts to diminish these effects through the application of high pressure.

^{*} NAVY/ASEE Summer Faculty Appointee, Permanent Address, Univ. of Texas at Dallas, Richardson, Texas 75080

EXPERIMENTAL

Acetylene was polymerized under Ziegler-Natta catalysis according to published procedures.^{6,7} The polymer was handled exclusively in inert atmosphere glove boxes and chemically modified by standard high vacuum line techniques. The cis-trans isomer distribution was controlled by careful post-polymerization heat treatment and low temperature storage.

The degree of doping was determined either by weight increase, conductivity enhancement and comparison with published data^{5,8} or by elemental analysis.⁹ Volume compression measurements were made at room temperature on samples of ca. 50 mg using standard piston-displacement techniques.¹⁰ The data were corrected for stretch of the apparatus ($\sim 20\%$ correction) and radial elastic expansion of the compound WC-steel cylinder ($\sim 11\%$ at the maximum pressure). The details of these corrections and of the data collection procedure are given in Reference 11. High pressure conductivity measurements were obtained at room temperature using a tetrahedral anvil press¹² which had been previously calibrated against several fixed point resistive transition.¹³ Sample resistance was measured with a Dana model 5000 Digital Multimeter using a four-lead technique through the anvils. This removes lead and contact resistances except for the spacer-sample contacts. Contacts to the sample were ohmic. In the sample arrangement shown in Figure 1, spacers were of either graphite or copper (see Results Section). In general, data points were taken at ca. 0.5 kbar intervals. Since the resistance settled slowly subsequent to pressure increments, readings were usually taken two minutes after a pressure increase so that a run could be completed in a reasonable time. Longer waiting periods result in discontinuities as noted in runs A, F, and E. Samples were maintained at pressure overnight in most cases, then decompressed the following day. Samples were subsequently examined by ESCA.

RESULTS

The average compressibility on duplicate runs of cis-rich undoped polyacetylene is shown in Figure 2. The data are reported as normalized changes in the sample height. There is an irregularity around 20 kbar possibly due to a transformation to a somewhat less compressible structure. Sharp popping noises were noted around this pressure each time the material was compressed, which may indicate sticking. At lower pressures the material behaved in a smooth plastic manner. The highest density achieved subsequent to these experiments was 1.135 gm cm^{-3} , approximately 95% of the calculated density for void-free polyacetylene. The pressure dependencies of the resistivity for undoped A, two lightly iodinated $(\text{CHI}_{0.0094})_x$, B and C and two heavily iodinated $(\text{CHI}_{0.219})_x$, F, and $(\text{CHI}_{0.03})_x$, G polyacetylene specimens are shown in Figure 3. Initial resistivity values are consistent with doping levels. All samples except for A and B were precompacted (6.1 kbar, 1 minute) prior to resistivity measurements.

Sample A displays a featureless pressure dependence of its resistivity. The conductivity in the doped sample is limited by inter-chain hopping, while the pure $(CH)_x$ has its conductivity limited by intrachain processes which would be unaffected by pressure. Upon standing overnight at ca. 60 kbar, a 30% increase in conductivity resulted but this enhancement was lost upon return to atmospheric pressure. This increase must be due to a physical change; for example, a possible alignment of the chains for better overlap. The reversibility could then be due to an "elastic" disordering on release of the pressure.

Sample B shows a 22-fold decrease in resistivity upon pressurization to 20 kbar but over half the effect occurs in the first 6.7 kbar. That precompaction should obviously aid the conduction process as manifested by sample C whose initial resistivity is some 6.3 times lower than its nonprecompacted counterpart. The resistivity minima occur at ca. 23 kbar for both specimens of lightly doped polymer. Excessive drift in resistance was observed between 47-50 kbar for B and the discontinuities in the curve reflect 15 minute intervals between points. Data for C were obtained at constant dp/dt . The inflection point around 48 kbar demonstrates the effect is reproducible but its exact cause has yet to be determined.

Heavily doped samples show the expected increase in conductivity at ambient conditions. The pressure dependence of both samples is similar with resistivity minima shifted to 16 kbar. When maintained at 60 kbar overnight, the resistivity of all doped samples deteriorated to the 10^5 to 10^6 ohm-cm range.

Two experiments on highly iodinated polymer were conducted using copper spacers in lieu of graphite (D, E). The results are shown with the graphite spacer runs in Figure 4. While the resistivity maxima in D are dramatic, they are non-reproducible (see G) and we suspect they are due to the reaction of I_2 with copper at high pressure to form CuI . ESCA examination of the Cu electrodes for E showed a considerable I 3d peak. Some iodine was also detected in the ESCA spectrum of the graphite electrodes for sample G in addition to a strong C 1s peak. Upon removal from its tetrahedron, one sample displayed a propensity to lose iodine and promptly discolored its storage vial. The differences in initial resistivity for specimens from the same batch with copper or graphite spacers was negligible so the use of copper was abandoned.

DISCUSSION

The initial decrease in resistivity for the acceptor doped samples is consistent with our expectations of reduced interfibril resistance and/or increased density of conducting filaments per cross section. The leveling off and subsequent increase in resistivity is probably due in part to several factors.

The loss of iodine from one depressurized sample was observed. We have noted such a loss of I_2 from iodinated $(CH)_x$ films as a result of thermal treatment (mass spectroscopy) and solvent^x extraction studies. In all cases loss of I_2 results in decreased film conductivities. Loss of I_2 can be accomplished without reduction of the polymer. Since there would be no change in the number of charge carriers it is believed that the reduced film conductivity arises from the reduced size and polarizability⁶ of the dopant species. However, the final resistivity values of ca. 10^6 ohm-cm with significant amounts of iodine still present argues against this as the sole cause. A distinct possibility exists for pressure induced iodination of the conjugated chain similar to that observed for iodine charge transfer complexes of polycyclic aromatics.¹⁴ We are pursuing mass spectral and ESCA studies to search for species containing the CI bond. IR experiments have been inconclusive. A plot of the resistance change with time at 65 kbar for sample G (Figure 5) indicates that chemical reaction alone cannot account for the entire observed resistance change. One might expect second or pseudo first order rate behavior (assuming only mild heterogeneity) but the effect appears to be linear. Furthermore, the natural retardation of rate as the iodine species is consumed will not allow for the magnitude of the overnight resistivity change. We suggest that the application of high pressure results in significant amounts of chain scission and/or cross-linking yielding an insulating system even in the presence of dopant.

Run H was held at 20 kbar for four days to ascertain if an extended soak at this pressure would afford transformation. The resistance increased by a factor of seven, an amount seen around 50 kbar in the comparable runs B and C. The pressure was then increased to 39 kbar, resulting in a 40% drop in resistivity, and then held at this pressure another two days resulting in a resistivity increase of 1.5 times. The magnitude of these changes suggests that the major irreversible effect on the lightly iodinated samples occurs upon pressurization in excess of ca. 50 kbar. At 65 kbar an overnight soak of runs B and C results in a resistance increase of some two orders of magnitude.

We recognize two possible problems with our experimental setup as it now stands. The first is the random geometry of the compacted foils. While this would be a severe problem for highly anisotropic materials such as TTF-TCNQ and $(SN)_x$, polyacetylene consists of randomly oriented fibrils in its pristine state. We suspect that any loss of information due to averaging anisotropic conductivities will be minimal. A possibly more serious criticism might be the use of a two probe method. Undoubtedly some contact resistance is folded into our results but its magnitude is probably less than interfibril resistances.

SUMMARY

This study has demonstrated that the conductivity of the I_2 doped $(CH)_x$ can be increased by the application of pressure to the samples. This^x is reasonable since it has been felt that conduction in the doped samples is limited by interchain hopping which can be more easily

facilitated by moving the chains closer together. The decrease in conductivity at the higher pressures is understandable in light of previous work with similar unsaturated hydrocarbon - I_2 charge-transfer systems which undergo chemical reaction at the higher pressures giving rise to saturation of the hydrocarbons. Such a reaction in the $(CH)_x$ case would lead to an insulating type structure and therefore lower the conductivity.

FUTURE STUDIES

We anticipate four probe resistivity measurements in a diamond anvil cell under hydrostatic or quasi-hydrostatic (at higher pressures) environments on oriented films of $(CH)_x$ as a function of temperature and pressure.

Preliminary experiments on heavily AsF_5 -doped polyacetylene display a four-fold decrease in resistivity from ambient to pressures of 5 kbar. There follows an essentially flat region to 30 kbar and then completely erratic behavior. Upon decompression, the sample appears black and brittle. X-ray studies and additional resistivity measurements are in progress.

REFERENCES

1. STOLETOV N. (1888) cited by VARTANIAN A. T., Izv. Akad. Nauk SSSR Ser. Fiz. **16**, 169 (1952) and SHCHIRO N. K. (1919) cited by VARTANIAN A. T., Zh. Fiz. Khim. **28**, 856 (1954).
2. "Molecular Metals," NATO Conference Series, VI: Materials Science, HATFIELD W. E., ed., Plenum Press, New York (1979).
3. YOFFE A. D., Chem. Soc. Rev. **5**, 51 (1976).
4. STREET G. B., GILL W. D., GEISS R. H., GREENE R. L. and MAYERLE J. J., J. C. S. Chem. Comm. 407 (1977).
5. SHIRAKAWA H., LOUIS E. J., MACDIARMID A. G., CHIANG C. K. and HEEGER A. J., J. C. S. Chem. Comm. 578 (1977).
6. ITO T., SHIRAKAWA H. and IKEDA S., J. Polymer Sci., Part A-1, Polymer Chem. **12**, 11 (1974).
7. a) SHIRAKAWA H. and IKEDA S., Polymer J. **2**, 231 (1971).
 b) SHIRAKAWA H., ITO T. and IKEDA S., Polymer J. **4**, 460 (1973).
 c) ITO T., SHIRAKAWA H. and IKEDA S., J. Polymer Sci., Part A-1, Polymer Chem. **13**, 1943 (1975).
8. CHIANG C. K., DRUY M. A., GAU S. C., HEEGER A. J., LOUIS E. J., MACDIARMID A. G., PARK Y. W. and SHIRAKAWA H., J. Amer. Chem. Soc. **100**, 1013 (1978).
9. Elemental analyses performed by Galbraith Laboratories, Inc., Knoxville, Tenn., U.S.A.
10. BRIDGMAN P. W., Proc. Am Acad. Arts Sci. **74**, 21 (1940).
11. WEBB A. W., TOWLE L. C. and CARPENTER, JR. E. R., High Temp.-High Press (in press).
12. HALL H. T., Rev. Sci. Instrum. **29**, 267 (1968). *Ibid.*, **33**, 1278 (1962).
13. WEBB A. W., J. Phys. Chem. Solids **34**, 501 (1973).
14. BENTLEY W. H. and DRICKAMER H. G., J. Chem. Phys. **42**, 1573 (1965).

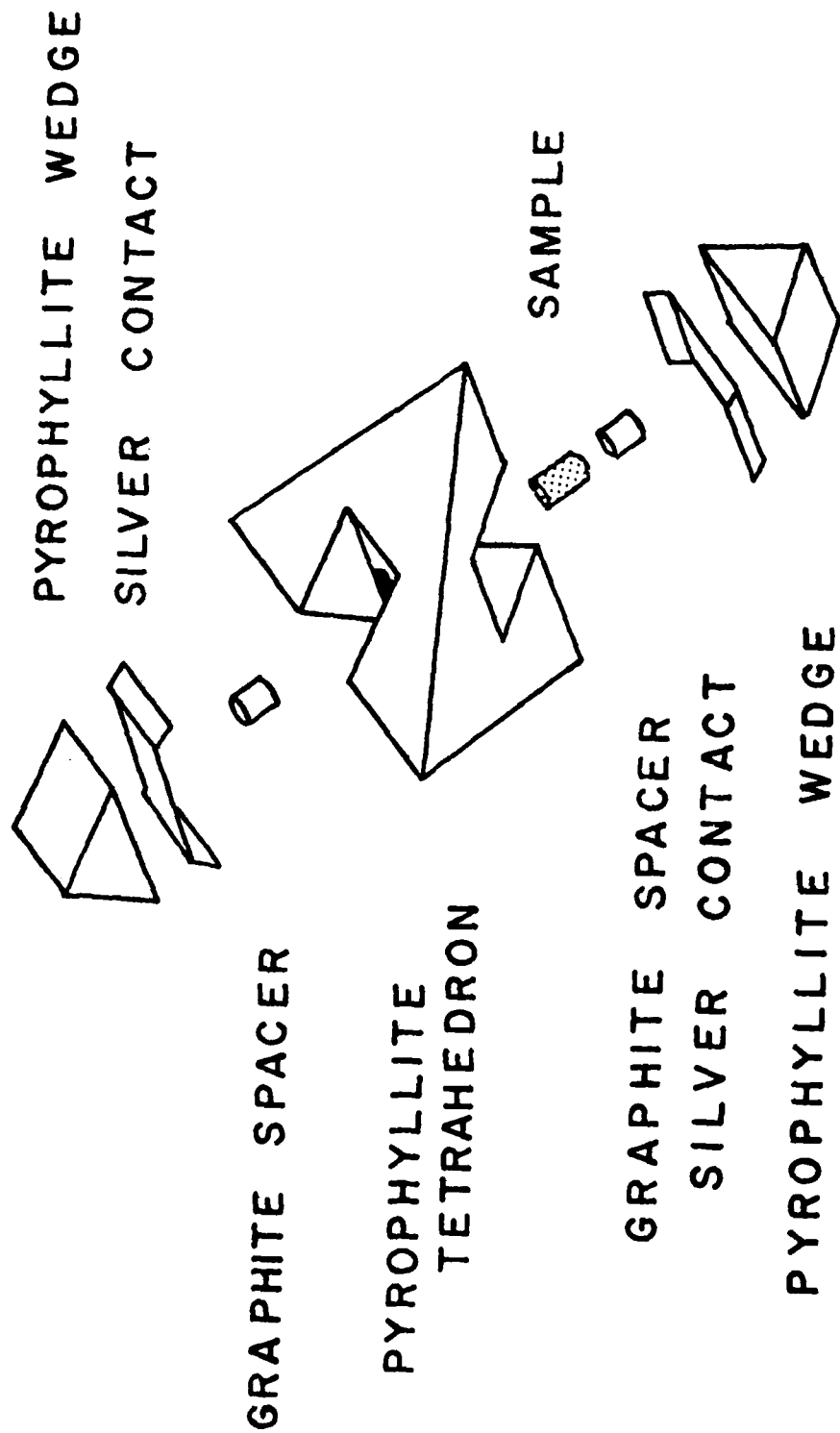


Fig. 1 - Schematic of pyrophyllite sample chamber tetrahedron

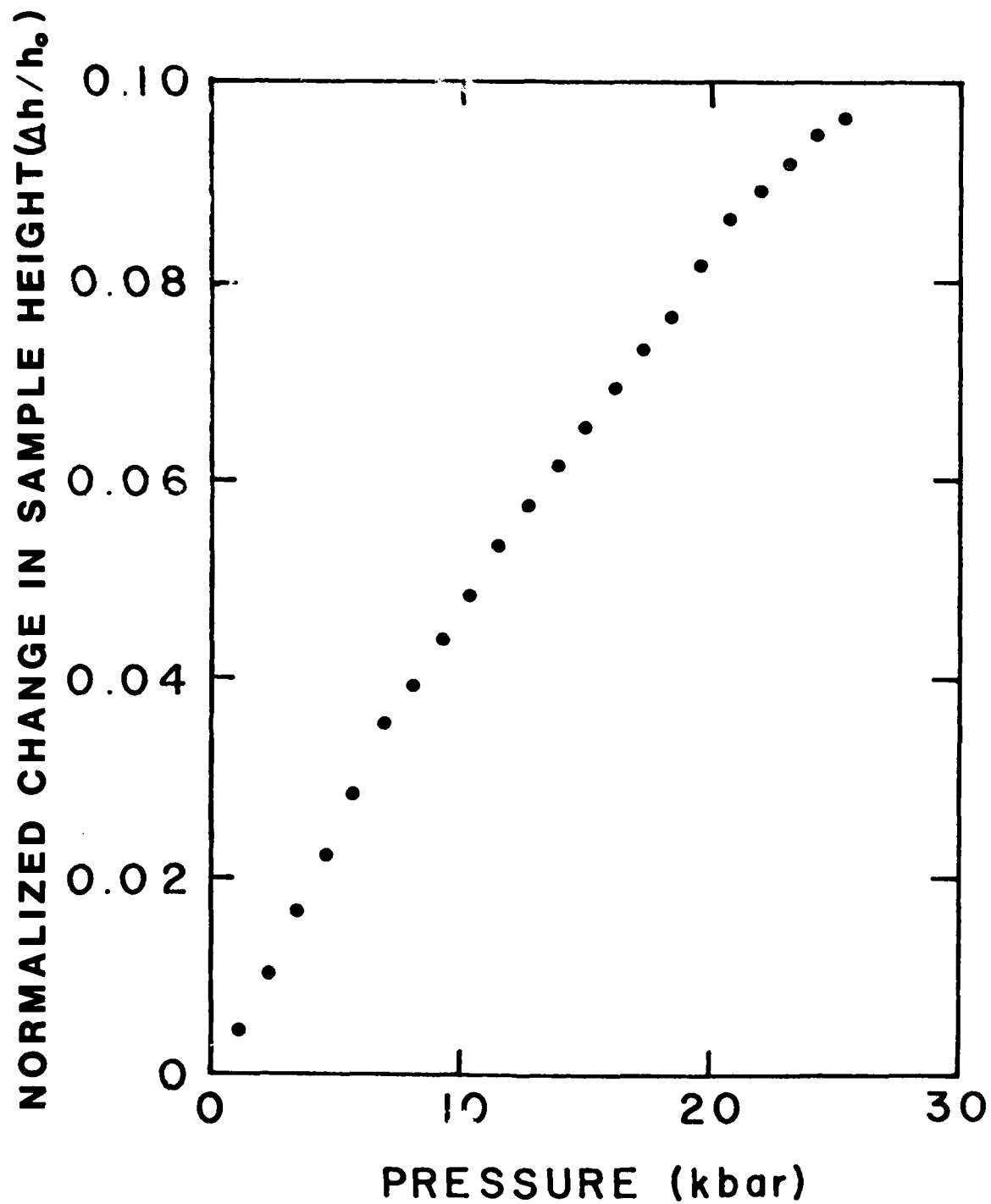


Fig. 2 - Compressibility of cis-rich undoped polyacetylene

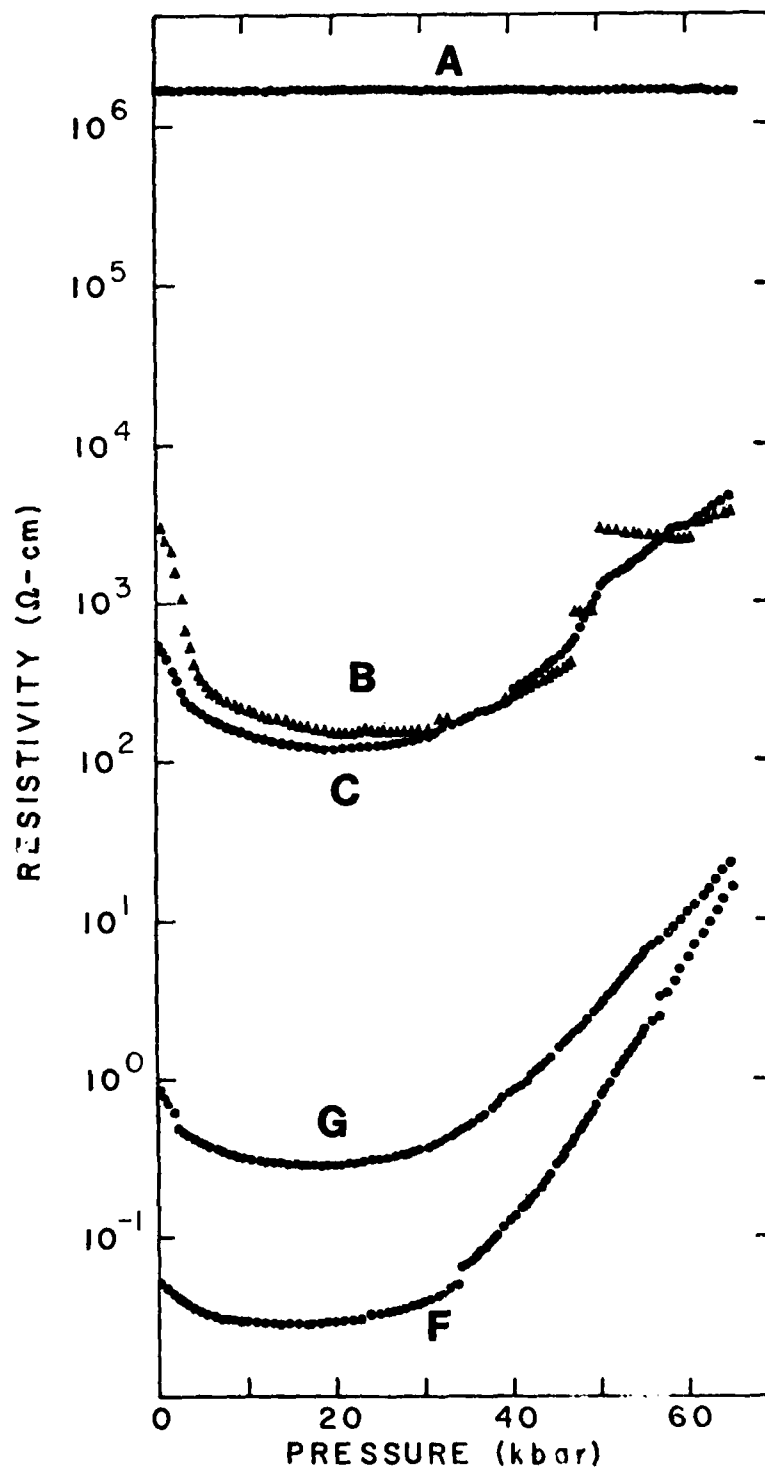


Fig. 3 - Resistivity vs. pressure for undoped $(\text{CH})_x$, A; $(\text{CHI}_{0.0094})_x$, B and C; $(\text{CHI}_{0.219})_x$, F; and $(\text{CHI}_{0.03})_x$, G.

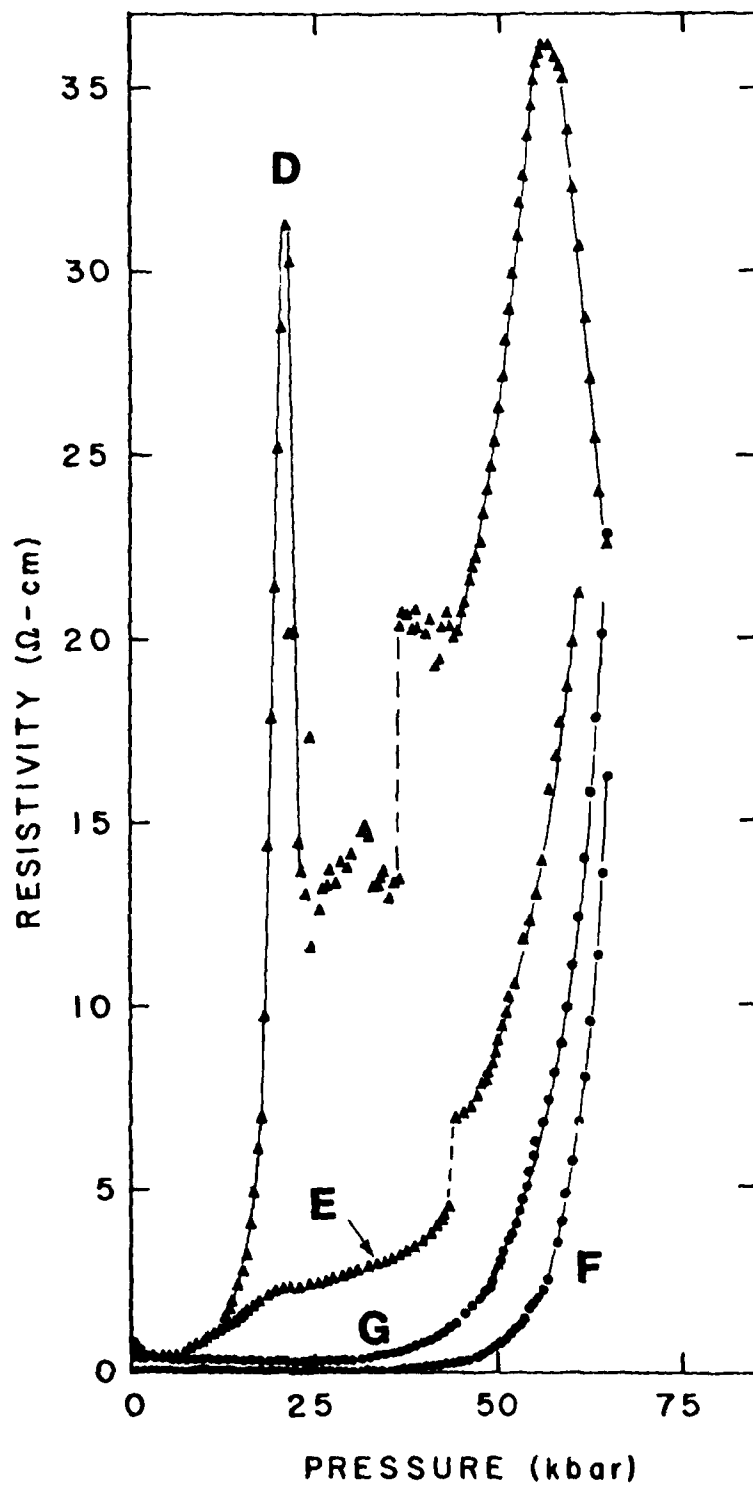


Fig. 4 - Resistivity vs. pressure for heavily iodinated $(\text{CH})_x$ with graphite (F and G) and copper (D and E)

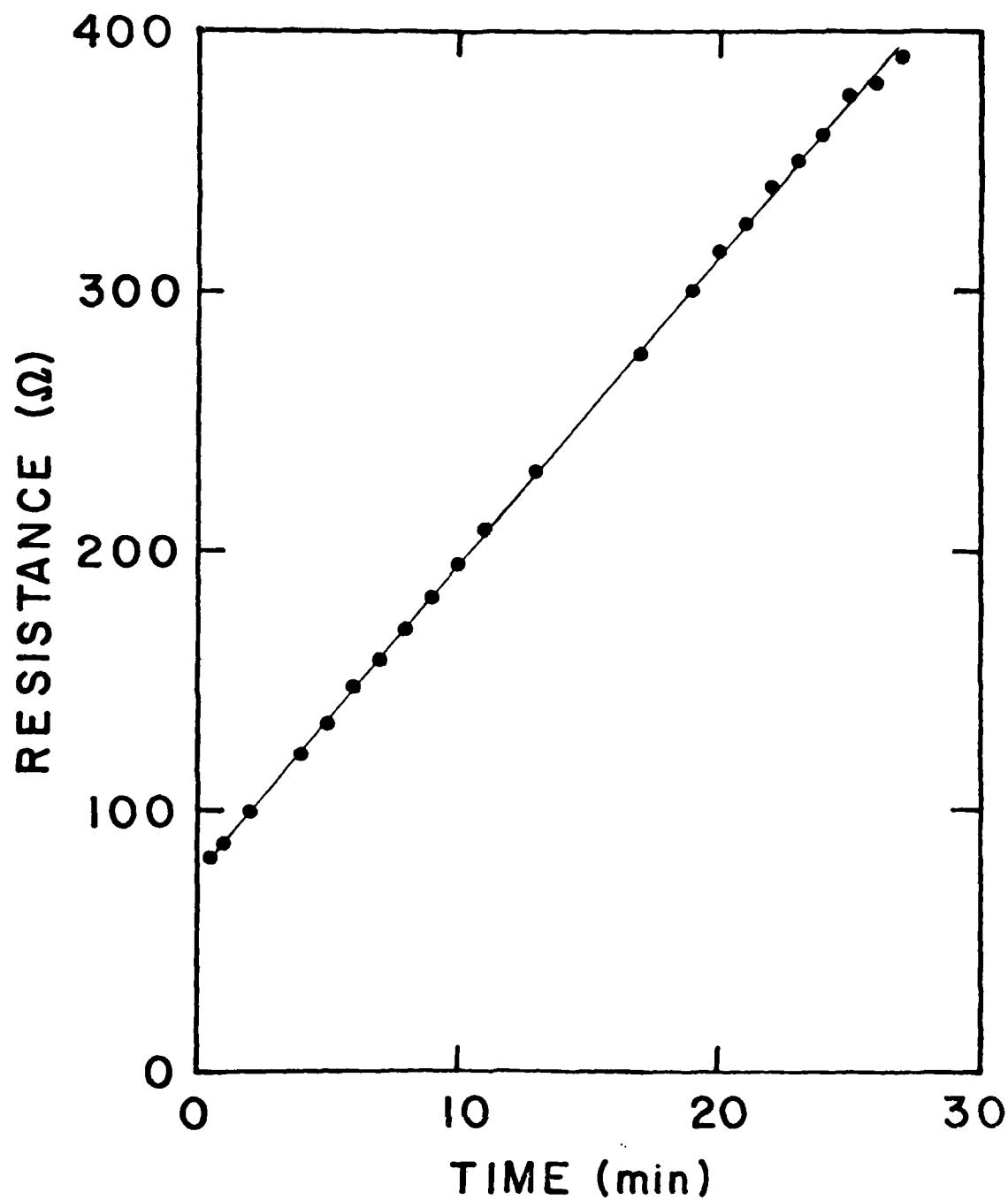


Fig. 5 - Resistance vs. time for sample G held at 65 kbar

PROGRESS NOTES ON STUDIES OF $(\text{SN})_x$, $(\text{CH})_x$, AND
RELATED MATERIALS

Patrick Brant, David C. Weber, Curtis T. Ewing, and
Joseph A. Hashmall
Inorganic and Electrochemistry Branch
Chemistry Division

INTRODUCTION

Since the last semiannual progress report, advances have been made in the interpretation of the x-ray photoelectron data for S_2N_2 , S_4N_4 , and $(\text{SN})_x$ and relationships between the bonding and charge distribution have been found. Experiments have been completed which elucidate the nature of the iodine-polyacetylene interactions in the doped polymer. Syntheses designed for molecular modifications of the polyacetylene backbone which will render more stable polymers with greater flexibility of polymer properties have been initiated. These new studies are summarized in the following pages.

X-ray Photoelectron Spectroscopic Study of $(\text{SN})_x$, Its Precursors, and Brominated $(\text{SN})_x$

In the previous report (1), XPS data for solid S_2N_2 , S_4N_4 , $(\text{SN})_x$, and $(\text{SNBr}_{0.4})_x$, as well as for S_2N_2 gas were reported and some interpretations of the data presented. All of the work has since been accepted for publication (2). With the completion of the data analysis, we now summarize our findings. We have compared the gas phase XPS data for S_2N_2 with the data previously published for S_4N_4 (3). The data, interpreted using the point charge potential approximation in conjunction with semi-empirical molecular orbital MNDO (4) and CHELEQ (5) (electronegativity equalization) calculations, show that the S-N charge transfer is greater in S_4N_4 than in S_2N_2 . The CHELEQ calculations further indicate that S-S bonding is present in S_4N_4 (but not in S_2N_2) and that the S-S bond order is ~ 0.2 . The results can be very satisfactorily understood without the inclusion of $\text{Np}\pi \rightarrow \text{Sd}\pi$ back bonding. A plot of observed versus calculated (by CHELEQ method) sulfur $2p_{3/2}$ gas phase binding energy shifts for S_2N_2 , S_4N_4 , and a variety of other sulfur compounds is shown in Fig. 1. Solid state binding energy data similarly show that S-N charge transfer is greater in S_4N_4 than in S_2N_2 and that the charge distribution in $(\text{SN})_x$ is the same, within experimental error, as that in S_2N_2 . Relative x signal attenuation of the nitrogen and sulfur core levels in brominated $(\text{SN})_x$ is consistent with

a bonding model in which the Br_3^- effectively sheaths the individual $(\text{SN})_x$ fibrils (6).

Solvent Extraction Studies of Iodinated Polyacetylene Films

An important question to consider in any reaction is whether or not it is reversible and, if so, under what conditions and to what extent. The reversibility of the iodination of polyacetylene films has been examined by solvent extraction techniques. Films exposed to iodine vapor with resultant compositions $(\text{CHI})_x$ $0.009 \leq x \leq 0.16$ were used in the study. In a qualitative examination to determine the effect of solvents on the doped films, it was initially discovered that iodine is readily removed from the film by all of the solvents tested: dichloromethane, nitromethane, dimethylsulfoxide, dimethylformamide, acetonitrile, tetrahydrofuran, and benzene. We chose tetrahydrofuran (dried and distilled) and benzene to conduct a more detailed and quantitative study of the effects of solvent extraction on the film properties and composition. Films placed in a Soxhlet extractor underwent repeated extractions under argon for periods of 12-26 hr. Data regarding composition and properties of extracted and unextracted films were obtained from weight and conductivity (four point probe) changes, elemental analyses (7), and mass and x-ray photoelectron spectroscopies. The iodine content of the extraction solutions was determined by coulometric titration (8) ($2 \text{S}_2\text{O}_3^{2-} + \text{I}_2 \rightarrow \text{S}_4\text{O}_6^{2-} + 2 \text{I}^-$) and uv-vis analysis (9). Film compositions before and after extraction could be crosschecked by the various analytical techniques employed. Some of the results for film extractions are summarized in Table I.

It is clear from the summarized analytical data that:

(1) The iodination reaction is "quasi-reversible" to the extent that 40-80% of the iodine incorporated in the film could be removed as molecular iodine. The iodine removed is identified as I_2 from its characteristic visible spectrum and from mass spectroscopy. Coulometric data are also consistent with this formulation.

(2) Decreased film conductivities track with the decreased iodine concentrations in the film in a manner which is also reversible.

The nature of the iodine dopant in extracted and unextracted films has been examined by XPS and mass spectroscopy. The $\text{I } 3d_{5/2}$ spectra of extracted and unextracted films are shown in Fig. 2, while the I_2^+ ion yield curves for such films are shown in Fig. 3. It is clear from the XPS and ion yield spectra that there are at least two different iodine environments in the unextracted film. In the XPS study, the skewed $\text{I } 3d_{5/2}$ peak could be deconvoluted into two symmetric $\text{I } 3d_{5/2}$ peaks with an intensity ratio of 2.0:1.0 separated by 1.5 eV. In contrast, the extracted film exhibits only a single, symmetric $\text{I } 3d_{5/2}$ peak. The results obtained from the solvent extraction study have important implications regarding the nature of the iodine-polyacetylene inter-

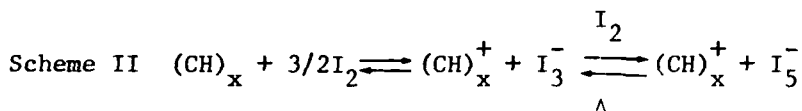
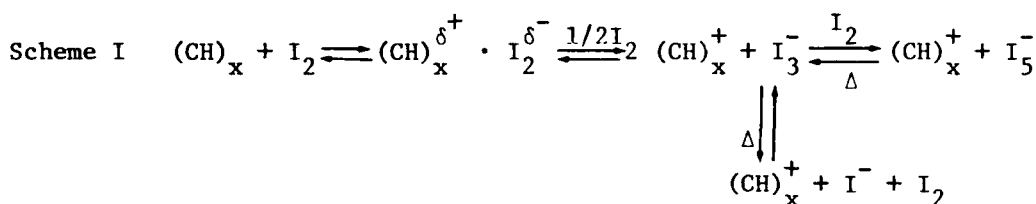
Table I

Effects of Solvent Extraction on Iodinated Polyacetylene

		$(\text{CHI}_{\frac{x}{y}})_y$	
<u>Analytical Method</u>		<u>Mole Ratio, I/(CH) = x/y</u>	
Before Extraction	{ Wt. gain	.115	.035
	{ Elem. anal.	.136	.066
After Extraction		THF extraction	BENZENE extractions
	Wt. loss	.065	.034
	UV-VIS		.043
	Coulometry		.041
	XPS		.030
	Elem. anal.	.074	.006
	Conductivity difference after extraction	$\downarrow \times 21$	$\downarrow \times 46$ $\downarrow \times 75$

action. In previous studies (10), the incorporated iodine was determined to be present in the film in two forms; the more robust species was identified by Raman spectroscopy as I_3^- while the less robust species, which can be depleted by mild thermal treatment, was attributed to I_5^- or a "strongly perturbed" iodine molecule.

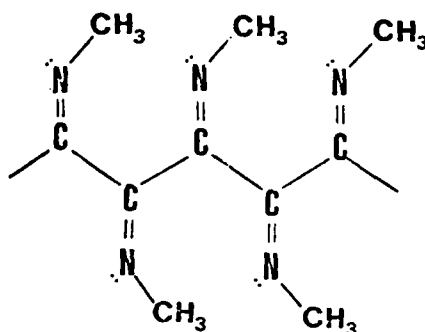
Two possible schemes for the incorporation of I_2 in polyacetylene and its subsequent removal by solvent extraction or thermal treatment are shown below:



An important question yet to be answered definitively from studies thus far completed is whether the removal of iodine as I_2 from the conducting polymer results in electron transfer back to the polymer. The decreased conductivities of the solvent extracted $(CHI_y)_x$ films may arise from the decreased size of remaining iodide species (I^- and I_3^-) relative to those in the unextracted films (I_3^- and I_5^-) since the larger anions may provide more efficient bridges for electron hopping from fibril to fibril.

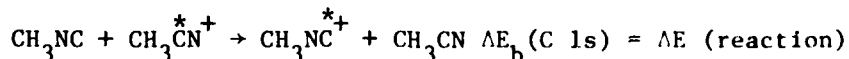
Molecular Modifications of Polyacetylene

Native polyacetylene films are inherent semiconductors but can be made highly conducting on treatment with a variety of dopants (e.g., I_2 , $NOPF_6$, and AsF_5) (11). There have been successful attempts to copolymerize acetylene with other substituted acetylenes such as 1-hexyne (12) and 1,1,1 trifluoropropyne (13), but the products proved to hold no particular advantage in stability and reactivity over pure $(CH)_x$. Nonetheless, it remains a reasonable assumption that copolymerization of acetylene with the proper compound can yield films with enhanced air stability and the capability to modify the polymer backbone in a desirable fashion as well as provide specific reactive dopant sites along the polymer chain. The compound we have chosen to attempt copolymerization with acetylene is methylisocyanide, CH_3NC . Methylisocyanide was prepared and purified according to the published procedure (14). It can undergo self-polymerization in the presence of a nickel catalyst to form spiroidal chains bound only through the (originally) divalent carbons (15-18).

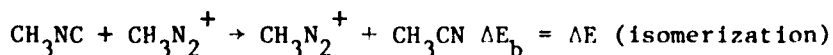


The $(\text{CH}_3\text{NC})_x$ polymer was prepared by catalysis with NiCl_2 in methanol following the literature procedure. The CH_3NC monomer was examined in the gas phase and the polymer in the solid state by x-ray photoelectron spectroscopy. These data are summarized in Table II and the N 1s spectrum of CH_3NC gas is shown in Fig. 4.

In the gas phase data, two different carbon 1s peaks of equal intensity can be deconvoluted from the C 1s spectrum. Ordinarily, the two peaks could not be unambiguously assigned to either the isocyanomethyl carbon. However, Jolly has pointed out that the shift in binding energy of a given core level can be equated to the energy of a chemical reaction (19). In this case, the difference in the C 1s core level binding energies between the cyano carbon in acetonitrile and the isocyanomethyl carbon in methylisocyanide is equivalent to the energy of the reaction



where the asterisks indicate 1s holes. Using the equivalent cores approximation to convert the above equation into one containing only ground state species, the C^* atoms are replaced by N atoms:



Thus, the difference in carbon 1s E_b 's is simply equal to the heat of isomerization of CH_3NC to CH_3CN . The heat of isomerization (20) is found to be -14.7 kcal/mol or -0.7 eV. The C 1s and N 1s binding energies for acetonitrile (21) are 293.2 and 405.9 eV, respectively (the methyl and cyano carbons are indistinguishable).

Based on the equivalent cores model then, the peak at 292.7 eV is assigned to the isocyanomethyl carbon, while the peak at 293.4 eV is attributed

Table II
X-ray Photoelectron Spectroscopic Data for CH_3NC Gas and Solid $(\text{CH}_3\text{NC})_x$

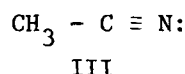
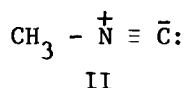
	<u>Binding Energies, eV</u>		
	<u>C 1s</u>	<u>N 1s</u>	<u>$\Delta\text{B.E. (N 1s-C 1s) (eV)}$</u>
CH_3NC^a	293.4 (1.4) ^b , 292.7 (1.4)	406.83 (1.15)	113.4, 114.1
$(\text{CH}_3\text{NC})_x^c$	~285.9 (2.0)	~399.0 (1.7)	113.1

^a All gas phase binding energies are referenced to the $2p_{3/2}$ core level B.E. of 248.62 eV for argon gas.

^b Values in parentheses are peak full widths at half maximum (fwhm), in eV.

^c C:N:O stoichiometry of 2.3:1.0:0.2 obtained from corrected relative areas of C 1s, N 1s, and O 1s peaks. The oxygen is present due to adsorption of C, O containing materials onto the surface of the sample from the residual atmosphere in the sample chamber of the X-ray photoelectron spectrometer.

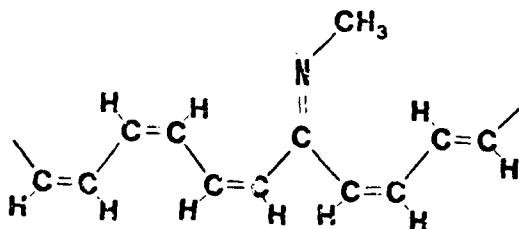
to the methyl carbon by the process of elimination. These results and the nitrogen 1s E_b 's are consistent with the simple valence bond pictures (structures II and III below) for the methylisocyanide and acetonitrile molecules, which suggest that there is greater N→C charge polarization in CH_3NC than in CH_3CN .



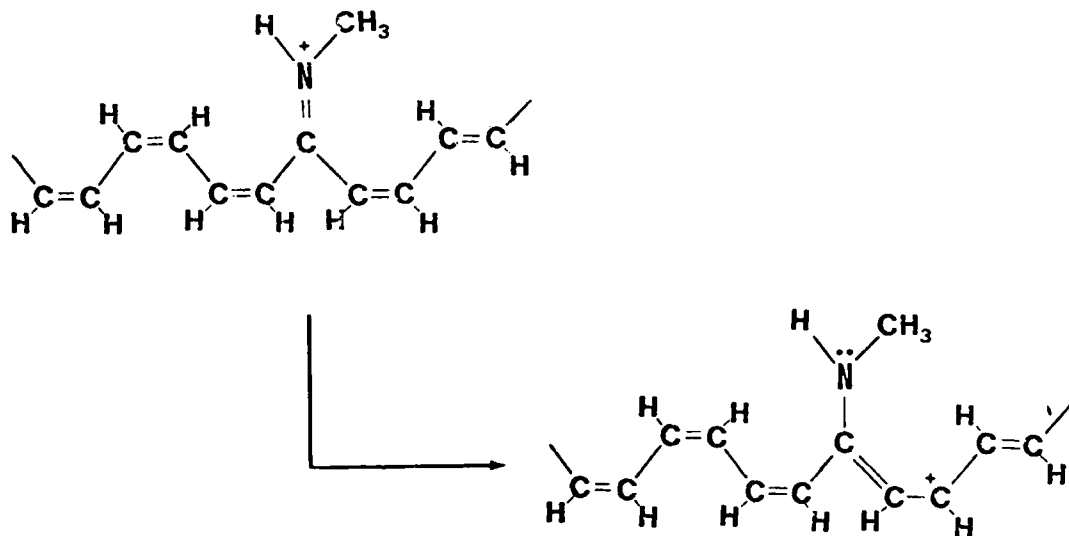
However, the equivalent cores model and correlation of core level E_b 's with ground state VB structures require the assumption that core hole relaxation effects in methylisocyanide and acetonitrile are equal, whereas calculations have been published for the model compounds HNC and HCN in which differential relaxation effects are reported to be large (22). The role of relaxation effects and the contribution of the potential from the other atoms in each of the molecules in the interpretation of the E_b data for these two isomers will be carefully investigated by CHELEQ and MNDO methods in the near future.

The $\overset{+}{\text{N}} \equiv \bar{\text{C}}$ formal charge polarization CH_3NC is lost on polymerization, and a lone pair of electrons is localized on the nitrogen in each monomeric unit (VB structure I). One would expect then that the [N 1s - (isocyano) C 1s] binding energy difference should decrease on polymerization in keeping with the less positive charge on nitrogen (and more positive charge on the isocyano carbon). In fact, such a result is found; the [N 1s-(isocyano) C 1s] (see C 1s peak assignments above) binding energy difference decreases ca. 1 eV on polymerization.

At present we have completed one copolymerization synthesis of acetylene with methylisocyanide in the presence of the Ziegler-Natta catalyst following the standard polyacetylene preparation procedure (24). The reaction rate was much slower and the silvery film which formed had a slightly reddish-brown sheen. After purification, XPS data were obtained for the material which, based on the N 1s and C 1s signals, indicated the film contained approximately 5% CH_3NC :95% HCCH. The N 1s binding energy of ~398.3 eV is reasonable. If the methylisocyanide is randomly incorporated in the polyacetylene backbone, we expect (25) the structure to be:



An important feature of the proposed structure is the nitrogen lone pair introduced by the insertion of the CH_3NC moiety in the backbone. This nitrogen lone pair provides a reactive site for the covalent attachment of Lewis acids and consequent modification of the electrical properties of the polymer. As shown below, such Lewis acid-base reactions provide a method for introduction of a positive hole charge carrier in the polymer backbone, as shown below.



REFERENCES

1. P. Brant, D. C. Weber, and C. T. Ewing in, "The NRL Program on Electroactive Polymers First Annual Report," NRL Memorandum Report 3960, Report period 10-77 to 10-78.
2. P. Brant, D. C. Weber, C. T. Ewing, F. L. Carter, and J. A. Hashmall, *J. Synthetic Metals* 1, 161 (1980).
3. W. R. Salaneck, J. W.-p Lin, A. Paton, C. B. Duke, and G. P. Ceasar, *Phys. Rev. B* 13, 4517 (1976).
4. M. J. S. Dewar and N. Thiel, *J. Amer. Chem. Soc.* 99, 4899 (1977).
5. (a) W. L. Jolly and W. B. Perry, *J. Amer. Chem. Soc.* 95, 5442 (1973).
(b) W. L. Jolly and W. B. Perry, *Inorg. Chem.* 13, 2686 (1974).
6. G. B. Street and W. D. Gill, in *Molecular Metals*, W. E. Hatfield, ed. NATO Conference Series, Materials Science, Vol. 1, Plenum Press, N. Y., 1979, p. 301.
7. Elemental analyses were obtained by Galbraith Laboratories, Inc., Knoxville, Tennessee.

8. D. T. Sawyer and J. T. Roberts, Jr., "Experimental Electrochemistry," Wiley and Sons, N. Y., 1974, p. 418.
9. H. A. Benesi and J. H. Hildebrand, J. Amer. Chem. Soc. 71, 2703 (1949).
10. (a) S. L. Hsu, J. Signorelli, G. P. Pez, and R. H. Baughman, J. Chem. Phys. 69, 106 (1978).
(b) W. N. Allen, J. J. DeCorpo, F. E. Saalfeld, J. R. Wyatt, and D. C. Weber, J. Synthetic Metals 1, 0000 (1980).
11. (a) C. K. Chiang, M. A. Druy, S. C. Gau, A. J. Heeger, E. J. Louis, A. G. MacDiarmid, and Y. W. Park, J. Amer. Chem. Soc. 100, 1013 (1978).
(b) S. C. Guy, J. Milliken, A. Pron, A. G. MacDiarmid, and A. J. Heeger, Chem. Comm. (1979).
12. A. G. MacDiarmid, et al., presented at the IBM Symposium on Conducting Polymers, March 31, 1979, San Jose, California.
13. D. C. Weber, P. Brant, and J. Ferarris, unpublished work.
14. J. Casanova, Jr., R. E. Schuster, and N. D. Werner, J. Chem. Soc., 4280 (1963).
15. W. Drenth and R. J. M. Nolte, Accts. Chem. Res. 12, 30 (1979).
16. R. J. M. Nolte, R. W. Stephany, and W. Drenth, Recl. Trav. Chim. Pays-Bas 92, 83 (1973).
17. R. J. M. Nolte and W. Drenth, Recueil 92, 788 (1973).
18. S. M. Aharoni, J. Polymer Sci. 17, 683 (1979).
19. W. L. Jolly, Topics in Current Chemistry 71, 150 (1977).
20. National Bureau of Standards Tech. Note 270-3, January 1968, Table 23 (49), p. 154.
21. M. Barber, P. Baybutt, J. A. Connor, I. H. Hillier, W. N. E. Meredith, and V. R. Saunders,
22. D. T. Clark, B. J. Cromarty, and A. Sgamettotti, J. Electron Spectroscopy 14, 175 (1978).
23. C. D. Wagner, Anal. Chem. 44, 1050 (1972).
24. H. Shirakawa, E. J. Louis, A. G. MacDiarmid, C. K. Chiang, and A. J. Heeger, Chem. Comm. 578 (1977).

25. J. A. Hashmall, L. C. W. Baker, F. L. Carter, P. Brant, and D. C. Weber, EAP Report.

AD-A089 312

NAVAL RESEARCH LAB WASHINGTON DC
THE NRL PROGRAM ON ELECTROACTIVE POLYMERS. (U)

F/O 11/9

SEP 80 R B FOX

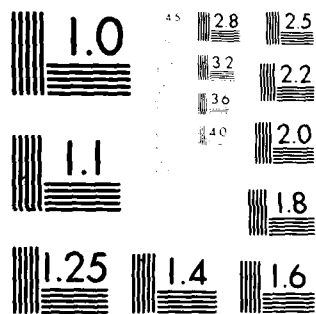
NRL-MR-4335

NL

2 of 2

2000

END
DATE
FRI MED
10-80
DTIC



MICROCOPY RESOLUTION TEST CHART
NATIONAL BUREAU OF STANDARDS 1963 A

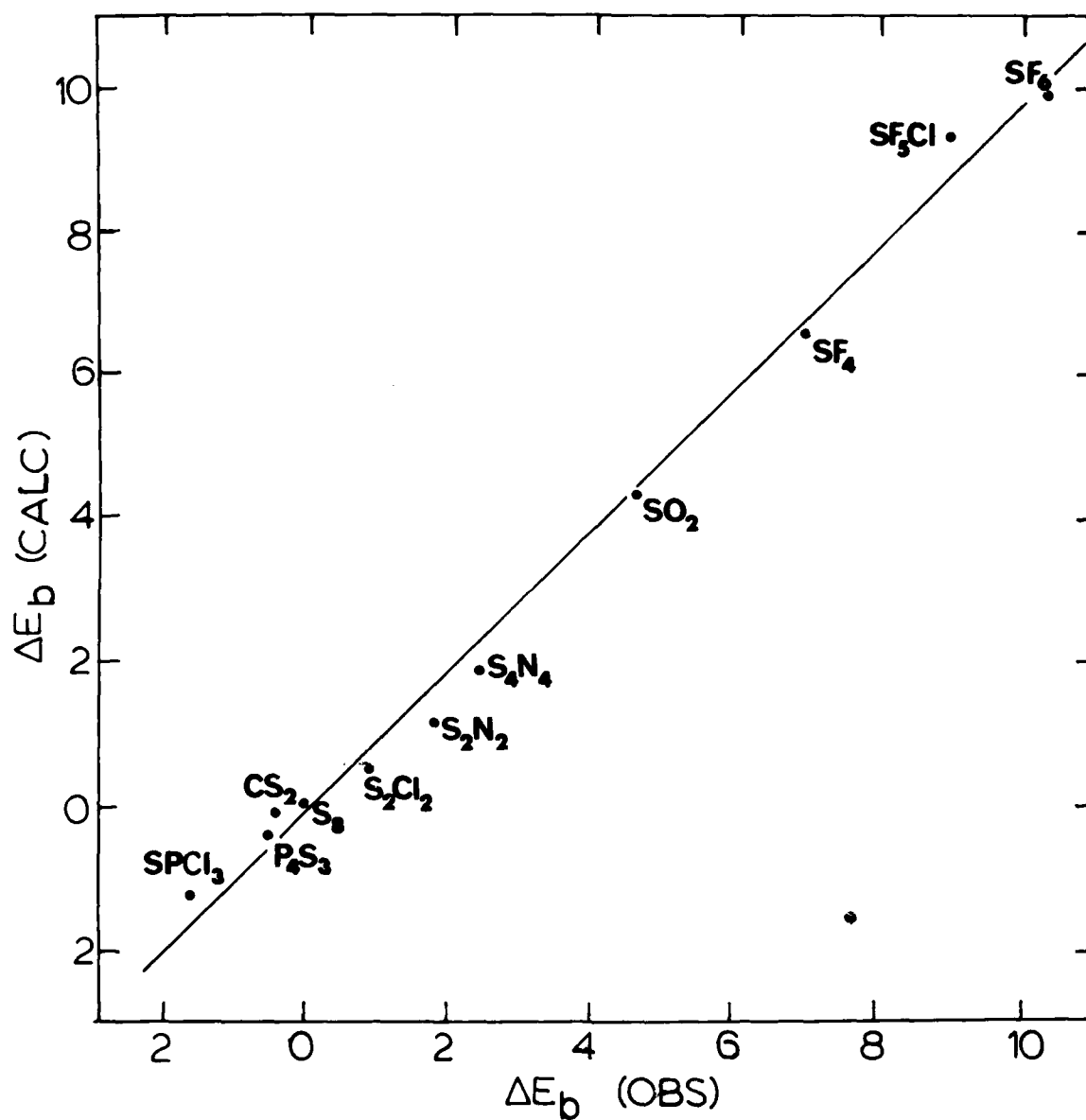


Fig. 1 - Observed versus calculated $S_{2p_{3/2}}$ binding energy shifts in S_2N_2 , S_4N_4 , and a variety of other sulfur containing compounds. The slope of the least squares fit line is 17 eV and its intercept is 170 eV.

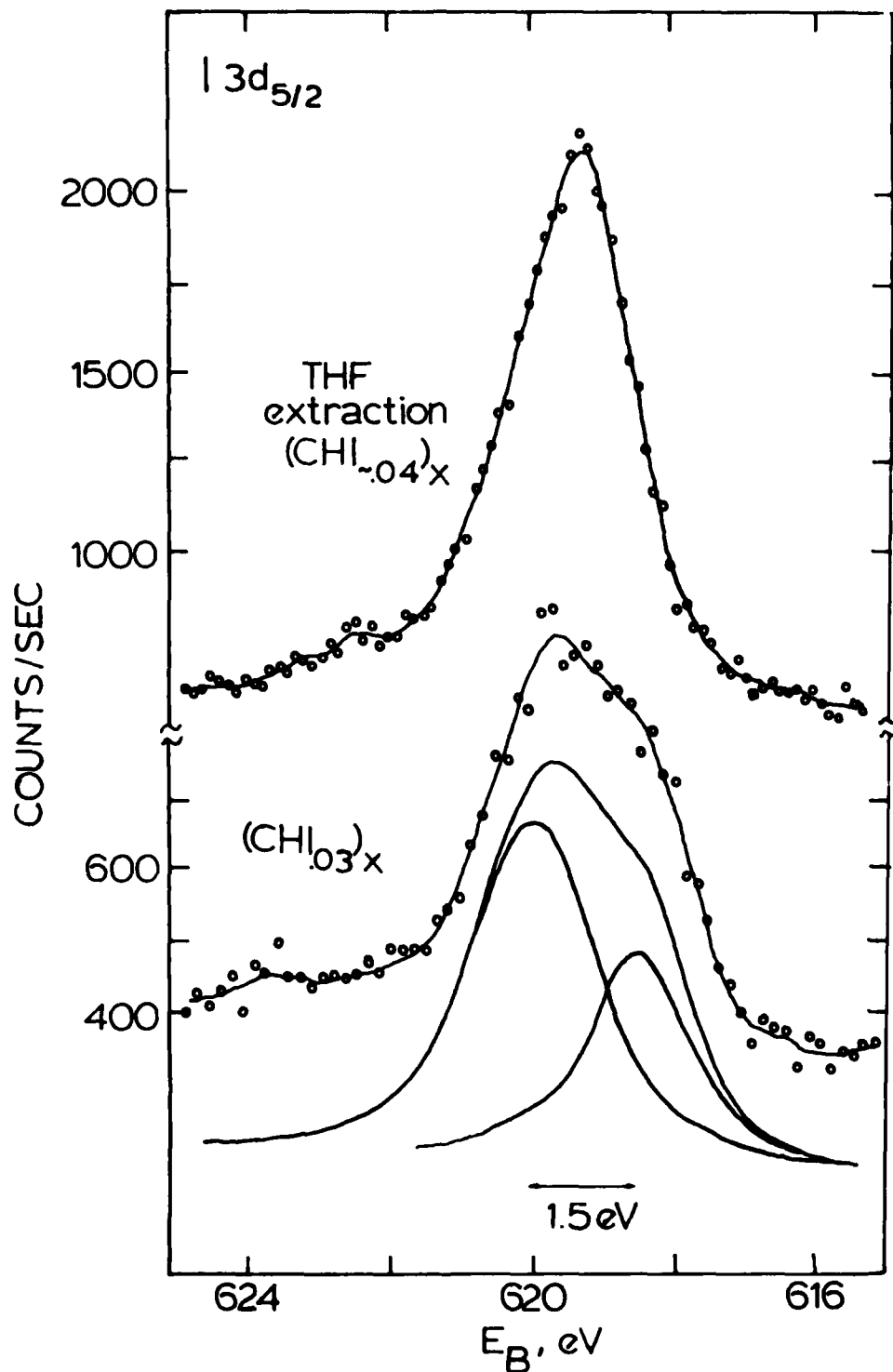


Fig. 2 - Iodine 3d_{5/2} spectra of solvent extracted and unextracted iodinated polyacetylene films. The curve deconvolution of the I 3d_{5/2} envelop recorded from the unextracted films suggests the presence of at least two different iodine environments. The area ratio of the two Gaussian peaks which were used to fit the envelop is 2.0:1.0 (higher B.E.:lower B.E.).

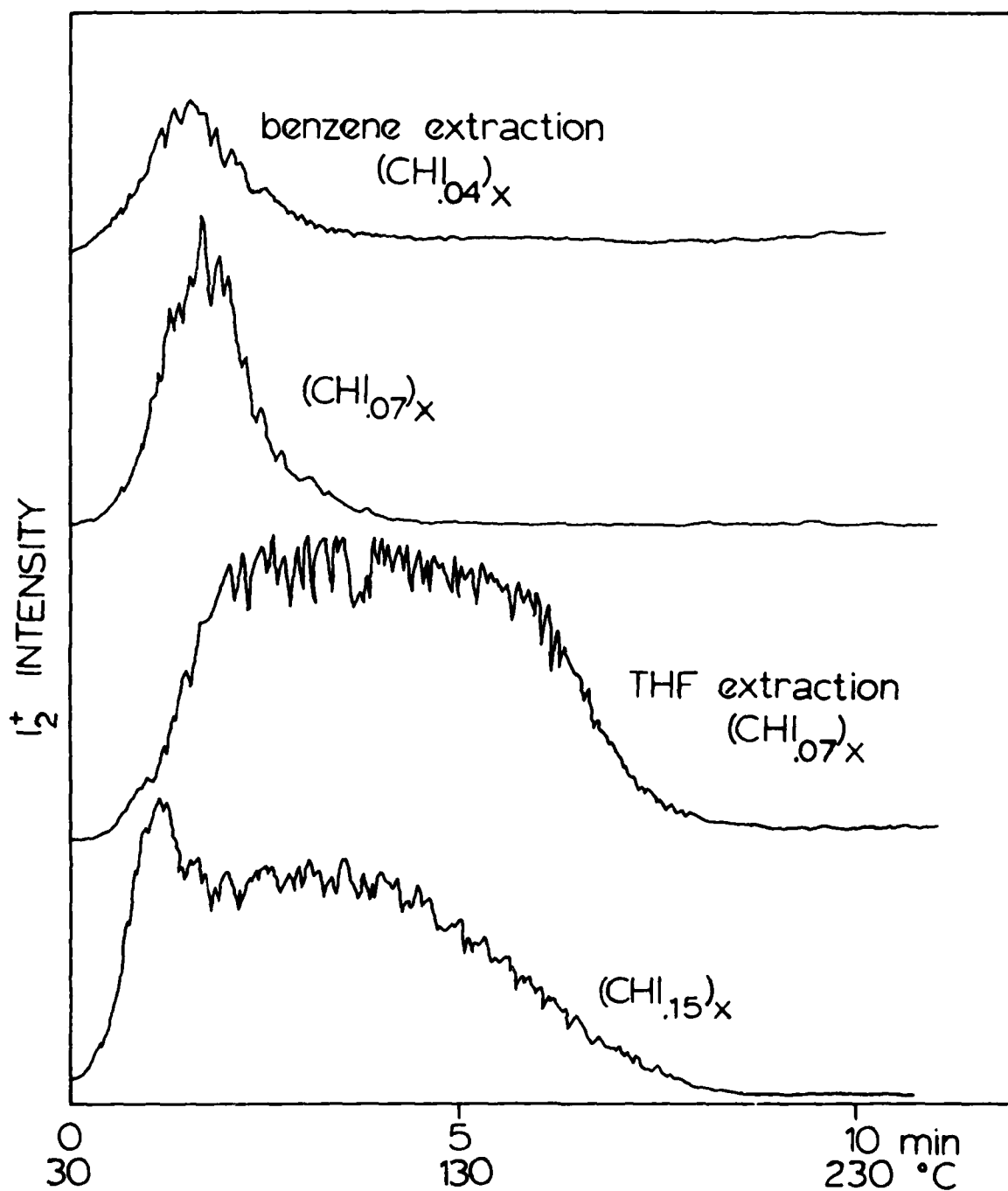


Fig. 3 - I_2^+ ion yield spectra as a function of temperature for extracted versus unextracted iodinated polyacetylene films

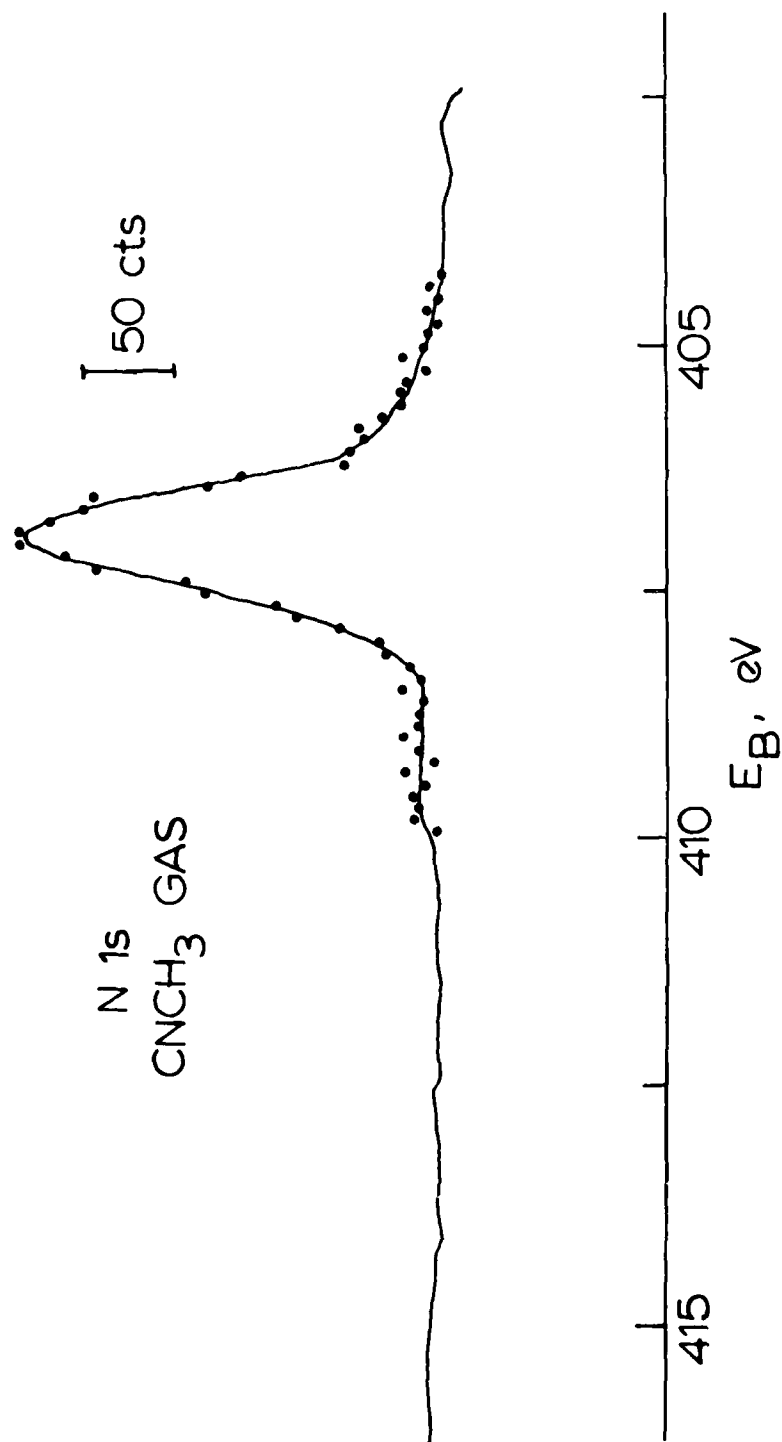


Fig. 4 - Nitrogen 1s spectrum of CNCH₃ gas

CHARACTERIZATION OF $(\text{SN})_x$ PASTE ELECTRODES IN NONAQUEOUS MEDIA

R. J. Nowak, C. L. Joyal, D. C. Weber and D. L. Venezky
Inorganic & Electrochemistry Branch
Chemistry Division

INTRODUCTION

Much effort has been devoted to the synthesis and characterization of inorganic and organic polymeric materials having semiconducting or conducting properties(1). The electrical properties of these polymers make them amenable to study by electrochemical techniques(2). The aim of this research is to: (i) gain fundamental knowledge concerning the surface redox chemistry which occurs at the polymer/solution interface at various applied potentials, and (ii) evaluate the feasibility of utilizing these new electrode materials in electrochemical devices. Prior to these studies it is necessary to demonstrate whether or not the polymer meets certain basic performance criteria which have been established for the use of more conventional electrode materials. In order to accomplish this, the following questions were addressed: (i) What solvent/supporting electrolyte systems can be used with these electrode materials?, (ii) Do the electrode materials influence the kinetics (electron transfer rate) or thermodynamics (formal potential) for solutes which behave reversibly relative to conventional electrode materials under the same experimental conditions?, (iii) For systems behaving reversibly at polymer electrodes, are fundamental current/voltage and current/time relationships obeyed?, and (iv) Do the electrodes behave reproducibly (a) during electrochemical experiments and (b) after storage?

The results of studies utilizing electrodes prepared from the conducting polymer, polymeric sulfur nitride or $(\text{SN})_x$, are reported here. The $(\text{SN})_x$ electrodes were studied in several solvent/supporting electrolyte systems, with and without electroactive solutes present. Parallel studies using well-characterized electrode materials such as glassy carbon and/or platinum were carried out so that non-ideal behavior resulting from differences in the electrode material could be distinguished from that caused by other variables. Results obtained using acetonitrile as the solvent and ferrocene and tetracyanoquinodimethane (TCNQ) as electroactive solutes are described.

ELECTRODE PREPARATION

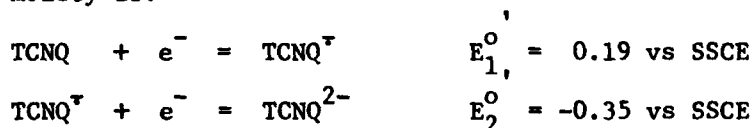
Initial studies which utilized (SN)_x crystals were hampered by difficulty in preparing electrodes that exhibited suitably reproducible electrochemical behavior. However, a technique similar to that used in preparing carbon paste electrodes(3) was used and promises to be very valuable in the rapid evaluation of new polymeric electrode materials. The (SN)_x paste is prepared by mixing (SN)_x and Apiezon M lubricant. First the Apiezon is thoroughly mixed with sodium lauryl sulfate, after which the (SN)_x is added to form an evenly dispersed mixture. The paste is compacted in the bottom of a disposable Pasteur pipette (ca. 1 mm in diameter) and ohmic contact is made with a platinum wire. A resistance of 50 ohms is typical for electrodes having a 3-4 mm plug of paste.

RESULTS AND DISCUSSION

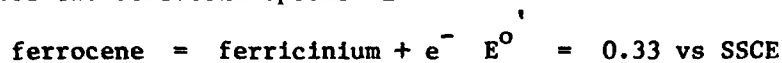
Cyclic Voltammetry:

The usable potential range and background currents for (SN)_x electrodes were found to be quite acceptable for studying the solution electrochemistry of ferrocene and TCNQ in acetonitrile. Breakdown currents, which are the result of electrolytic decomposition of the (SN)_x rather than the solvent or supporting electrolyte, are under investigation and will be reported elsewhere.

Figure 1 shows cyclic voltammograms obtained for TCNQ (A,B) and ferrocene (C,D) in acetonitrile solution at glassy carbon (A,C) and (SN)_x (B,D) paste electrodes. The electrochemical reactions for the TCNQ_x moiety is:



and for the ferrocene specie is:



where SSCE = sodium saturated calomel electrode. Both the qualitative and quantitative features of these cyclic voltammograms are the same for the (SN)_x and glassy carbon electrode. These features and their significance are: (i) similar values of formal potential, E° (Table I) - the thermodynamics of the electrode reactions are unaffected by the electrode material, (ii) similar values of peak current potential differences - the electrochemical reversibility is unaffected by using (SN)_x as the electrode material and (iii) similar values for (a) the slopes of plots of i_p/A vs $V^{1/2}$ where i_p = peak current, A = electrode area and V = potential sweep rate, and (b) peak current ratios (Table I) - Fundamental current/voltage relationships are adhered to when (SN)_x is employed as the electrode material.

Table I summarizes the cyclic voltammetric data obtained using (SN)_x, glassy carbon and platinum electrodes. The (SN)_x data represent three different paste compositions (nine electrodes total) and were acquired over a period of approximately six weeks. Qualitative and quantitative features of cyclic voltammograms were similar on the short term (repetitive cycling in solution) or long term (after extensive periods of storage). The above attest to the long term stability of this electrode material.

Chronoamperometry:

Chronoamperometry was used in order to determine if the current/time behavior of (SN)_x electrodes was consistent with theoretical equations. The technique involves measuring the current transient following a potential step from a potential region in which no electrochemical reaction is occurring to a region in which an electrochemical reaction occurs at a diffusion controlled rate. For planar unshielded electrodes, the current is expressed as:

$$i(t) = \frac{nFA D^{1/2} C}{\pi^{1/2} t^{1/2}} + \text{constant} \quad (1)$$

where n = number of electrons, F = Faraday, A = electrode area, D = diffusion coefficient, and C = concentration of electroactive species. If D is known for a substance under a particular set of conditions, e.g., ferrocene in 0.2M LiClO₄ in acetonitrile(4), the electrode area can be calculated from a plot of i vs. (t)^{-1/2}. This was done for an (SN)_x paste electrode with the result that the electrochemically determined electrode area (1.11 x 10⁻² cm²) compared quite favorably with the geometric area (1.12 x 10⁻² cm²). Thus, as would be expected for an inert electrode, equation (1) is obeyed using (SN)_x as the electrode material.

CONCLUSIONS

Paste (SN)_x electrodes have been found to behave no less ideally than more conventional solid electrode materials in nonaqueous media. With respect to the criteria outlined above, (SN)_x electrodes: (i) Can be used in acetonitrile; (ii) do not influence the thermodynamics or kinetics of solutes which undergo simple outer sphere electron transfer; (iii) obey fundamental current/voltage (cyclic voltammetry) and current/time (chronoamperometry) relationships; and (iv) exhibit a response which is unaffected by continuous use or storage.

These findings have provided the foundation for ongoing studies of the electrochemical decomposition reactions of (SN)_x as well as properties (such as catalytic activity) which may be unique to this novel electrode material.

Reference

1. See, for example, "Molecular Metals", William E. Hatfield, ed., Plenum Press, NY, NY, 1978.
2. R. J. Nowak, H. B. Mark, Jr., A. G. MacDiarmid and D. C. Weber, J. Chem Soc., Chem. Comm., 9 (1977).
3. L. S. Marcoux, K. B. Prater, B. G. Prater and R. N. Adams, Analytical Chemistry, 37, 1446 (1965).
4. T. Kuwaua, D. E. Bublitz and G. Hoh, J. Amer. Chem. Soc 82, 5811 (1960).

TABLE 1
CYCLIC VOLTAMMETRIC DATA^a

Electrode Material	Ferrocene/Acetonitrile ^b		TCNQ/Acetonitrile ^c	
	E^o	i_{pc}/i_{pa}	E_1^o	i_{pc}/i_{pa}
Platinum	$0.328 \pm 0.007(57)^d$	$0.90 \pm 0.08(57)$	$0.194 \pm 0.002(31)$	$1.03 \pm 0.02(15)$
Glassy Carbon	$0.328 \pm 0.005(56)$	$0.90 \pm 0.06(56)$	$0.192 \pm 0.003(30)$	$1.05 \pm 0.03(10)$
(SN) _x paste ^e	$0.330 \pm 0.008(326)$	$0.87 \pm 0.07(326)$	$0.196 \pm 0.005(25)$	$1.05 \pm 0.03(16)$
				$-0.352 \pm 0.004(18)$
				$-0.349 \pm 0.005(16)$

^aE values in V vs SSCE

^b0.2M LiClO₄; V = 0.5, 0.2, 0.1, 0.05, 0.02, V/s; 0.52, 1.01, 2.00, 2.02, 5.03 mM ferrocene

^c0.1M tetraethylammonium perchlorate; V = same as a; 0.49 mM TCNQ

^dNumbers in parenthesis = number of voltammograms averaged

^eNine electrodes (three separate batches of paste) used for ferrocene data; three electrodes for TCNQ data

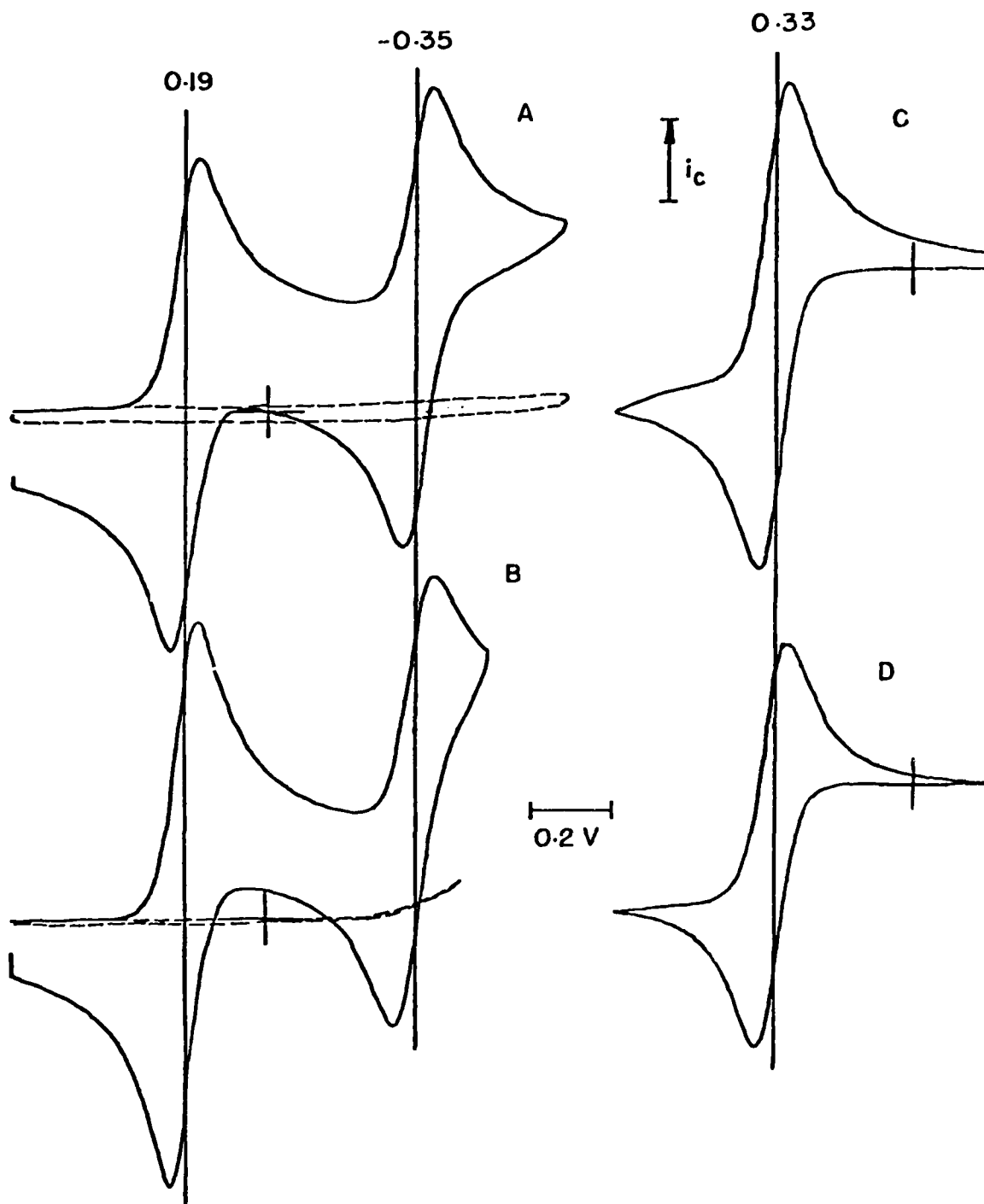


Fig. 1 - Cyclic voltammograms for 0.5 mM TCNQ (A,B) in 0.1 M tetraethylammonium perchlorate/acetonitrile and 1.0 mM ferrocene (C,D) in 0.2 M lithium perchlorate/acetonitrile solution. Glassy carbon electrode: A,C; $y=5.0 \mu\text{A/division}$. (SN) electrode: B,D; $y=1.0 \mu\text{A/division}$. Potential sweep rate = 0.2V/s. Dotted curves: no TCNQ present in solution.

ELECTRICAL CONDUCTIVITY OF TCNQ SALTS DISPERSED IN
POLY(VINYLACETALS) AS MATRIX POLYMERS

Oh-Kil Kim and R. B. Fox
Polymeric Materials Branch
Chemistry Division

INTRODUCTION

Many radical-anion salts of 7,7,8,8-tetracyanoquinodimethane (TCNQ) are organic semiconductors (1). A complex salt, $M^+(TCNQ)_2^-$, usually has a higher conductivity than the corresponding simple salt, M^+TCNQ^- (1,2). This is rationalized in terms of decreased electron-electron repulsion in complex salts. Polymeric semiconductors incorporating TCNQ anion-radicals onto polycationic macromolecules as sites for the attachment have been studied by several groups of investigators (3,4,5). The properties of polymeric semiconductors of the polycation-TCNQ type have some advantages over their monomeric derivatives in that they are processable and their conductivity can be controlled by varying the TCNQ concentration. However, the matrix polymer is brittle due to its ionic nature, and its stability is lowered (6,7) by sensitivity to moisture.

Another approach is to disperse TCNQ salts into non-ionic matrix polymers so that advantage can be taken of the mechanical properties and higher stabilities of the polymer (8). However, this kind of system may be more than a simple physical mixture of components as with conducting fillers such as Al or Cu powder or carbon black in a plastic carrier. If electron donor groups are present in the matrix polymer, interaction is expected between these groups and TCNQ or its derivatives. This interaction will not only increase the compatibility of the electrically active additive with the matrix, but will strongly affect the electrical and mechanical properties of the system as well.

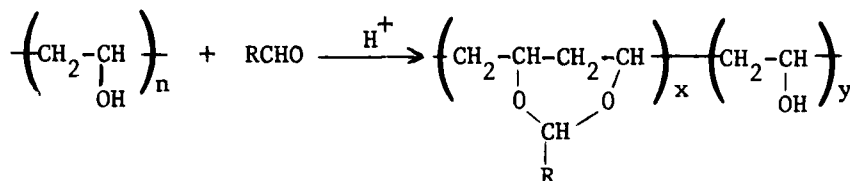
Poly(vinyl acetals) derived from high molecular weight poly(vinyl alcohols) are generally film-forming materials with good stability and mechanical properties. Synthetically, a wide variety of donor or acceptor groups can be incorporated into these polymers. Accordingly, the present study deals with the electric conductivity of systems consisting of TCNQ salts dispersed in poly(vinyl acetals) whose side groups have electron-donating properties. In this paper, we report preliminary conductivities and their chemical significance.

EXPERIMENTAL

Materials

Salts such as $K^+(TCNQ)^-$, $NH_4^+(TCNQ)^-$, $NH_4^+(TCNQ)_2^+$, and N-Ethyl-Quinolium $(TCNQ)_2^+$ were prepared according to procedures described by Melby and coworkers (1). Characterization of the TCNQ derivatives was made by elemental analysis, IR and visible spectra.

Poly(vinyl acetals) were synthesized from poly(vinyl alcohol) (PVA) (Polyscience, 99% saponification, molecular weight 25,000) and the appropriate aldehyde in the presence of acid catalyst. Both reactants were commercial products and used as received. The general reaction is



The reaction of N-ethyl-3-carbazolecarboxaldehyde (ECZ) with PVA represents a typical synthesis. The aldehyde, ECZ, 22.3g (0.1 mole) was dissolved in 130 ml DMF in which was suspended 3.3g (0.075 mole) of pulverized PVA, and p-toluenesulfonic acid hydrate, 2.5g (0.013 mole) was added. The mixture was warmed up to 80°C with stirring. In about 3 hours the solution became homogeneous. After 20 hours the solution was poured into a large amount of acetone to precipitate a grey-colored polymer. Dissolution in DMF and precipitation with acetone and then with water was repeated several times. Finally the precipitated polymer was filtered, washed with acetone, and dried under reduced pressure to give a light grey solid (5g). The nitrogen analysis, 4.26%, corresponded to 71% acetalization; IR (solid film): ν_{CH} 3050, 2920 and 2870 cm^{-1} ; δ_{CH} 1480 and 1420 cm^{-1} ; ν_{COC} , 1270 cm^{-1} ; ν_{OCO} , 1120 and 1020 cm^{-1} and ν_{CO} , 935 cm^{-1} .

Other poly(vinyl acetals) from aldehydes such as 9-anthraldehyde (ANT), 4-quinolinecarboxaldehyde(QUN), and p-(dimethylamino)benzaldehyde (DMB) were synthesized as described above. The basic aldehydes QUN and DMB were neutralized with the acid used as catalyst, with an excess performing the catalyst function. At the conclusion of the heating period in these cases, the reaction mixture was poured into a large volume of water and neutralized with sodium acetate.

The conditions of the acetalization and the analytical results are given in Table I.

Table I

Reaction Conditions^a and Analyses for Poly(vinyl acetals)

<u>RCHO</u>	<u>RCHO</u> <u>mole</u>	<u>PVA</u> <u>mole</u>	<u>Acid</u> ^b <u>mole</u>	<u>% N</u>	<u>% Acetalization</u> ^c
ANT	0.1	0.075	0.008	d	39
ECZ-1	0.1	0.075	0.018	4.26 ^e	71
ECZ-2	0.1	0.15	0.013	3.28	40
ECZ-3	0.1	0.15	0.013	3.11	36
DMB	0.1	0.075	0.13	3.29	30
QUN	0.03	0.03	0.04	5.39	46

^aIndicated amounts of reactants were dissolved in 130 ml of DMF and the reaction allowed to proceed for 20 hrs except for ECZ-2 (8 hrs) and ECZ-3 (4 hrs).

^bp-Toluenesulfonic acid except with QUN, for which conc. H₂SO₄ was used.

^c% Acetalization = $100[2x/(2x + y)]$, where x and y are the mole fractions of acetal and hydroxyl units, respectively, determined from the analyses.

^d% C 73.37, % H 6.66.

^e% C 70.16, % H 7.41.

Preparation of Conducting Film Samples

Typically, the poly(vinylacetal), 47 mg, was dissolved in 1.5 ml of dry DMF (DMF and DMSO are the best solvents) that had been purged with dry nitrogen and then a weighed amount of the TCNQ salt was added to the solution. Stirring of the green solution was continued for several hours to several days (very low concentrations, e.g. 7.15×10^{-3} M, of TCNQ salts require 2 to 3 days treatment) at room temperature. Films were cast by spreading the solution on a glass or aluminum plate and evaporating the solvent over a period of about one hour at approximately 30°C under reduced pressure. The resulting film was further dried at 40°C in vacuo overnight. A smooth black-green film is formed

with a uniform dispersion of heavily inter-connected microcrystals, often in a fan shape. The thickness of film samples for the electric measurement was in the range of 3 to 5×10^{-3} cm. Anhydrous conditions were used in the film preparation because water reacts with TCNQ and its salts.

Electrical Measurements

The electrical resistance of the conducting film was measured with Keithley 610C electrometer in most cases. The film was made up as a surface-type cell; on both sides of the film were Au-vapor-deposited electrodes whose diameter was 2.0 cm. The d.c. current induced under various applied voltages was measured in air at room temperature. The resistance of the conducting film was calculated by Ohm's law. Ohmic behavior was observed in all conducting films. The resistivity was computed from $\rho = R \cdot A/d$, where R is the measured resistance (Ω), A is the area of the electrode in cm^2 , and d is the sample thickness in cm. For a four-probe method a Keithley 164 TT digital multimeter was used in the milliohmeter mode. Four-probe and two-probe measurements gave approximately identical resistivity values. The temperature dependence of the electrical resistance was measured in vacuo in a temperature controlled chamber. Activation energies were determined from Arrhenius plots obtained by measuring the resistance (R) at 5° intervals over 10° to 50°C . The activation energy, E_a was computed from the relation:

$$R = R_0 \exp (E_a / kT)$$

where R_0 is the resistance at infinite temperature, k is the Boltzmann constant, and T is the absolute temperature.

RESULTS AND DISCUSSION

Compositions of the film samples and their resistivities and activation energies are given in Table II. All polymer samples of the present system showed linear current-voltage characteristics regardless of the nature of the polymer and the concentration of components; examples are illustrated in Fig. 1. The temperature dependence of the electrical resistance shown in Fig. 2 is typical of semiconductors.

Electrical conduction in these films may depend in part on the formation of a continuous network of uniformly dispersed conducting species into the polymer matrix. The uniformity of the dispersion of the added conducting species is probably a consequence of interaction between those species and the matrix polymer. If there were no or negligible interaction, the conductivity would be independent of the chemical structure of the polymer. Conductivity is, however, highly dependent on the polymer matrix, as shown in Table II; the contribution of P(ANTA) to the conductivity is 10^3 times smaller than that of P(ECZA). This is indicative of a selective binding of donor groups in the polymer to TCNQ or the TCNQ salts. Among the vinyl acetal polymers, N-ethylcarbazolyl and (N,N-dimethylamino)phenyl moieties are

electrically-active components in the matrix, unlike the anthracenyl moiety. A preliminary result indicated that poly(vinyl-4-quinoline-aldehyde acetal), P(QUNA), was as electrically active as P(ECZA).

The reasons for such functional differences in component species are not clear but may result from differences in charge-transfer interaction. These interactions, as reflected by film resistivities, involve more than charge transfer between TCNQ^0 and donor moieties in the polymer matrix, since the transparent films formed from TCNQ^0 and P(ECZA)-1 or P(DMBA) (Samples X and XI, Table II) were nonconducting. Rather, the interactions appear to involve the polymer donor groups, TCNQ^0 , and a TCNQ salt, as shown by a comparison of samples I, IV, and X.

The formation of charge-transfer complexes between neutral donors and aromatic cations has been reported (9). An interaction between a neutral donor polymer and a heterocyclic cation was suggested by Shinohara and his coworkers (8) in the systems of quinolinium or acridinium- TCNQ complex salts dispersed in donor polymers such as poly(4-vinylpyridine) and poly(N-vinylcarbazole). A homogeneous dispersion and a higher conductivity were obtained with the former polymer, but the electrical stability of the film was inferior to that obtained with the latter polymeric system. This seems to imply that for good conductivity and stability matrix polymers should overcome such conflicting effects by somehow moderating their interactions with TCNQ salts. It has been noted that n-donors and π -donors are contrasted by very large differences in their degree of association with σ -acceptors compared with π -acceptors (10). There is, however, not always a clear division between n-donors and π -donors; for example, N,N-dimethylaniline behaves as n-donor toward some acceptors and as a π -donor toward other acceptors (11).

Ionization potentials for model compound analogs of P(ECZA), P(ANTA), and P(DMBA) are in the range of 7.3 to 7.5 eV, and therefore this parameter cannot account for five orders of magnitude variation in conductivity between dispersed systems in P(ANTA) and in the nitrogen-containing poly(vinylacetals). Differences in the degree of acetalization are also not overriding, since this value is higher in P(ANTA) than in P(DMBA) (Table I) and the resistivities obtained with dispersions in P(ECZA)-2 and in P(ECZA)-3 were only one order of magnitude higher than those in P(ECZA)-1 with approximately twice the degree of acetalization. While undoubtedly a variety of factors can affect interactions in complex polymer systems, attention is drawn to the electronic character of the donor moieties in the poly(vinylacetals). The anthracenyl groups in P(ANTA) are surely π -donors and complexes with TCNQ will be π - π complexes. Each of the nitrogen-containing moieties in the other poly(vinylacetals) has the capability of acting as an n-donor. Consequently, it is suggested that the observed higher conductivity in the nitrogen-containing poly(vinylacetals) is rooted in the formation of n- π complexes with TCNQ .

It was found that the addition of neutral TCNQ to the simple salt, K^+TCNQ^+ , increased the conductivity (Samples XII-XIII and XVI-XVII in Table II), as expected (3,12,13). Addition of poly(ethylene oxide) (PEO), whose effects for plasticization and interaction were expected to enhance the compatibility of a TCNQ salt with a matrix polymer, also increased the conductivity of the K salt dispersion to some extent (Samples XIII-XIV).

As shown in Samples I-III in Table II, conductivity in the $NH_4^+(TCNQ)_2^-/P(ECZA)-1$ system increases with increasing concentrations of the added TCNQ salt up to about 20 wt%; little further effect is observed with additional increments of the salt. Up to 40% by weight TCNQ salt in P(ECZA), the conductivity is uniform throughout the entire film, but above that concentration the films become heterogeneous and the flexibility lessened. Such observations indicate that there is a saturation in the dissolution of TCNQ salt in the polymer matrix. The level of saturation in PMMA and PAN was found to be much lower than that in the poly(vinylacetals), because the phase separation took place at lower TCNQ salt concentrations.

An unusual effect was observed when $TCNQ^0$ was added to a complex salt. As shown in Samples I, IV, and V in Table II in the case of the $NH_4^+(TCNQ)_2^-/P(ECZA)-1$ system, the resistivity was lowered to 4×10^4 from $2 \times 10^8 \Omega\text{-cm}$ by introducing only 4% by wt $TCNQ^0$ but additional $TCNQ^0$ did not further decrease the resistivity. The decreasing resistivity with increasing $TCNQ^0$ can be explained in terms of the activation energy. It is reported (3,12) that the addition of $TCNQ^0$ to poly(vinylpyridinium)- $TCNQ^-$ salt, (PVP^+TCNQ^-) , increases the conductivity up to the mole ratio of $TCNQ^0$ to PVP^+TCNQ^- of about 0.5, with added $TCNQ^0$ introduced between $TCNQ$ radical-anions, and hence charge resonance interaction takes place, but beyond that ratio, the conductivity decreases, probably because the excess $TCNQ^0$ hinders electron transfer. A similar situation could be produced by the addition of $TCNQ^0$ to the complex salt in the present system. However, the addition of $TCNQ^0$ to the complex salt in the present system makes $TCNQ^0/TCNQ^+ > 1$. A sharp increase in the conductivity under this condition cannot be explained without considering an interaction between $TCNQ^0$ and the donor component of the matrix polymers, through which $TCNQ^0$ can participate in the conducting path by packing the gap between $TCNQ$ complex salt species aligned in the polymer. As indicated above, there is a good possibility that the charge-transfer interaction with the matrix produces $TCNQ^-$ through electron-transfer. Recently, Schulz et al. (14) and Braun et al. (15) reported that charge-transfer interaction between naphthalenealdehyde acetal polymers and $TCNQ^0$ in dichloromethane is followed by an electron transfer to give $TCNQ^-$ species, confirmed by absorption and ESR spectra. (15) The monomeric analog of the polymer does not produce the radical-anion under the same conditions. This suggests a cooperative interaction among two or more donor moieties in the same polymer molecule. Moreover,

this cooperative effect is strongly structure-dependent, probably as a result of ionization potential differences or steric factors. It was shown, (15) for example, that identically prepared dichloromethane solutions of TCNQ⁰ with poly(1-naphthalenealdehyde acetal) and with poly(2-naphthalenealdehyde acetal) initially had a TCNQ⁻ concentration ratio of 40:1; after 24 hours, this ratio had become 10:1, indicating a difference between the isomeric polymers in the rate of equilibration.

In a similar way, additional TCNQ⁻ will be formed when excess TCNQ⁰ is added to a solution of the complex salt and one of the poly(vinylacetals) used in the present study. The rate of attainment of equilibrium will depend upon the structure of the poly(vinylacetal). It was found that the electrical conductivity of TCNQ complex-dispersed poly(vinylacetal) systems depends upon how long the solution was allowed to stand before casting the film. Such conductivity dependence on the pre-treatment time was noticeable when the salt concentration was low and especially in the presence of additional neutral TCNQ, suggesting that a time-dependent interaction was in progress. A sample solution required 2-3 days pre-treatment at room temperature to give maximum conductivity, when the sample solution contained a low concentration ($>7.5 \times 10^{-3}$ M) of TCNQ salts; with a high concentration ($>1.5 \times 10^{-2}$ M) of TCNQ salts the pre-treatment was not normally necessary. In the low concentration case, the conductivity of the cast film was increased two orders of magnitude by allowing the solution to equilibrate.

All of the poly(vinylacetals) were soluble in DMF or DMSO, and P(DMBA) was soluble in THF or dichloroethane; other common solvents were not suitable. As a solvent, DMF was preferred to DMSO because it had a lower tendency to absorb atmospheric moisture. It is conceivable that such highly polar solvent molecules can dissociate the TCNQ complex salt. A brief spectral study strongly indicated that the complex salt, $\text{NH}_4^+(\text{TCNQ})_2^-$, in DMF solution is dissociated almost completely to TCNQ⁻ and TCNQ⁰; the $(\text{TCNQ})_2^-$ absorption (1) of the complex salt at 395 nm (in acetonitrile) did not appear, but absorption bands due to TCNQ⁻ at 420 nm and TCNQ⁰ at 340 nm were evident. Other spectral evidence showed that neutral TCNQ in DMF solution forms TCNQ⁻, although the absorption due to TCNQ⁻ was gradually diminished with time. Another strong solvent interference was observed in THF, a strong donor solvent, in which $(\text{TCNQ})_2^-$ is destabilized as evidenced by a rapid decrease in the absorbance at 395 nm. By analogy, it can be expected that $(\text{TCNQ})_2^-$ is destabilized in the strong donor environment of the matrix polymer in solid state. When THF was used instead of DMF in the system of $[\text{NH}_4^+(\text{TCNQ})_2^- + \text{TCNQ}^0]\text{P(DMBA)}$, the conductivity of the film produced was extremely low, compared with that produced from a DMF solution. In such strong donor solvents, the charge-transfer interaction between the dissolved components is ordinarily greatly reduced. In order to eliminate the interference of such a donor solvent, an inert solvent was used to examine the interaction between the dissolved components. Therefore one of the

poly(vinylacetals), for example P(DMBA), was examined in dichloroethane for the charge-transfer interaction with TCNQ⁰. It was observed in this system that there are absorption bands characteristic of TCNQ⁻, as observed with TCNQ⁰ and the naphthalene aldehyde poly(vinylacetal),⁽¹⁵⁾ mentioned above. Clearly, such an electron-transfer interaction would be even stronger in the donor-rich environment of the polymer solid.

The electrical stability of the conductive films was examined in air at room temperature as a function of time; the data are shown in Figure 3. It was found that P(ECZA) and P(DMBA) are useful matrix polymers for stability as well as conductivity. Among them, the P(ECZA) system was the most stable one; only negligible changes in resistivity in these films occurred over a period of almost two months.

SUMMARY

Poly(vinylacetals) having different donor moieties such as N-ethyl-3-carbazolyl, 9-anthracenyl or p-(dimethylamino)phenyl were synthesized and employed as matrix polymers for dispersions of TCNQ anion-radical salt conductors with the aim of developing a new film-forming polymeric conductor. The effect of the donor component of the poly(vinylacetals) was evaluated in terms of the conductivity, film-forming properties and electrical stability. Comparison was made with common vinyl polymers. Discussion was focussed on the polymer donor effect in relation to the charge-transfer interaction with TCNQ salts and neutral TCNQ. Electrical properties of the present polymeric system showed typical semiconducting behavior.

The electrical conductivity of the dispersed systems was strongly influenced by the type of matrix polymer and the type of donor moiety in the poly(vinylacetals). Conductivity of these dispersions was not related to the ionization potentials of the donor groups.

Addition of only a few percent of neutral TCNQ to the TCNQ complex salt-dispersed poly(vinylacetal) system increased the conductivity dramatically. The presence of excess neutral TCNQ cannot explain the enhanced conductivity without considering a charge-transfer interaction between the donor component of the poly(vinylacetal) and neutral TCNQ. Absorption spectra indicated a possible formation of TCNQ radical-anions by an electron transfer from the polymeric donor. A decrease in the activation energy parallels an increase in the conductivity by the addition of neutral TCNQ.

An increase of TCNQ salt concentration up to about 40% by weight in the poly(vinylacetal) system increased the conductivity, but additional increments had little effect. This corresponds to changes in the properties of the resulting films; at over 40% by weight of TCNQ salts a heterogeneous phase separates, and a lessened film flexibility is produced. The stability of the conducting films in air was found to be excellent with poly(vinylacetal) matrices, especially those which have the N-ethylcarbazole moiety.

TABLE II
Sample Compositions and Electrical Properties

Sample	Polymer	mmol/g. polymer		$\rho (\Omega\text{-cm})$	Ea (eV)
		$\text{NHET}_3^+(\text{TCNQ})_2^-$	TCNQ^0		
I	P(ECZA)-1	0.24	-	2.5×10^8	0.094
II	P(ECZA)-1	0.48	-	1.5×10^4	0.078
IIa	P(ECZA)-2	0.48	-	3.6×10^4	0.11
III	P(ECZA)-1	0.95	-	7.2×10^3	-
IV	P(ECZA)-1	0.24	0.24	4.4×10^4	0.065
V	P(ECZA)-1	0.24	0.59	2.9×10^4	0.048
VI	P(ANTA)	0.24	0.24	7.8×10^7	0.41
VII	P(DMBA)	0.24	0.24	2.7×10^5	0.22
VIII	PMMA	0.24	0.24	5.0×10^6	-
IX	PAN	0.24	0.24	8.9×10^8	-
X	P(ECZA)-1	-	0.24	1.2×10^{12}	-
XI	P(DMBA)	-	0.24	1.2×10^{12}	-
		K^+TCNQ^-	TCNQ^0		
XII	P(ECZA)-1	0.44	-	5.2×10^{10}	-
XIII	P(ECZA)-1	0.44	0.44	9.1×10^6	-
XIV	P(ECZA)-1 ^a	0.44	0.44	4.5×10^5	-
XV	P(ANTA)	0.44	0.44	1.1×10^8	-
XVI	PMMA	0.44	-	1.8×10^{11}	-
XVII	PMMA	0.44	0.44	1.9×10^7	-

^a320 mg. PEO added per g. P(ECZA)-1.

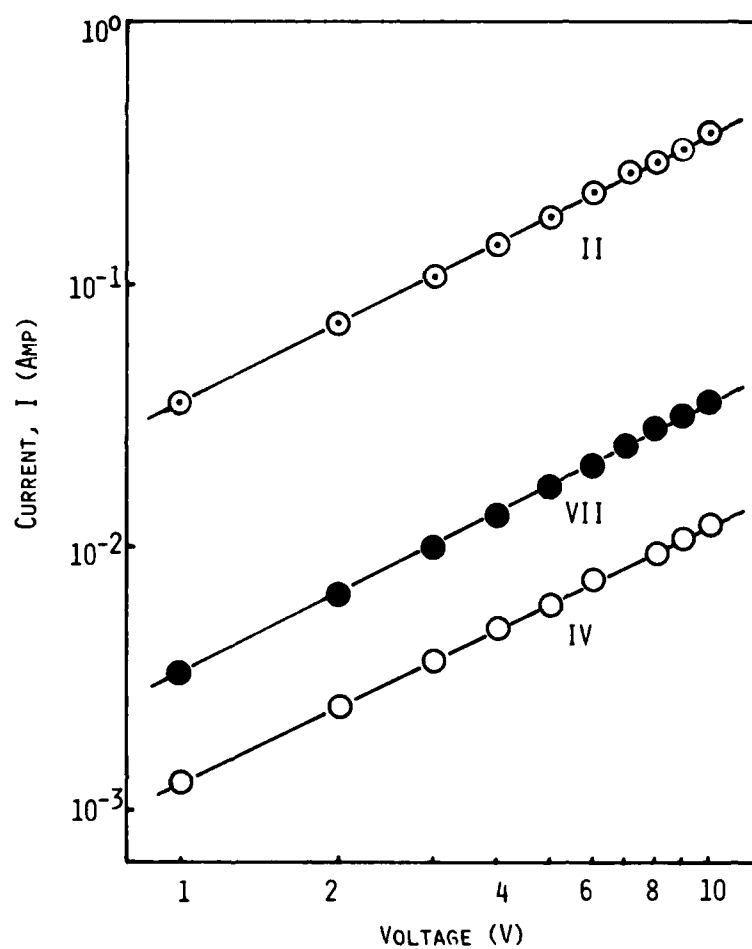


Fig. 1 - Current-voltage relation of TCNQ salt-polyacetal systems. Sample numbers are identified in Table II.

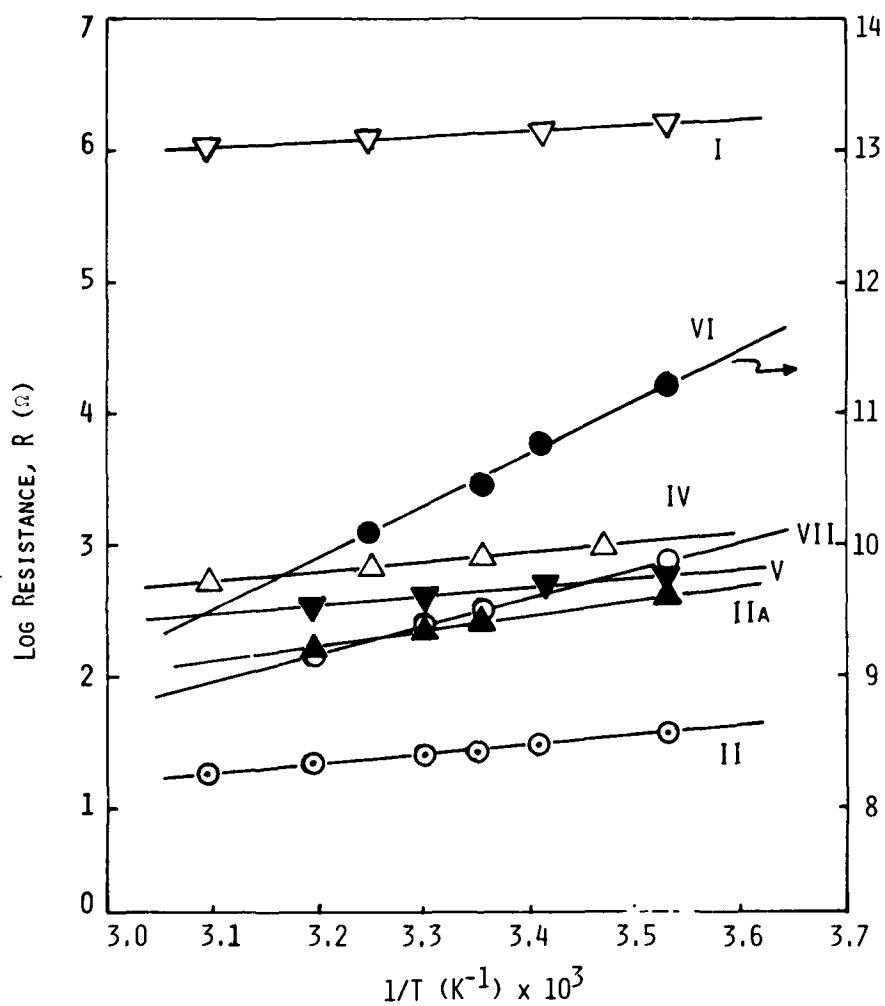


Fig. 2 - Temperature dependence of electrical resistance of TCNQ salt-polymer systems. Sample numbers are identified in Table II.

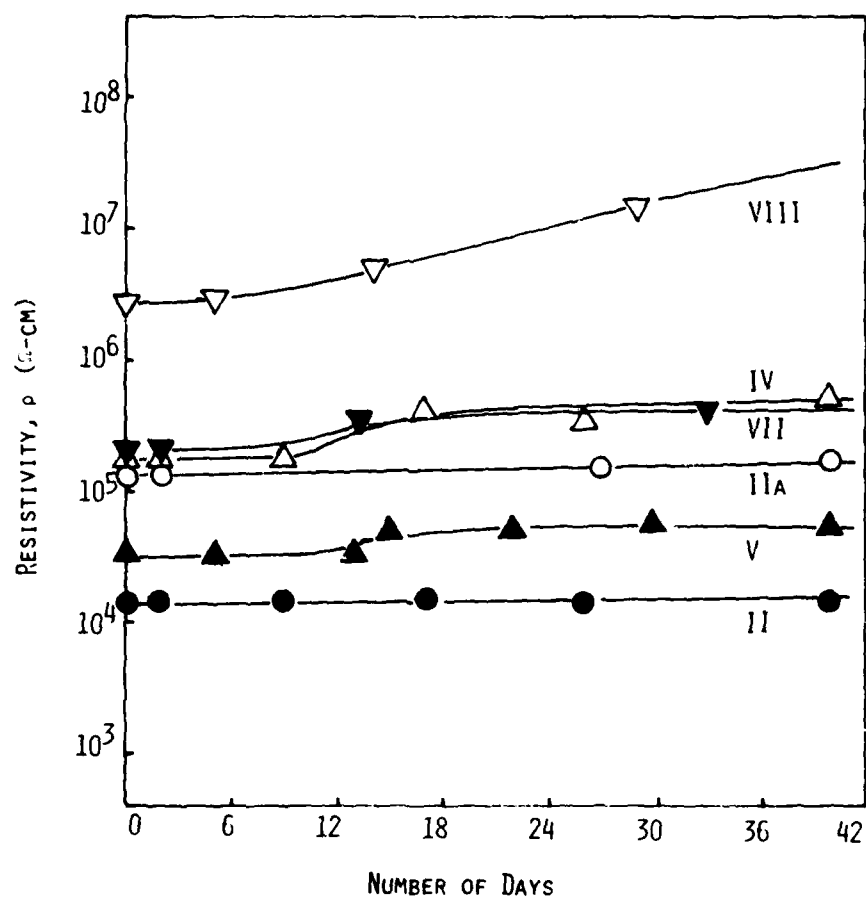


Fig. 3 - Resistivity changes of conducting films as a function of time. Sample numbers are identified in Table II.

REFERENCES

1. L. R. Melby, R. J. Harder, W. R. Hertler, W. Mahler, R. E. Benson and W. E. Mochel, J. Am. Chem. Soc., 84, 3374 (1962).
2. D. W. Bonniface, M. J. Braithwait, O. D. Eley, R. G. Evans, R. Pethig and M. R. Willis, Discuss. Faraday Soc., 51, 131 (1971).
3. J. H. Lupinski, K. D. Kopple and L. J. Hertz, J. Polym. Sci., Part C, 16, 1561 (1967).
4. A. Rembaum, A. M. Hermann, F. E. Stewart and F. Gutmann, J. Phys. Chem., 73, 513 (1969).
5. K. Mizoguchi, T. Suzuki, E. Tsuchida and I. Shinohara, Nippon Kagaku Kaishi, 1973, 1760.
6. J. M. Bruce and J. R. Herson, Polymer, 8, 619 (1967).
7. K. Nakatani, T. Sakata and H. Tsubomura, Bull. Chem. Soc. Japan, 48, 2205 (1975).
8. K. Mizoguchi, T. Kamiya, E. Tsuchida and I. Shinohara, J. Polym. Sci., Polymer Chem. Ed., 17, 649 (1979) and references therein.
9. R. Foster, "Organic Charge-Transfer Complexes", Academic Press, London (1969), p. 293-294.
10. Ref. 9, p. 190.
11. H. Tsubomura, J. Am. Chem. Soc., 82, 40 (1960).
12. K. Nakatani, T. Sakata and H. Tsubomura, Bull. Chem. Soc. Japan, 48, 657 (1975).
13. K. Mizoguchi, T. Suzuki, E. Tsuchida and I. Shinohara, Nippon Kagaku Kaishi, 1973, 1751.
14. R. C. Schulz and U. Geissler, Makromol. Chem., 179, 1355 (1978).
15. H. Löligier and A. Braun, Makromol. Chem. 179, 1369 (1978).

ELECTRICAL CONDUCTIVITY OF CONJUGATED ORGANIC POLYMERS

T. M. Keller and J. R. Griffith
Polymeric Materials Branch
Chemistry Division

INTRODUCTION

The phenomenon of electrical conductivity of organic compounds has evoked a great deal of interest in recent years. In spite of this intense research interest, however, the mechanism of conduction remains largely obscure.

The conjugated system is probably the most universally recognized structural parameter in this area of research. The orbitals of the π electrons in a conjugated molecule can be considered as overlapping with the resultant mixing of wave functions to form delocalized molecular orbitals encompassing all nuclei of the conjugated system. Orbital delocalization, besides permitting an electrical charge to be transferred readily along the molecule, causes a reduction in the excitation energy required to promote π electron to triplet or other excited states. This decrease in the promotional energies is reflected in an enhanced conductivity when a potential is applied across a material.

Maximum overlap of the π orbitals and a high degree of polymerization seem to be of paramount importance for high conductivity. Although a charge carrier can move through a conjugated chain without much interruption, its movement is interrupted at the end of the chain where an intermolecular barrier constitutes a large energy gap for further charge transport. To facilitate the charge transport across the intermolecular barrier, the polymer can be complexed with a suitable acceptor (or donor) or its structure can be modified such that extended conjugation is obtained. Enhanced conductivity is generally obtained in polymers with extended conjugation.

In practice, one cannot prepare infinite network polymers which contain only a single molecule. Side reactions and/or immobility terminate polymer growth such that the material is generally composed of a number of very large polymer molecules rather than a single molecule. Nevertheless, the amount of cross-chain hopping should be greatly reduced and increased conductivity expected as the polymer structure approaches an infinite network.

Although many kinds of polymeric semiconductors have been synthesized, a large portion have consisted of carbon-carbon conjugated systems. When nitrogen, which contains a free pair of electrons, is involved in a conjugated system, the polymer would be expected to have different electrical properties than a carbon-carbon conjugated system. In such polymers, current carriers

should appear quite easily and, with a sufficiently high regularity of the polymeric structure, the electron dispersion should be small.

Dopants are being increasingly used to enhance the conductivity of polymeric materials. A wide variety of compounds (1-6) have shown an increase in conductivity of many orders of magnitude when chemically doped with electron-attracting (acceptor) or electron-donating (donor) species. For example, polyacetylene films, when treated with certain dopants, e.g. I_2 , AsF_5 , etc., exhibit the highest conductivity observed for any covalent organic polymer (7). Polyacetylene is, however, both thermally and oxidatively unstable, and other highly conductive polymeric materials are being sought.

RESULTS AND DISCUSSION

Polyphthalocyanines

The reaction of four phthalonitrile units can produce a phthalocyanine nucleus either when heated neat or in the presence of a metallic additive (Figure 1).

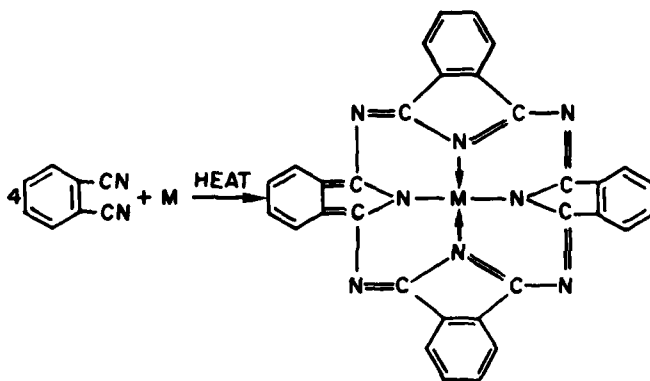


Figure 1

To utilize this reaction for polymer synthesis, two of these units must be linked together. Self-condensation of such a resin would yield an infinite network polyphthalocyanine (Figure 2). In order to achieve the free movement of electrons throughout the system and thus conductivity, the linking structure (R) must also be completely conjugated. Several different approaches have been pursued in an attempt to produce a highly conductive polyphthalocyanine.

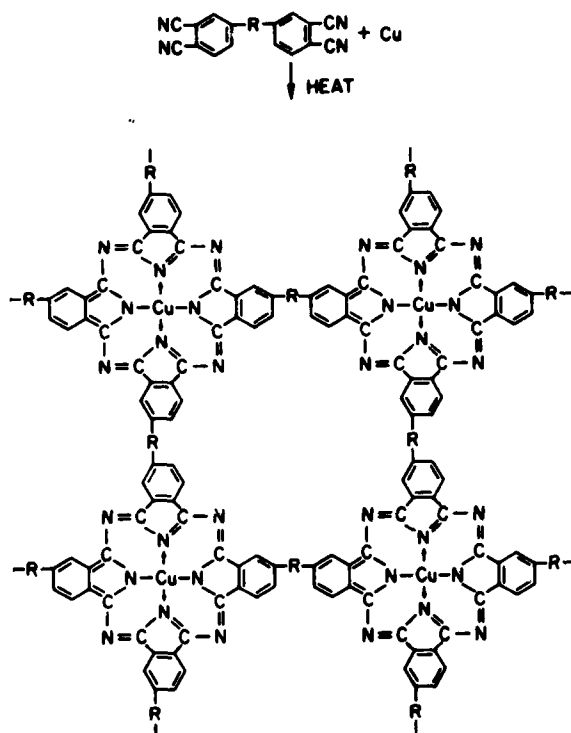
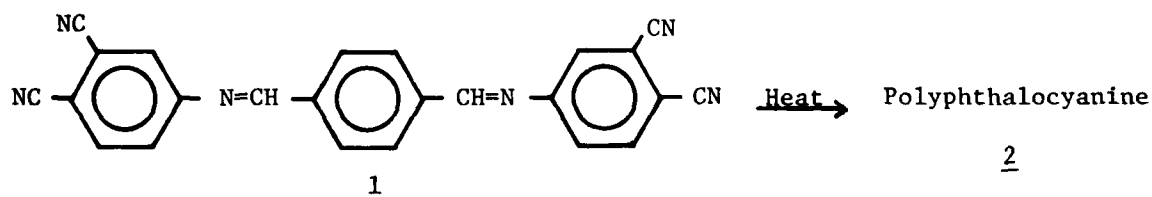


Figure 2 - Bis(phthalonitrile) Polymerization Reaction

The dianil phthalonitrile monomer 1 can be polymerized by simply heating it above the melting point, usually at 280-300°C for 24 hours. At this stage, the polyphthalocyanine is a dark brown solid and is an electrical insulator



as determined by the four-probe DC conductivity method (8,9). Conductivity studies on postcured materials reveal that little change occurs below 450°C. However, at this temperature, the cyano moieties have completely reacted as determined by the absence of the cyano absorption peak ($\sim 2240\text{cm}^{-1}$) in the infrared spectrum. As the temperature is slowly increased, there is a corresponding enhancement in the conductivity that can be attributed to the polymeric chains becoming more highly ordered and/or more closely packed. For example, at 500°C, resistivity rapidly drops to 10^5 ohm-cm and continues to decrease with time, leveling off at 10^2 - 10^3 ohm-cm after 800 hours at this temperature.

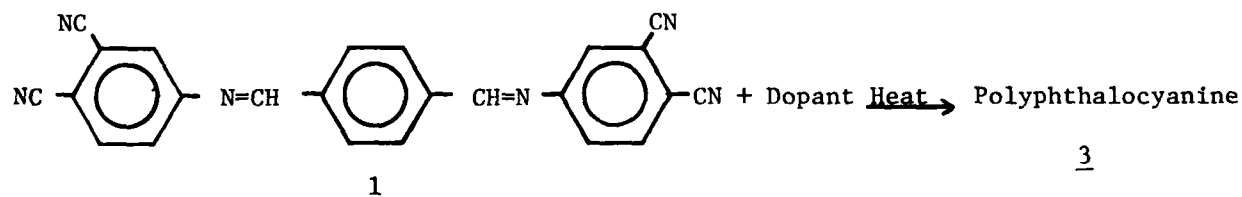
When a metal is reacted directly with a phthalonitrile monomer, there is always some unreacted metal due both to a density difference and to gelation occurring before a high molecular weight polyphthalocyanine has completely

formed. The stoichiometry of the reaction requires two resin molecules per metal atom for incorporation of a covalent-bonded metal atom into each phthalocyanine nucleus (Figure 2). Since the polymerization occurs even in the absence of metals, one has the option of using less than stoichiometric amounts. The insertion of metal atoms into only a few of the phthalocyanine rings may be sufficient to modify the electrical properties of the polymer.

To learn the effect of a metal on the conductivity of a polyphthalocyanine, two experiments were devised in which the metal is dispersed throughout the resin system. A stoichiometric amount of phthalonitrile 1 and activated copper was stirred at 150°C in dry dimethyl sulfoxide in an inert atmosphere until the copper had completely dissolved. The isolated brown powder, which was an insulator, was slowly heated to 500°C in a sealed tube. The resistivity of a pressed pellet prepared at 18000 psi was 10^4 ohm-cm. Next, a sample of phthalonitrile 1 was heated at 300°C until the melt became extremely viscous. After cooling and pulverizing to a fine powder, the prepolymer was thoroughly mixed with a stoichiometric quantity of activated copper. The mixture was heated at 300°C in an inert atmosphere until gelation had occurred. The temperature was then slowly increased to 500°C where it was held for 65 hours. Visual inspection of the sample showed that the copper had not completely reacted but was dispersed throughout the system. However, the sample did have a resistivity of 10^1 ohm-cm which was a 10^4 fold decrease relative to the corresponding metal-free polyphthalocyanine.

Doped Polyphthalocyanines

It has been observed that partial oxidation of a number of metal and metal-free phthalocyanines with iodine yields mixed-valence solids with high electrical conductivity (10,11). Consequently, several polymerization reactions involving phthalonitrile 1 and dopants, e.g. I_2 , SnI_2 , and SnI_4 , were carried out in an attempt to enhance the conductivity of the polymer.



In all cases, 1 and the dopants were sealed in evacuated, thick-walled tubes and postcured at elevated temperatures. The results are shown in Table 1. It was found that iodine does not increase the conductivity, which probably indicates that it is not being incorporated into the polymeric system. However, SnI_2 and SnI_4 do markedly affect the conductivity with iodine being liberated, as expected, when the latter salt was used. Perhaps the iodine molecule is too large to become entrapped within the framework of a highly crosslinked polymer, whereas the metal atom becomes chemically bound within the cavity of the phthalocyanine ring.

In an attempt to incorporate iodine within the matrix of a polyphthalocyanine, less highly crosslinked polymeric systems were investigated. For example, crosslinking can be diminished by copolymerization of dianil phthalonitrile 1 and phthalonitrile. When this reaction was performed in the

presence of iodine, an enhancement in conductivity was observed (Table 2), which suggests some complexation of iodine with the completely conjugated system.

Table 1
Dopant Effect on the Resistivity of
Postcured Dianil Polyphthalocyanine

<u>Dopant</u>	<u>Temp. °C</u>	<u>Resistivity (ohm-cm)</u>
None	450	$>10^8$
I ₂	450	$>10^8$
SnI ₂	450	4.1×10^6
SnI ₂	500	2.4×10^3
SnI ₂	520	2.9×10^1
SnI ₄	500	5.2×10^3 (Pellet)

Table 2
Dopant Effect on the Resistivity of Postcured
Copolymers of Dianil Phthalonitrile 1 and Phthalonitrile

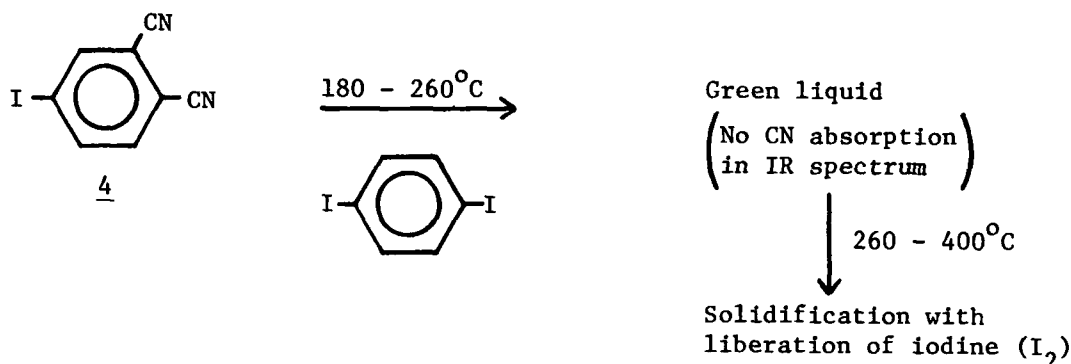
<u>Dianil Phthalonitrile (Mole)</u>	<u>Phthalonitrile (Mole)</u>	<u>Dopant</u>	<u>Temp. °C</u>	<u>Resistivity (ohm-cm)</u>
1	None	I ₂	450	$>10^8$
1	2	I ₂	450	1.4×10^5 (Pellet)
1	4	None	450	$>10^8$
1	4	I ₂	450	1.8×10^5 (Pellet)
None	1	I ₂	450	1.5×10^3 (Pellet)

Polyphthalocyanines through Free Radical Coupling

Even though phthalocyanine formation is believed to be the principal reaction during the polymerization of a compound terminated by a phthalonitrile unit, other cyano-addition reactions can be envisioned involving divalent 3-diminoisoindoline intermediates (12). For phthalocyanine formation to occur, four of these intermediates must interact followed by cyclization which might be extremely difficult in a rigid system such as the dianil monomer 1. Moreover, gelation, which greatly reduces the mobility of the individual molecules, may occur before four phthalonitriles have

reacted. Thus, other reaction pathways may be less energetic and more prominent.

In order to dramatize the effect of the phthalocyanine ring on the conductivity of a network polymer, a stepwise polymerization reaction was investigated. When p-diiodobenzene, which acts as both solvent and reactant, and 4-iodophthalonitrile 4 were heated at 180°C for 66 hours in a thick-walled, evacuated tube, a green color formation took place, presumably due to formation of tetraiodosubstituted phthalocyanine.

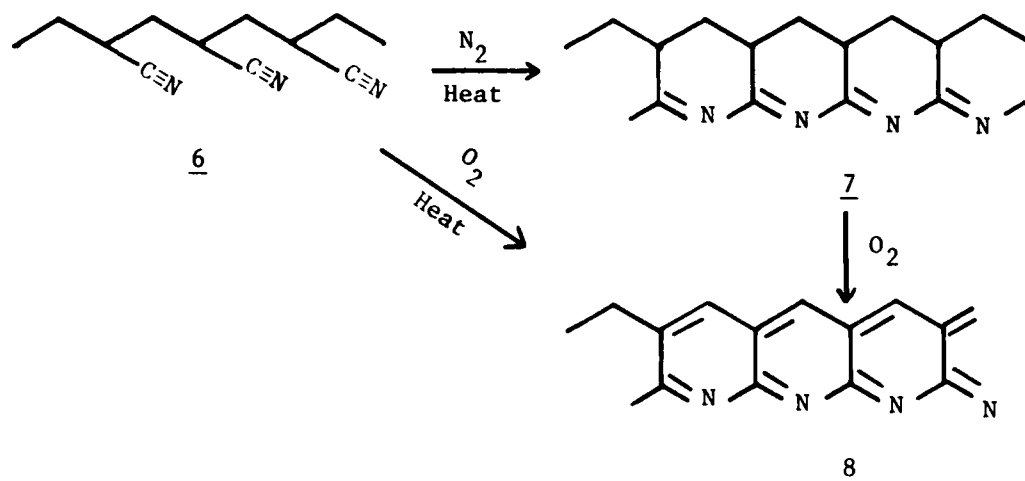


Further heating resulted in the evolution of iodine at 280°C and solidification at 300°C. The release of iodine produces aromatic radical units from either 4-iodophthalonitrile 4 or p-diiodobenzene which can combine to form a highly conjugated network polyphthalocyanine. The resistivity values for the sample heated at 300°C for 70 hours and at 400°C for 96 hours are 10⁵ ohm-cm and 10⁴ ohm-cm, respectively.

Pyrolysis of Polyacrylonitrile

High molecular weight polyacrylonitrile (PAN) was prepared (13) and its thermal degradation was investigated. Below 200°C, the material remains essentially unchanged. As the temperature is raised, progressive color changes from yellow to red to brown to black occur. With the onset of color, the material becomes insoluble in dimethylformamide. Infrared absorption spectra of these residues indicate that as heating progresses the cyano absorption at 2220 cm⁻¹ disappears with concurrent appearance of a strong absorption at 1580 cm⁻¹ assigned to C=N units.

The course of the pyrolysis is speculative, but it appears that the major reaction is the formation of naphthyridine-like structures. It is believed that PAN undergoes the following changes (14):



When PAN is heated to 300°C either in an inert atmosphere or in an evacuated sealed tube, nitrile cyclization occurs to produce a carbon-nitrogen conjugated system. The resistivity of the material was too high to measure by the four-probe method. On exposure to methyl iodide at 300°C, a tremendous reduction in the resistivity was achieved ($\rho = 3.9 \times 10^4 \text{ ohm-cm}$). For comparison purposes, the resistivity of 8 has been reported as $5 \times 10^8 \text{ ohm-cm}$ at 400°C (15). Further work is planned on doping both the cyclized form 7 and the oxidized form 8.

CONCLUSIONS

A series of experiments were carried out in an attempt to enhance the conductivity of dianil-linked polyphthalocyanine. A stoichiometric amount of activated copper dispersed in the polymer and co-reacted increased the conductivity by $10^4 \text{ ohm}^{-1}\text{-cm}^{-1}$. Similarly, incorporation of SnI_2 and SnI_4 improved the conductivity. The results from the copper experiment are especially encouraging and other experiments employing powdered copper are planned.

Iodine as dopant was found to enhance the conductivity of both the dianil-linked polyphthalocyanine in certain instances and the pyrolysate produced from PAN. The dianil phthalonitrile monomer cured in the presence of iodine exhibited no improvements in conductivity. However, when the cross-linking network was diminished by incorporation of phthalonitrile, an increase in conductivity was observed.

REFERENCES

1. D. J. Berets and D. S. Smith, *Trans. Faraday Soc.*, **64**, 823 (1968).
2. G. M. Holob and P. Ehrlich, *J. Polym. Sci., Polym. Phys.*, **15**, 627 (1977).
3. H. Akamatu, H. Inokuchi, and Y. Matsunaya, *Bull. Chem. Soc. Japan*, **29**, 213 (1956).

4. J. S. Miller and C. H. Griffiths, J. Am. Chem. Soc., 99, 749 (1977).
5. J. L. Petersen, C. S. Schramm, D. R. Stojakovic, B. M. Hoffman, and T. J. Marks, J. Am. Chem. Soc., 99, 286 (1977).
6. W. D. Gill, W. Bludau, R. H. Geiss, P. M. Grant, R. L. Greene, J. J. Mayerle, and G. B. Street, Phys. Rev. Lett., 38, 1305 (1977).
7. C. K. Chiang, M. A. Druy, S. C. Gau, A. J. Heeger, E. J. Louis, A. G. MacDiarmid, Y. W. Park, and H. Shirakawa, J. Am. Chem. Soc., 100, 1013 (1978).
8. L. B. Valdes, Proc. I.R.E., 42, 420 (1954).
9. W. R. Runyan, "Semiconductor Measurements and Instrumentation", McGraw-Hill Book Co., New York, 65 (1975)
10. J. F. Myers, G.W.R. Canham, and A.B.P. Lever, Inorg. Chem., 14, 461 (1975).
11. R. Taube, Pure Appl. Chem., 38, 427 (1974).
12. K. Venkataraman, "The Chemistry of Synthetic Dyes", Academic Press, New York, 283 (1971).
13. W. R. Sorenson and T. W. Campbell, "Preparative Methods of Polymer Chemistry", Interscience Publishers, Inc., New York, 168 (1971).
14. A. V. Topchiyev, M. A. Geyderikh, B. E. Davydov, V. A. Kargin, B. A. Krentsel', I.M. Kustanovich, and L. S. Polak, Chemistry and Industry, 184 (1960).
15. M. A. Geiderikh, B. E. Davydov, B. A. Krentsel', I.M. Kustanovich, L.S. Polak, A. V. Topchiev, and R. M. Voitenko, J. Poly. Sci., 54, 621 (1961).

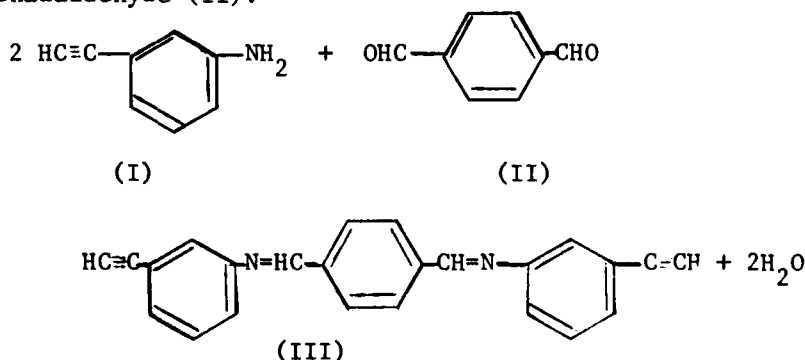
ELECTRICAL CONDUCTIVITY OF NETWORKS DERIVED FROM ACETYLENE-TERMINATED DIANIL PREPOLYMERS

Theodore R. Walton
Polymeric Materials Branch
Chemistry Division

INTRODUCTION

During the past several years we have had an interest in highly aromatic network polymers (1). By designing the prepolymer to have a conjugated structure between reactive end groups which chain extend and crosslink through reactions that form additional conjugated and/or aromatic connecting structures, a completely conjugated polymer network can be formed. In our earlier work, the conjugated prepolymers end-capped with ortho-dinitrile groups were converted to a structure that is consistent with a polyphthalocyanine (2). These conjugated polyphthalocyanines exhibited high thermal stability and electrical conductivity that could be varied from that of an insulator to a semiconductor (3).

This paper reports a similar study of a prepolymer end-capped with terminal acetylenic groups. The new resin, N,N'-(1,4-phenylenedimethylidyne) bis(3-ethynylaniline) shown as structure III, is readily synthesized in high yield by the reaction of 2 moles of 3-aminophenylacetylene (I) with 1 mole of terephthalaldehyde (II):



The resin melts at about 139°C and on continued heating at 150°C for a few hours, slowly solidifies into a hard black solid. The strength and conductivity of the polymer are increased by postcure at elevated temperatures.

EXPERIMENTAL

Monomer Synthesis

(a) A solution of terephthalaldehyde (13.4 g, 0.10 mole) in toluene (300 ml) was added dropwise over a 1-hr period to a stirred, refluxing solution of 3-aminophenylacetylene (24.6 g, 0.21 mole) in toluene (200 ml). A slight excess of the 3-aminophenylacetylene was used to insure reaction of both aldehyde groups. After 26 hours, 3.5 ml of water (theory, 3.6 ml) had been isolated from the reaction. Further refluxing did not produce more water. The mixture was filtered hot, and the filtrate volume reduced to 100 ml. Upon cooling, 30.4 g (91.6% yield) of crude III was obtained. Recrystallization from abs. ethyl alcohol (95% recovery) gave a product melting at 138.5–139.5°C.

(b) A solution of terephthalaldehyde (1.34 g, 0.01 mole) in dry acetonitrile (32 ml) was added at room temperature over a 10-minute period to a stirred solution of 3-aminophenylacetylene (2.45 g, 0.021 mole) in dry acetonitrile (20 ml). Stirring was continued at room temperature for 6 hours, the solution filtered through a drying agent (anhydrous Na_2SO_4) to remove the water formed in the reaction, and the solvent stripped off. Recrystallization (abs. ethyl alcohol) gave an overall yield of III comparable to the synthesis in toluene.

The infrared spectrum (KBr pressed pellet) of III showed a strong acetylenic hydrogen absorption at 3280 cm^{-1} and the complete absence of any NH or carbonyl absorption. The imine -N=C- absorption was observed at 1620 cm^{-1} , consistent with values reported for extended conjugation (4). The elemental analysis results were: calculated; C = 86.71%, H = 4.86%, N = 8.43%, Found; C = 86.75%, H = 5.00%, N = 8.24%.

Polymerization

Because III melts into a free flowing, low viscosity liquid, it can be cast or molded using conventional polymer processing techniques. At 150°C, the liquid melt slowly increased in viscosity and changed in color from a light yellow to black. After approximately one hour at 150°C, the resin became a glassy solid. The cure was continued at 150°C for an additional hour, then postcured 1 hour at 200°C, 1 hour at 250°C and 50 hours at 300°C. The cure was done in a furnace with no attempt to exclude air. Weight loss during cure was less than 0.1%.

After this initial cure, the material could be removed without breaking from the aluminum planchet in which it was prepared. Its conductivity was less than $10^{-12}\text{ (ohm-cm)}^{-1}$. Further heating at higher temperatures produced a material with greater conductivity. Typically a cured sample approximately 1 inch in diameter and 0.1-inch thick was further heated under an inert atmosphere in a tube furnace or under vacuum in a sealed glass tube. If a sealed tube was used, it was evacuated and flushed with nitrogen or argon several times before final sealing. If the tube furnace was used, a stream of oxygen-free nitrogen or argon was passed through the 1-inch diameter

furnance tube at a flow rate of 50 ml/min. The outlet of the tube furnance was restricted with a capillary tube to reduce back diffusion of air. The heat up and cool down rate for the furnances were approximately 0.5°/min. After the 300°C cure in air, the sample was heated to 400°C for 100 hours, then 500°C for 100 hours, and then 600°C for 100 hours. Thus the 600°C sample had received the previous heat treatments and was not taken directly from the 300°C cure to 600°C.

Measurements

After each heat treatment measurements were made of sample weight, thickness, and electrical resistance. The sample resistance was measured with a Keithly 610A electrometer. The sample was sandwiched between soft conductive mats which were held between copper electrodes under a constant load of approximately 1.2 Kg. Resistivities were calculated from the measured resistance, sample thickness, and a conservative estimate of the contact area. The measurements were made in air and the apparatus was not shielded.

The reliability of the resistance determined with this apparatus was verified by measurements made on other conductive polymers and comparison with more refined procedures using shielding, guard electrodes, and a van der Pauw four-probe technique.

RESULTS

In Table 1 are summarized the results for heat treatment of the cured polymer. The 300°C results are part of the initial cure in air. It should also be emphasized that for a given heat treatment, the weight loss and shrinkage includes the values of the earlier heat treatments. The values in

Table 1

EFFECT OF POSTCURE-HEAT TREATMENT ON SAMPLE
WEIGHT LOSS, SHRINKAGE, AND CONDUCTIVITY

<u>Temp. °C</u>	<u>Time, Hrs.</u>	<u>Atm.</u>	<u>Weight Loss, %</u>	<u>Shrinkage, %</u>	<u>Conductivity (ohm cm)⁻¹</u>
300	50	air	<0.1	-	<10 ⁻¹²
400	100	Inert	4.4	3.2	<10 ⁻¹²
500	100	Inert	10.9	8.1	1.6 X 10 ⁻⁵
600	100	Inert	13.2	12.0	3.3 X 10 ⁰

Table 1 are the average for two samples through 500°C. The values for the 600°C treatment is for a single sample. There was no apparent decrease in material strength at these higher temperatures, and in fact, strength appeared to increase. Generally, crack-free samples were obtained even after the 600°C treatment.

DISCUSSION

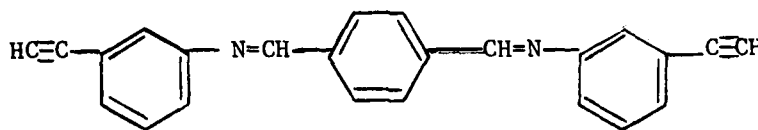
The literature is fairly abundant on the use of terminal acetylene groups as a polymerization site for preparation of high molecular weight polymers (5). In some of the initial work in this area, it was generally assumed that the cure reaction involved the trimerization of three acetylene groups into a benzene ring. However, work by Kovar, et al (6) and Herenrother (5) indicate that the trimerization reaction is probably minor and that the polymerization occurs by a number of simultaneous, complex reaction paths. It is expected that most of these reactions lead to aromatic or condensed aromatic rings, and conjugated linear chains which are probably further converted to aromatic systems at elevated temperatures. Thus the polymer structure can be depicted in only general terms. In Figure 2 we have made an attempt to do this, where the square blocks represent some undefined conjugated ring or chain formed from the reacting acetylenic groups. The concept we want to project here is that the prepolymer is completely conjugated, and if the cure process of the acetylene groups yields conjugated connecting and crosslinking groups, then the complete polymer system is represented by an extended conjugated network. This somewhat unique structure would be expected to confer high thermal stability and electrical conductivity, since, the delocalized π -electrons could provide both a source of charge carriers and a path of high mobility.

The weight losses in Table 1 indicate the high stability to thermal degradation exhibited by this polymer. Even in an air environment at 300°C for 50 hours, the polymer showed essentially no weight loss. At higher temperatures in an inert atmosphere some weight loss occurs, but even after the extended thermal treatment to 600°C, the total weight loss was only 13.2%. At present we do not know what this weight loss represents in terms of products or changes in the polymer structure. The physical appearance of the material is not obviously changed as a result of the thermal treatment. The sample undergoes some shrinkage, approximately 12% at 600°C, but the shape is undistorted and is essentially a smaller replicate of the original sample. The sample does not become fragile and a 0.1 inch thick sample can withstand considerable hand-held flexing force without breaking.

The fact that the material changes from an insulator to a semiconductor during the thermal treatment is indicative of important changes in the polymer structure. We believe that the increased conductivity results from an extension of the conjugated polymer network depicted in Figure 1 and the removal of impurities that serve as traps for the charge carriers. Because the temperature of the heat treatment did not exceed 600°C, graphite formation cannot be responsible for the increased conductivity. Attempts to obtain an infrared spectrum on a powder of the material has been unsuccessful because of the intense dark color of the polymer. The spectrum was nondescript with the only identifiable absorption occurring in the aromatic region at 1600-1500 cm^{-1} . It is hoped that other analytical techniques will determine if the material still has significant organic structure or has reverted to some form of elemental carbon. Because of the integrity and strength of the material, we favor an organic crosslinked polymeric structure.

SUMMARY

A new prepolymer, N,N'-(1,4-phenylenedimethyldiynyl)bis(3-ethynylaniline), has been prepared in high yield:



It is converted through the terminal acetylene groups into a conjugated polymer network by heating it in its molten state at 150°C for a few hours and finally at 300°C for 50 hours. Further heating in an inert atmosphere at higher temperatures results in an increase in the electrical conductivity ($3.3 \times 10^0 \text{ (ohm-cm)}^{-1}$ after 600°C). Weight loss at higher temperatures is also low (13% after 100 hours at 600°C) and appears to have no effect on the integrity of the sample.

Since the resin melts into a free flowing liquid at 140°C and polymerizes at 150°C with no evolution of volatiles, it is readily processable using conventional molding techniques. Once polymerized, the material possesses the inherent stability and solvent resistance characteristics of highly crosslinked polymers.

ACKNOWLEDGEMENTS

The author would like to express his appreciation and thanks to Charles M. Selwitz, Gulf Research and Development Company, for providing a sample of 3-aminophenylacetylene.

REFERENCES

1. (a) J. R. Griffith, J. G. O'Rear and T. R. Walton, "Copolymers, Polyblends, and Composites," ACS Advance in Chemistry Series No. 142, Edited by N. A. J. Platzer, 458 (1975), (b) T. R. Walton, J. R. Griffith and J. G. O'Rear, "Adhesion Science and Technology," Polymer Science and Technology, Vol. 9B, Edited by L. H. Lee, Plenum Press, 665 (1975), (c) T. R. Walton and J. R. Griffith, Applied Polymer Symposium No. 26, Edited by N. A. J. Platzer, John Wiley & Sons, 429 (1975).
2. T. R. Walton, J. R. Griffith and J. G. O'Rear, Org. Coatings and Plastics Chem., Preprints, 37 (2), 180 (1977).
3. J. P. Reardon and T. R. Walton, manuscript submitted for publication in "Synthetic Metals", Prof. F. L. Vogel, Ed., Elsevier, Publ.
4. "Infrared Spectroscopy", Robert T. Conly, 2nd Ed., Allyn and Bacon, Inc., 147 (1972).
5. D. M. Herenrother, Macromol. 11, 332 (1978) and references therein.
6. R. F. Kovar, G. F. L. Ehlers, and F. E. Arnold, J. Polymer Sci. 15, 1081 (1977).

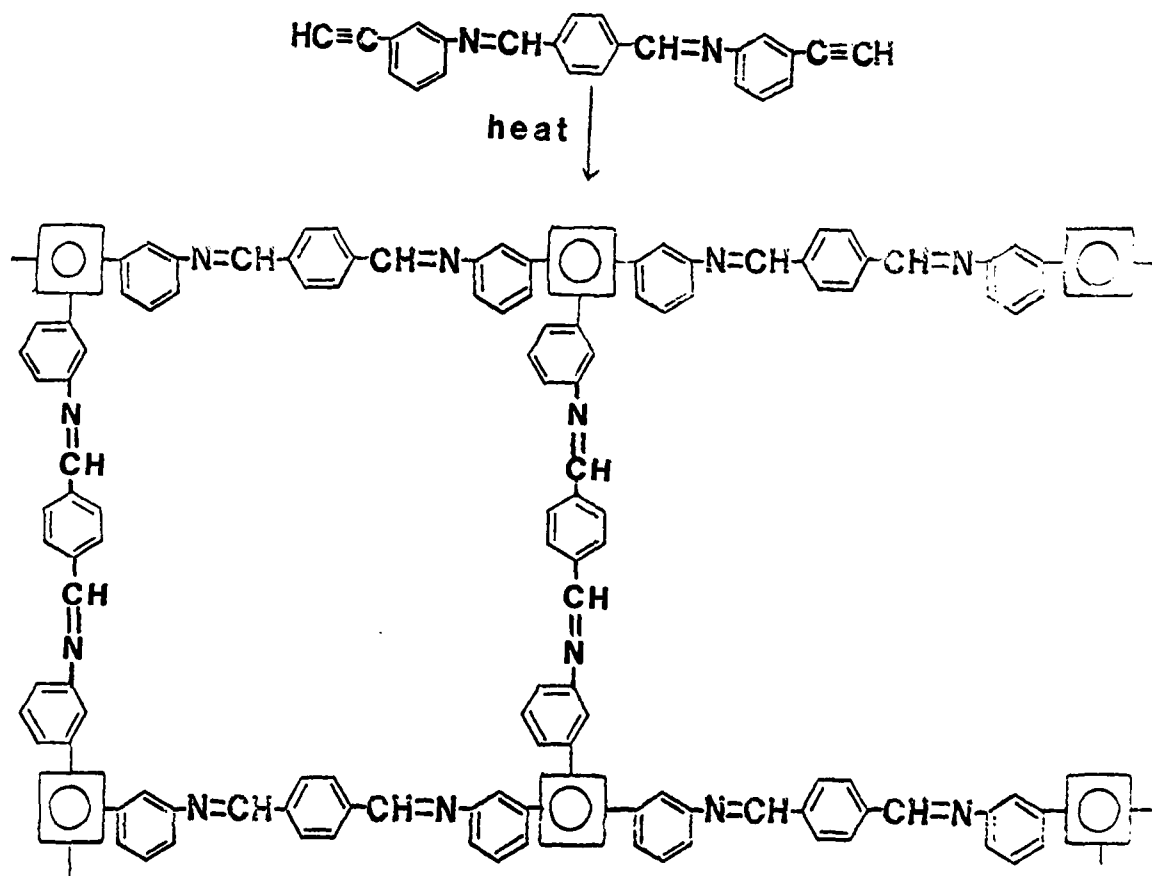


Fig. 1 - Polymerization reaction

¹⁹F NMR SPECTROSCOPIC AND RELAXATION STUDIES OF SbF₅, AsF₅, AND
OTHER INTERCALANTS IN GRAPHITE, GRAPHITE FIBERS, AND POLYACETYLENE

Henry A. Resing
Polymeric Materials Branch
Chemistry Division

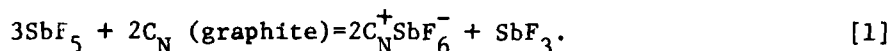
INTRODUCTION

The conductivities of the conjugated solids graphite and polyacetylene are increased several orders of magnitude to the level of copper by the solid "solution" of various electron donors or acceptors (1,2). At lower concentrations of donors/acceptors, useful semiconducting properties are evident (2) in polyacetylene. Graphite fibers show the properties of high tensile strength, low density, low coefficient of thermal expansion, and good thermal stability; these, and the anisotropic conductivity exhibited upon intercalation of electron acceptors (which promises a reduction of eddy current losses), make them potentially useful in power transmission applications (3). We seek here to find the chemical mechanism of action of "intercalants" in producing high conductivity graphite and polyacetylene and to assess the stability of these compounds; the principal tool we employ is Nuclear Magnetic Resonance (NMR).

Herein we use the term intercalation with respect to both graphite and polyacetylene to indicate the process of incorporation of foreign atoms or molecules in their respective solid states and call the incorporated matter the intercalant. For graphite, at least the structural location of the intercalated or "dissolved" entities is clear; they reside between the layers of the graphite. For polyacetylene the location of the dopant entities is still controversial; are they homogeneously distributed throughout the 400 Å diameter polyacetylene fibers or only on or near the surface thereof. But, aside from geometry, neither the chemistry (the reactions occurring on intercalation) nor the physics (mode of generation of charge carriers) of intercalation is clear, especially for those intercalants which accept electrons from the host and leave hole carriers on the host lattice. Thus the relation between the chemistry and the physics is unclear as well. A class of donors that has proven highly successful in raising conductivity for both polyacetylene and graphite consists of the group V pentafluorides, especially those of arsenic and antimony. We report here a group of ¹⁹F NMR studies, the purpose of which is to discover the chemistry of intercalation, or, at least, to test hypotheses (4) concerning this chemistry.

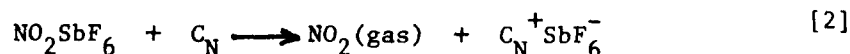
The plan of this report is as follows. In the remainder of the introduction we briefly present: (a) proposed intercalation reactions, (b) the opportunities presented by the NMR experiment, (c) a hypothesis made to interpret some of our early NMR spectroscopic results in terms of carrier concentration, and (d) additional questions we hope the data may answer. A brief experimental section follows. Then the ^{19}F NMR results for the various systems are presented and discussed, with division according to the group V element employed: antimony, phosphorus, and arsenic. Finally, a set of conclusions is assembled.

Intercalation may occur in several modes: as a result of a chemical reaction, by an electrochemical reaction, by ion implantation, or perhaps even by insertion of a neutral species. It is currently believed that AsF_5 enters polyacetylene as the molecule AsF_5 (5). In contrast, SbF_5 (and AsF_5 (6), *mutatis mutandis*) have been proposed (7) to enter graphite according to the reaction

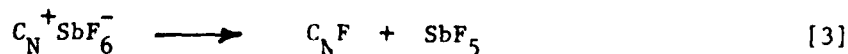


Suppose first that reaction [1] goes to completion and that the only intercalated species are the SbF_6^- ions. Under the assumption that every positive charge on the graphite lattice (right hand side of [1] represents a hole carrier, at the maximum degree of intercalation there would be about four times as many hole carriers in the graphite as are deduced from electronic transport measurements (4). This adverse situation can be relieved if reaction [1] does not go to completion, but leaves a match between the "proper" number of carriers and the number of SbF_6^- ions. To test these possibilities requires an analytical tool capable of looking inside the graphite to confirm or deny the existence of the species proposed on the basis of the models. Are SbF_3 , SbF_5 , and SbF_6^- all present in graphite or only some of them? Likewise, is AsF_5 the only species present in polyacetylene?

A mode of intercalation in which a chemical reaction definitely occurs is that in which the nitrosyl or nitryl salts of group V hexafluoro-anions (PF_6^- , AsF_6^- , SbF_6^-) react with the substrate as (8)



Clearly, by this reaction, one hole or positive charge is placed on the graphite lattice for each SbF_6^- anion so that electroneutrality is maintained. These materials also show a high conductivity that has not yet been studied in detail (9). Here one asks, however, the extent of fluorination of the graphite, i.e. does the reaction (10)



occur and thus reduce the number of positive charges on the graphite lattice? A reaction analogous to [2] may be performed on polyacetylene; and polyacetylene may be fluorinated as in [3] as well. Another reaction in these systems with high-vapor-pressure fluorides is attack of the glass container (as in NMR experiments) with resultant production of water; a cyclic fluorination and hydrolysis ensues with a buildup of SiF_4 in the ampoule.

There are some contrasts between the antimony and arsenic fluoride systems. SbF_5 is a viscous polymeric liquid at room temperature (11), while AsF_5 is a monomolecular gas. SbF_3 is solid, while AsF_3 is a monomolecular liquid. The states monomolecular, polymeric, and ionic imply differences in NMR behavior which may be of use in our analysis. The contrasts are such that intercalation of graphite with SbF_5 takes weeks, while that with AsF_5 takes hours.

For intercalated graphite the unit of concentration is the stage, or number of layers of graphite between layers of intercalant, as determined by X-ray diffraction. Gravimetric measurements coupled with X-ray measurements show that when a given gallery or interlayer space is completely full with SbF_5 , the ratio of carbon atoms in the plane below, say, to the number of SbF_5 units is about eight. For a first stage compound (layers of graphite and of intercalant alternate) the overall composition is C_8SbF_5 ; for a second stage compound (two layers of graphite between layers of intercalant) it is $\text{C}_{16}\text{SbF}_5$; etc. Specimens of homogeneous composition, i.e. with stage uniform throughout the specimen, can be formed (12). A given range of external vapor pressure of intercalant corresponds to a given stage; the higher the pressure, the lower the stage (12). One might view the intercalant as a two dimensional gas or a two dimensional liquid, with a corresponding two dimensional pressure. Higher stages might be expected to have lower two dimensional pressures and hence be more mobile. For intercalated alkali metals X-ray studies do show two-dimensional ordered arrays (13).

Though polyacetylene shows a crystal structure by X-rays (14), from a more macroscopic point of view, the material consists of parallel strands of fibers, each about 40 nm in diameter. Concentrations of AsF_5 as high as $(\text{CH}(\text{AsF}_5)_{0.3})_x$ have been made. In Fig. 1 is shown the relative size of an AsF_6^- ion with respect to the chains of cis-polyacetylene viewed end on (14). It is immediately clear that there are in the lattice no interstitial spaces large enough to receive AsF_5 or AsF_6^- species. For low AsF_5 concentrations the intercalant may reside at lattice defects (vacancies, dislocation cores, etc.) but for $(\text{CH}(\text{AsF}_5)_{0.3})$ the distinction between host and guest is lost.

Ion implantation can also be used for intercalation (15). Here only monatomic ions can be loaded into the polyacetylene, and among these the fluoride ion has shown promise in giving conductivity increases. Here, the chemical fate of the ions is difficult to

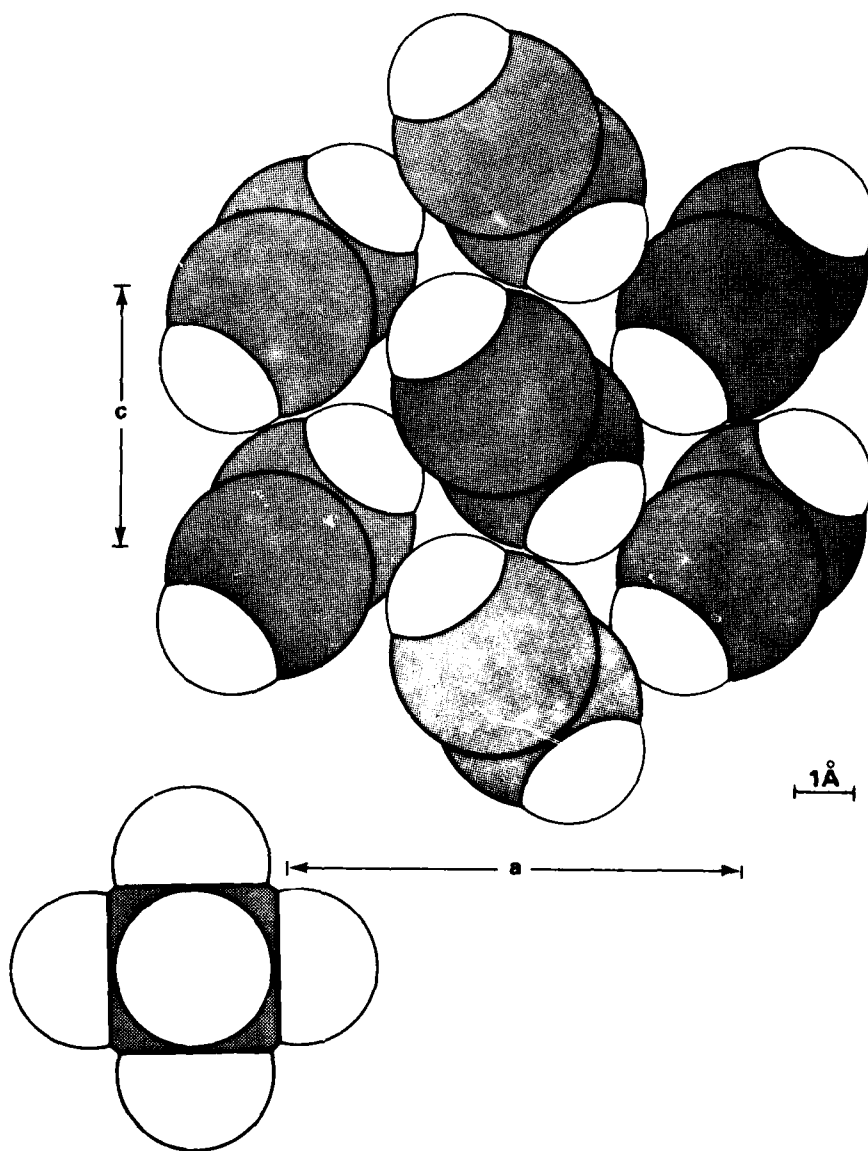


Fig. 1. Comparison of dimensions of MF_6^- ion (M=P, As, Sb) with those of polyacetylene. The MF_6^- ion is viewed along the four fold axis. The cis-polyacetylene chains are viewed end on, as adapted from ref. (14).

determine, although their geometric location is determined by the kinetic energy of the deposited ions. ^{19}F NMR may be helpful in such implanted systems. Are these mobile ions, F_2 molecules, or is the lattice fluorinated? A problem may well be the deposition of a sufficient fluorine density for adequate NMR signal in this case.

For the group V fluorides all of the nuclei ^{19}F , ^{31}P , ^{75}As , ^{121}Sb and ^{123}Sb can in principle be studied by NMR: the host should allow study of ^1H , ^{13}C , and perhaps ^2H as well. Of these, ^{19}F has intrinsically the highest relative NMR signal strength for the intercalants and ^1H for the host polyacetylene. In this report we concentrate on the ^{19}F NMR of the intercalated species using both spectroscopic and relaxation studies. NMR spectroscopy yields chemical shifts and coupling constants, both useful as fingerprints of chemical species. The coupling constant is rather unique in its ability to count the atoms in a local configuration. Relaxation studies provide estimates of jumping rates for rotation and diffusion, as well as measurements of inter-nuclear distances (from the strength of the magnetic dipolar interaction between nuclei). The diffusion information is useful in estimating stability, as it gives a measure of the tendency of the intercalated particle to reach the surface. The stability of spectroscopic features with time is also a measure of chemical stability. For instance the hydrolysis reaction produces SiF_4 which shows up in the NMR spectra. Because the conductivity of these intercalates is highly anisotropic, the NMR experiment is able to sample the bulk of the intercalate, unlike for three dimensional conductors where skin depth problems limit the penetration depth of the radio frequency radiation. Thus the NMR experiment is a valuable probe of intercalation chemistry.

It is clear that the central problem of intercalation chemistry is that of establishing the molecular and ionic species that actually exist within the substrate. Only if this chemistry is known can reasonable mechanistic interpretations of conductivity be made. We turn now to a preliminary interpretation of our first ^{19}F NMR spectra for the graphite- SbF_5 system (4) as an example of a hypothesis which relates NMR observations with the chemistry and electronic properties. We do this essentially to provide a jumping off place in terms of new experimental possibilities suggested by the data. We depend on the linewidth as the measure of molecular mobility, according to well established NMR theory (16). For molecules effectively not moving (jumping rates $< 10^5 \text{ s}^{-1}$) the linewidth can be calculated by theory (17,18) and is a measure of inter-atomic separation. For faster motion, the linewidth is inversely proportional to the jumping rate for "isotropic" motions (16).

In Figure 2 are displayed ^{19}F NMR spectra for first stage compounds of SbF_5 in graphite. Although the natural and synthetic graphites give rise to spectra that are somewhat different, both spectra show a narrow line sitting on top of a broad line, and both narrow and the broad lines

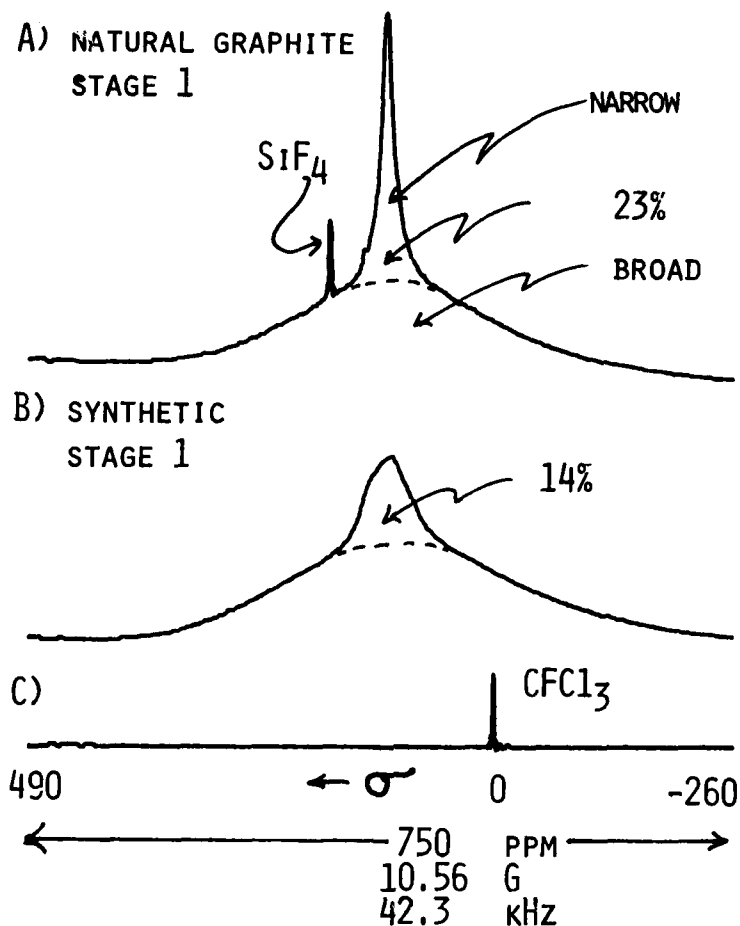


Fig. 2. Fluorine-19 NMR spectra of SbF_5 intercalated to stage I in natural (a) and synthetic (b) graphite. The fractional intensities of the narrow lines are indicated. The SiF_4 arises from hydrolysis of SbF_5 in the presence of glass. All spectra in this paper are referred to CFC1_3 as in (c). The scan width in three systems of units is indicated: parts per million (PPM); Gauss (G), and kilohertz (KHz).

are centered at about the same chemical shift in each case. These spectra and our preliminary interpretation are discussed more completely in the literature (4). In recapitulation, the narrow line represents a set of fluorine nuclei of higher mobility than those of the broad line. In the free liquid state it is known that SbF_5 is a long chain polymer (19); in the pure solid, it is a planar tetramer (20). The width of the broad line is consistent with an immobile (jumping rate for rotation or diffusion $> 2 \times 10^4 \text{ s}^{-1}$) SbF_5 molecule (monomer), linear polymer, tetramer, or even an immobile SbF_6^- ion. The width of the narrow line implies molecules both rotating and diffusing. Since the octahedral SbF_6^- ion is the most symmetric of the species in the intercalation reaction [1], it is the most likely candidate for the higher mobility implied by the narrow line, and we thus assigned the narrow line to the SbF_6^- ion. We assigned the broad line to the SbF_5 , and examined the consequences of these hypothetical assignments. The integrated intensities thus measure the relative numbers of fluorine nuclei represented in the broad and narrow lines, and we have counted the hole carrier density for the natural and synthetic graphite. In both cases it is the same within a few percent as that deduced from analysis of electromagnetic measurements (4), about 20%. Because of the ease of this NMR measurement of carrier density, we wish to confirm its validity; we have designed some tests of this broad-narrow line hypothesis, and we ask some other questions as well. (1) Does the fraction of SbF_6^- (per hypothesis, the narrow line intensity) depend on temperature? (2) Has equilibrium been established, i.e., does the SbF_6^- fraction depend on time? (3) Is there a difference between intercalation compounds for graphites of different history? (4) Is the product of intercalation the same in polyacetylene as it is in graphite? (5) Can MF_6 be inserted into the graphite lattice by other oxidation reactions? (6) Is the ^{19}F chemical shift a strong function of stage? (7) Or are any of the other NMR parameters such as lineshape, linewidth, or spin-lattice relaxation time strong functions of stage? (8) Can any of these NMR parameters be used to measure the stage of intercalation, and therefore perhaps, the crystallinity of graphite fibers? (9) What are the motions of the intercalated species?

This report represents the first phase of a parallel study of the group V fluorides in both polyacetylene and graphite. The intention is that what is learned in one system will suggest interpretations and experiments in the other. But the question is this: Is the mode of chemical action of the intercalants the same in both systems or are there fundamental differences? On the basis of the work reported here the only difference clearly apparent thus far is the rapidity of translational diffusion of the intercalant. The intercalant is orders of magnitude more mobile in the graphite than in the polyacetylene.

EXPERIMENTAL ASPECTS

For the graphite-SbF₅ system the graphite specimens were in the form of powders; equilibration with the SbF₅ occurred at temperatures ranging from 80 to 120°C. Stage was determined by X-ray analysis. Graphite fibers, polyacrylonitrile (PAN) and pitch based, were equilibrated with AsF₅ at room temperature; they were mounted with fiber axis perpendicular B₀ in the NMR experiment. Polyacetylene was prepared by the usual Ziegler-Natta catalyst procedure (21), and dosing was done by means of AsF₅ gas at reduced pressure. Reaction of polyacetylene as well as graphite powder with NOSbF₆ was carried out in dry solvent under inert atmosphere. Quantitative reaction of NO₂PF₆ with graphite powder was done under cover of solution. With the exception of the graphite-SbF₅ compounds, most of the specimens were not well characterized as to electrical properties, concentration, etc; they were for the purpose of rapid survey only.

A Bruker SXP NMR spectrometer was used as a fourier transform spectrometer. Spin-Lattice relaxation times were determined by the 180-t-90 method at 56.4 and at 26 MHz; relaxation plots for graphite-SbF₅ powders were nonexponential, and T₁ was taken at the 1/e point. The transverse relaxation plots were likewise nonexponential in some temperature regions; thus T₂ represents the 1/e point.

RESULTS AND DISCUSSION

Graphite - SbF₅ System. Several categories of information are provided: (a) fractional intensity of the narrow line of Fig. 2a as a function of temperature (Fig. 3); (b) spectra for various new preparations of first and higher stage compounds of SbF₅, as well as spectra for SbF₆⁻ and PF₆⁻ intercalants (Fig. 4); (c) relaxation times T₁ and T₂, as functions of temperature and frequency (Figs. 5 and 6). The data suite is as yet incomplete so that our conclusions are in some cases tentative. Thus our discussion is in terms of opportunities as well as in terms of conclusions. In general, however, the data reveal differences among the different nominally first stage preparations that we did not expect and have not yet explained.

In Fig. 3 is shown the temperature dependence of the fractional intensity of the narrow line for the natural graphite - SbF₅ compound of Fig. 2a (22). This dependence is most marked at room temperature, and the narrow line only reaches constant relative intensity above about 320K where it is about 2/3. This constant value implies a carrier concentration about three times that deduced from electrical measurements. Note here that the integrated intensity of the NMR spectrum is proportional to the number of nuclei in the effective sample volume; when all chemical species are homogeneously distributed the ratio of the integrated intensity of any spectral feature, to the total gives the fraction of nuclei contributing to that feature, i.e. to the narrow line, say. This relative intensity of the narrow line,

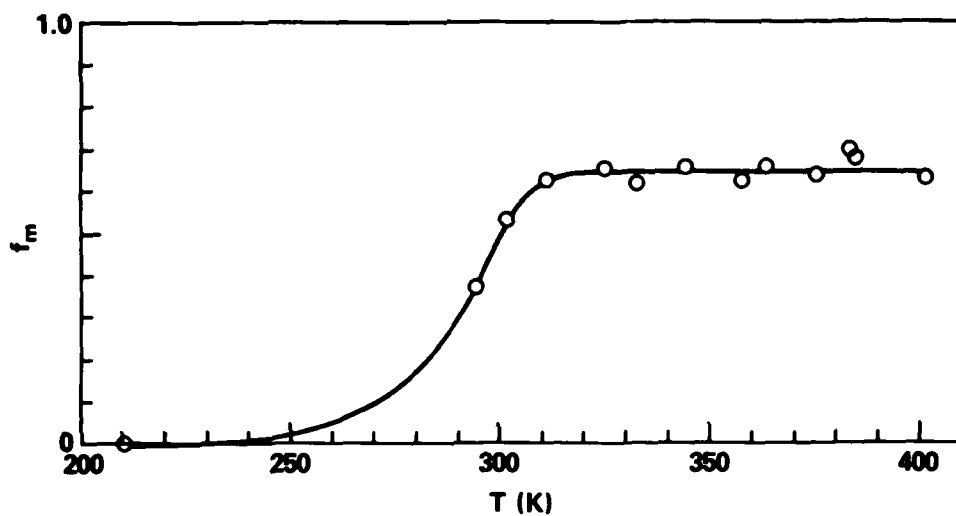


Fig. 3. For the graphite-SbF₅ stage I compound of Fig. 2A, the relative fractional intensity in the narrow line, i.e. the mobile fluorine fraction, f_m as a function of temperature.

coupled with the stoichiometry of stage I, allows the carrier density to be estimated under the joint hypotheses that (a) reaction [1] holds, and (b) there is a one to one correspondence between the narrow line intensity and the SbF_6^- ion concentration. For the synthetic graphite specimen of Fig. 2b the broad line disappears completely above 320K, in marked contrast. Furthermore, at about 0°C, the narrow central peak in the spectrum assumes the multiplet structure characteristic of liquid polymeric SbF_5 . This indicates the presence of the free liquid, most likely exterior to the graphite lattice because it does not seem likely that a polymer molecule could perform, between the graphite layers, the near isotropic motions required to give the narrow lines observed. To heighten the contrast, a spectrum representative of three newer preparations of first stage compounds of SbF_5 in the same natural graphite (Fig. 4b) shows no broad line at all at room temperature. Given this disparity of results, it is quite clear that the room temperature fractional intensity of the narrow line is not simply related to the carrier concentration as we earlier (4) hypothesized.

In connection with our discussion of relaxation times, further on, it becomes quite clear that in most of the graphite SbF_5 compounds (and in the other graphite compounds studied here as well) the molecular two dimensional translational diffusion is quite rapid, as the narrow line implies (16). As the sample is cooled, this motion and the rotational motion of the intercalant is slowed, and the lines must eventually broaden till the rigid lattice (17) value is attained. Now the line width (i.e., second moment) for the broad component in the spectra of Fig. 1 is already at a value consistent with expectations for a rotating SbF_5 (or SbF_6^-) molecule fixed in position in a two dimensional array of rotating SbF_5 units (4).

For the graphite-nitrate compound there has been found a liquid-solid transition for the intercalated nitric acid (23). For intercalated alkali metals, ordered arrays of metal atoms in the interlayer space have been found by X-ray methods (24). Thus it becomes possible that the broad component of SbF_5 spectra, representing a more rigid portion of the intercalated SbF_5 , corresponds to some ordered, solid-like array, and that the tendency toward formation of this solid depends on the degree of filling of the interlayer space. It is difficult to test this notion, because the attainment of compositional equilibrium in the graphite- SbF_5 system is quite sluggish; specimen equilibration requires weeks (9), and the degree of filling is not easily varied.

Spectra of a first stage reaction product of NO_2SbF_6 with graphite, of a stage II SbF_5 intercalate, and of the stage II reaction product of NO_2PF_6 with graphite are also compared in Fig. 4. That for the SbF_6^- ion (Fig. 4c) is almost identical in center frequency and width with the stage I SbF_5 intercalate immediately above it. That for the stage II SbF_5 intercalate (as well as for a stage III compound, not shown) gives a much narrower main line as well as a subsidiary

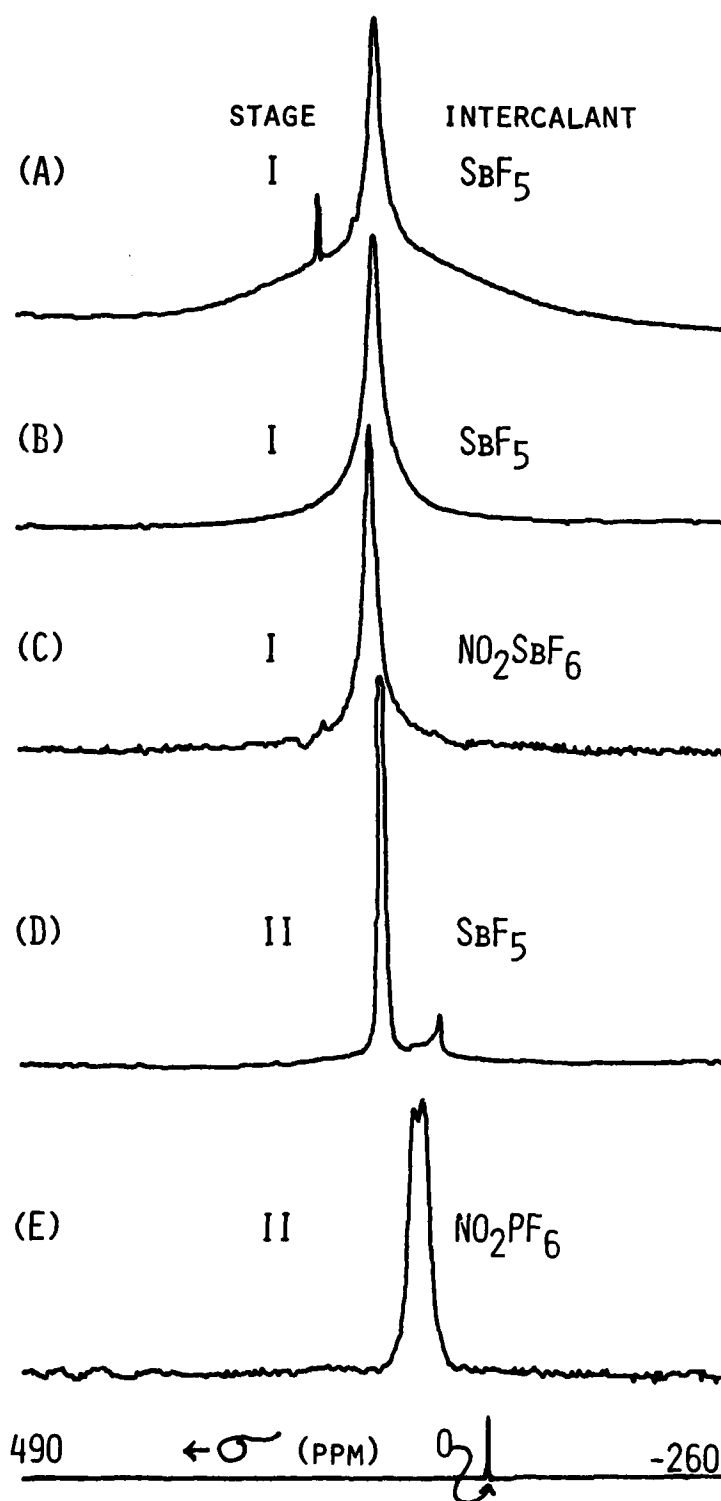


Fig. 4. Fluorine-19 NMR spectra for various group V fluoride intercalants ordinary in graphite at room temperature. The stage is indicated on the left, and the intercalant on the right.

spectrum at higher field (which on closer examination appears to be two lines of unequal intensity which bracket the shift expected for SbF_3). The last spectrum, for a graphite compound of composition approximately C_{16}PF_6 , consists of a doublet that is due to coupling of fluorine to the central ^{31}P nucleus. Since ^{31}P with spin $1/2$, has two equally populated energy levels, the attached ^{19}F nuclei divide themselves into two classes depending on which of these levels the ^{31}P to which they are attached finds itself. The splitting J_{PF} , called the coupling constant, is about 700 Hz and corresponds (25) to that seen for the PF_6^- ion in aqueous solution. This coupling is an interaction transmitted via the valence electrons in molecular orbitals, and actually gives us a method of counting the number of ^{19}F nuclei bonded to ^{31}P , as discussed below.

Since this spin-spin coupling interaction is so potentially valuable it may be instructive to inquire briefly into its use with the nuclei of antimony and arsenic which, like phosphorus, have magnetic moments and the associated sublevels. The coupling constants are of the order of kHz, i.e. as large or larger than in PF_6^- , so that we should have easily seen them on the basis of the resolution available, especially since six or eight line spectra should have resulted (i.e. the nuclear spin of ^{121}Sb is $5/2$, that of ^{75}As is $3/2$). But no splittings are apparent for the antimony fluoride species (Fig. 4) or for the arsenic fluoride species (Fig. 8, presented later). Observation of the multiplet requires that the fluorine nucleus remain attached to a second nucleus M for a time greater than J_{MF}^{-1} , and that while it is attached to the nucleus M, it must remain in one of its magnetic sublevels also for a time greater than J_{MF}^{-1} . Thus fast fluorine ligand exchange or rapid transitions among the sublevels of M (i.e. of As or Sb) lead to multiplet collapse (26). When nuclei with quadrupole moments (i.e. with spin greater than $1/2$) are situated at sites with lower than cubic symmetry (i.e. those at which electric field gradients exist), molecular or lattice motion modulates the electric field gradients; this may cause such rapid transitions among the nuclear sublevels that the coupling interaction may be averaged away. This is why the multiplet structure in the ^{19}F spectra of SbF_6^- and AsF_6^- has only been seen in cubic solids (27) and in solution in liquids of high dielectric constant (28). Now the octahedral ions MF_6^- are the most symmetric species postulated in the reaction schemes above as far as the intramolecular site symmetry of the central M atom is concerned (cubic symmetry). All of the other species have inherently unsymmetric central-atom sites, and ^{19}F splittings due to the central atom have not been seen for them in any phase. But the symmetric anion MF_6^- requires a counter charge on the graphite lattice. The MF_6^- ions are therefore sandwiched between positively charged graphite planes in a two-dimensional negatively charged fluid. The symmetry of this arrangement is less than cubic, and thus quadrupolar relaxation should average away the splittings expected in MF_6^- ions (M = As, Sb). Thus we will not be able to call upon the indirect nuclear dipolar coupling

(J coupling) to aid in assignment of intercalated antimony or arsenic fluoride species, and we are left with the chemical shift interaction and the direct nuclear dipolar interaction as NMR tools applicable to these species. For the PF_6^- ion, however, the J coupling is useful.

Unlike the spin-spin coupling, a completely intramolecular effect, the nuclear dipolar coupling is a through-space interaction of one nuclear magnet with another that couples all the nuclei of the body (29). Motion of nuclear magnets with respect to one another, e.g. by molecular rotation or diffusion, gives a time-varying magnetic field; Fourier analysis of this field allows assignment of its power to various frequency ranges. The power at the nuclear resonant frequency induces the transitions that allow the nuclear spin system to relax to thermal equilibrium with all the other degrees of freedom of the body; this is the spin-lattice relaxation process. The power in the frequency range close to zero frequency induces the transitions needed to keep the system of identical nuclear spins in internal thermal equilibrium (29); this is the spin-spin relaxation process. In homogeneous liquids and in solid single crystals each of these decay processes is exponential and can be characterized by a single parameter, the respective relaxation time. In polycrystalline solids each orientation has its own relaxation time and one observes a sum of exponential decays. This is known not to be a serious problem in cubic solids which turn out to be almost isotropic (30). But the motion of molecules between graphite layers is not isotropic, especially in so far as translational diffusion is concerned, and the relaxation time is a strong function of the orientation of the platelet normals with respect to the external large magnetic field direction (23). The theory for relaxation in two dimensional systems is unfortunately not complete (23). In summary, a proper relaxation study requires: (a) a system in which the molecular species are known; (b) a single graphite crystal, or at least a body in which the normals to the graphite planes are to a good approximation parallel to one another, and (c) a complete theory for relaxation due to diffusion in two dimensions. The theory is under development. An oriented specimen of the SbF_5 graphite system is under study. But what we are really trying to do is to survey a large number of random powder specimens, using an incomplete theory which is qualitatively correct, to get some clues as to the identity of chemical species between the graphite layers.

Spin lattice relaxation times T_1 for ^{19}F nuclei of SbF_5 in graphite are shown in Figs. 5 and 6. In Fig. 5, T_1 values for three stage I preparations are compared among themselves and with those of a stage II compound. The temperature dependence and T_1 values of the specimen that showed a broad and narrow line together at room temperature (as in Fig. 5A) are clearly different from those of the other stage I compounds. These latter show the T_1 minimum (as does the stage II compound) that is predicted by the theory appropriate to three dimensional solids. In Fig. 6, the T_1 values are seen to shift to lower values as the ^{19}F nuclear resonant frequency is changed from

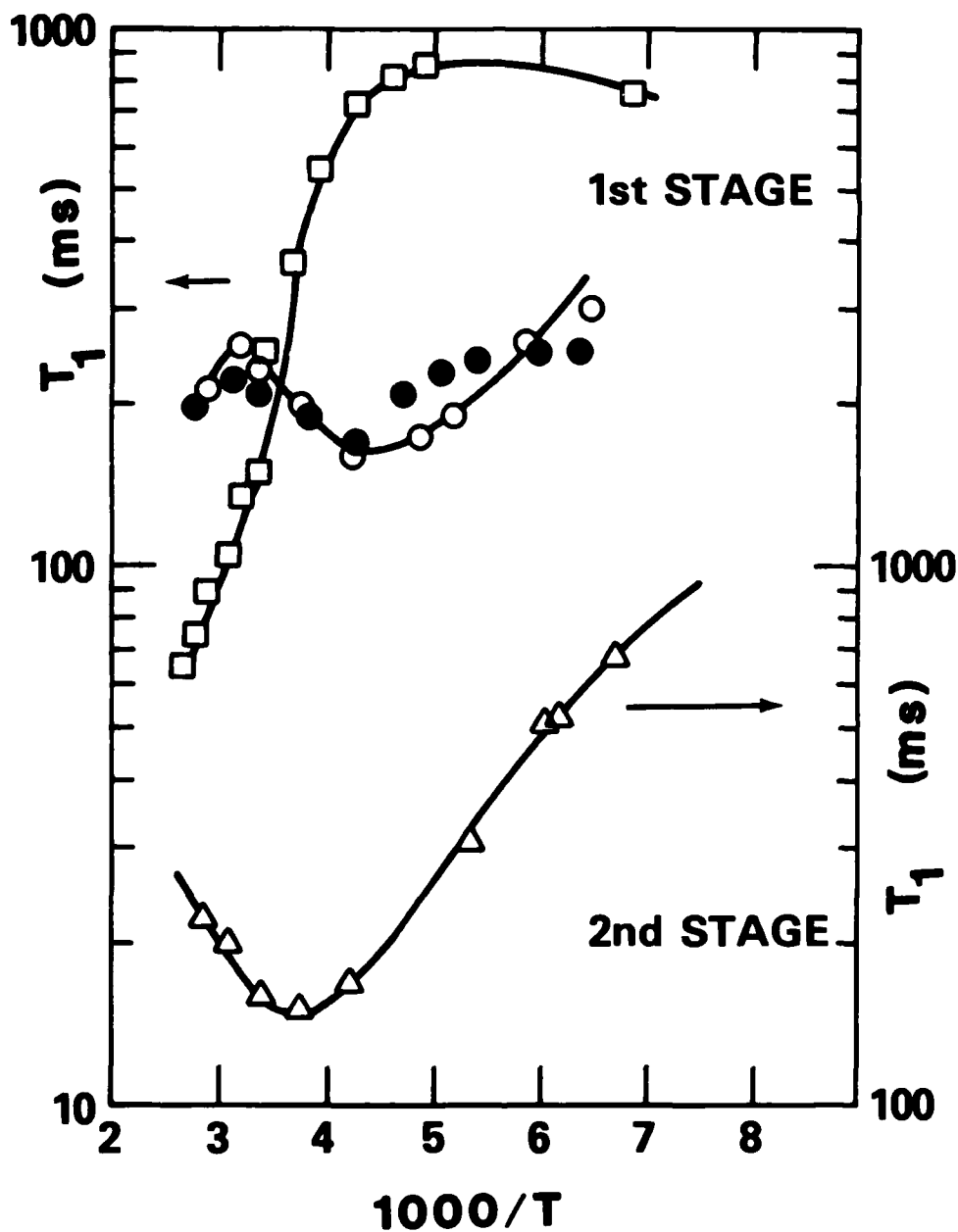


Fig. 5. Spin lattice relaxation times T_1 as functions of reciprocal temperature for various graphite-SbF₅ compounds. The scale T_1 for stage II (triangles) is on the right; for stage I is on the left. Squares: compound of Fig. 4a which showed broad and narrow lines at room temperature. Circles: specimen of Fig. 4b (open) and another stage I compound with the same lineshape (closed).

56.4 to 26 MHz (Fig. 6c); this shift is in accord with expectations based on "three dimensional" theory. Because the T_2 values shown in Fig. 6b are so large (i.e., near T_1), we know there is little power density of the internuclear magnetic field at zero frequency; that is we know that molecules are moving rapidly in space with respect to one another. At the minimum in T_1 we find from the relation $\omega\tau \sim 0.61$ (16) that the time between molecular translational jumps is about 6×10^{-9} s (ω is the resonant frequency). Thus we estimate the diffusion coefficient in the interlayer space to be about 10^{-6} cm²/s at room temperature with an activation energy for the diffusion process of 5 ± 1 kcal/mol. For a 0.1 mm diameter crystal this diffusion coefficient allows a molecule to reach the edge of the crystal once every 30 s on the average. The implication for long term stability of graphite conductors is that the intercalate, once formed, does not lock the intercalant in position, and that unless the edges of the graphite sandwich are sealed, or the whole composite somehow protected, reactive intercalants are readily available at the layer edges for degradation by and of the environment. Still, the differences in T_1 between the various stage I compounds are not yet explained. For the "anomalous" specimen in Fig. 5, the high temperature value of the spin lattice relaxation time T_1 is lower than any theory based on molecular motion can support, and is tending to lower values still. This anomalous downward trend in T_1 appears for the stage II compound as well (Fig. 6, A). Interaction of the nuclear magnets with paramagnetic centers (conduction electrons?) or with molecular rotational magnetic moments may play some role, but a final interpretation of this feature is not at hand. Our interpretation that the minimum observed in T_1 is due solely to the diffusion process is based on the fact that the mean square internuclear field strength deduced there (via the relation $T_1(\text{min}) = 3\omega/(2.84\gamma^2\Delta H^2)$, (16)) is only about one fourth of the total available. The remainder should then be available for modulation by molecular rotation to give another T_1 minimum at some lower temperature, as extrapolated schematically in Fig. 6d.

The NMR linewidth $\Delta\omega$ as in Figs. 2, 4, etc. is in some cases a measure of the transverse relaxation times, as $T_2 = (\Delta\omega)^{-1}$; the faster the motion, the narrower is the line and the longer is T_2 . However, in powders of irregularly shaped particles with large magnetic susceptibility, the linewidth actually observed may be due to contributions from this diamagnetic susceptibility. Thus the "narrowest linewidth" observed is indicated as T_2 (inhomogeneous) by the dashed line in Fig. 5g. The true transverse relaxation time, T_2 , may be recovered by the pulse sequence devised by Carr and Purcell (31), and the T_2 values determined in this way are shown in Fig. 6. Note that T_2 rises with temperature, goes through a maximum and then decreases with temperature as at Fig. 6b. The theory for relaxation due to motional processes predicts T_2 to rise with temperature. The fall (Fig. 6b) at higher temperature is explainable as due to fluorine exchange between a mobile (long T_2) species, i.e. SbF_5 or SbF_6^- , and some relatively immobile fluorine species, perhaps SbF_3 or fluorine bound to the lattice; the

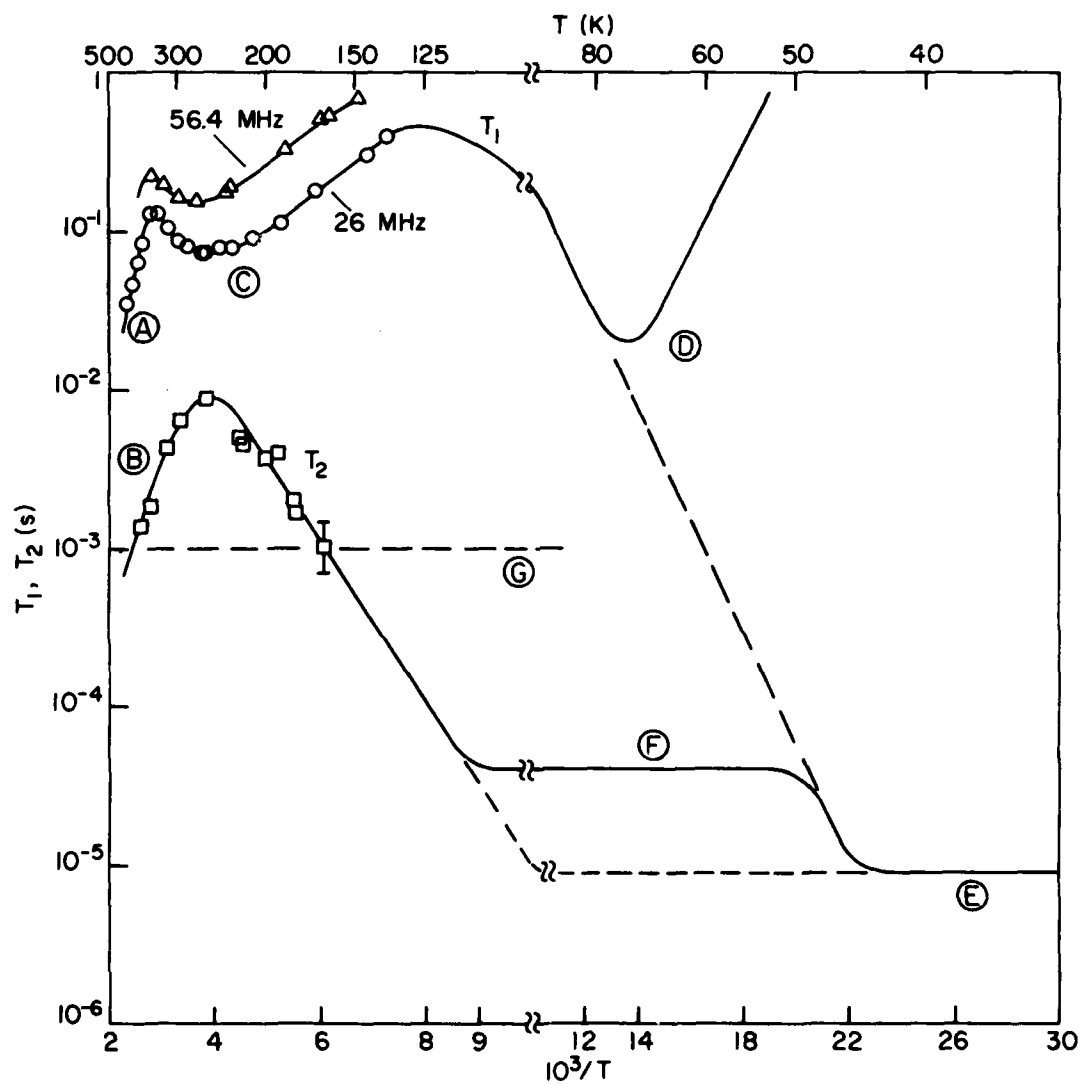


Fig. 6. Relaxation times T_1 and T_2 vs. reciprocal temperature for ^{19}F nuclei of a stage II graphite- SbF_5 compound, i. e. that of Fig. 4d. T_1 values at 56.4 and 26 MHz are indicated. See text for explanation of letter codes.

measured T_2 value in this region is a lifetime against exchange (32). Somewhat aside, there even exists an NMR method for determining the exchange rate between the broad and narrow lines of Fig. 2 (33). Raising the temperature may give rise to yet another kinetic effect, a coalescence of the lines due to different species, say those of Fig. 4d, caused by rapid chemical exchange (34). Lowering the temperature may quench chemical exchange processes and cause the appearance of new spectral features not apparent at room temperature (34). Finally, at lower temperatures T_2 should decrease in two stages (Fig. 6e and f) if molecular rotation and diffusion have vastly different activation energies. In the temperature regions E and F (Fig. 6) where T_2 is independent of temperature, mean square internuclear distances may be estimated from T_2 (17).

The chemical shift remains as the most direct indicator of the variety of species present, yet for most of the SbF_5 spectra of Fig. 4, there is a single sharp peak which occurs at shifts in the range 111-119 ppm, depending on the specimen. This range includes the shift of pure SbF_5 and that of the SbF_6^- ion (4) so that we cannot say that either species is present alone. We can say, since only a single line is observed, that if both these species are present, they are exchanging rapidly enough so that only a single line is observable. By the same token we can say that when we see a broad and narrow line (Fig. 4a) or a set of sharp lines (Figs. 4d, e) that the fluorine nuclei are not rapidly sampling the set of environments or of chemical shifts. Since we suspect rapid chemical exchange processes at room temperature, perhaps we can quench the exchange process at lower temperature. But there, the nuclear dipolar line broadening may limit our resolution. However, there is a technique which should recover the resolution, a technique which disposes of the uninteresting dipolar width and leaves only the chemical shift; this is the multiple pulse line narrowing technique (35). This technique will put the immobile species SbF_3 , graphite fluoride, SbF_5 polymer on an equal footing with the room temperature mobile species; at the lower temperature they will all be immobile and will respond to the spectrometer in the same way.

In summary, experiments at this point are well begun. The difficulty of sample irreproducibility has been met and not yet accounted for. Preliminary estimates of molecular diffusion coefficients have been made, and limitations on stability have been shown. We don't know the species between the graphite layers, but we know how fast it moves. Many experimental avenues remain open. Among these are: work with highly oriented pyrolytic graphite specimens (specimen in hand); work at temperatures down to 20 K (equipment in calibration), to include spectra and various relaxation measurements; and development of two-dimensional relaxation theory.

The Graphite - NO_2PF_6 - Intercalation System. The doublet pointed out previously in Fig. 4e for this specimen shows that for the PF_6^- ion, a clear identification of intercalated species based on NMR coupling

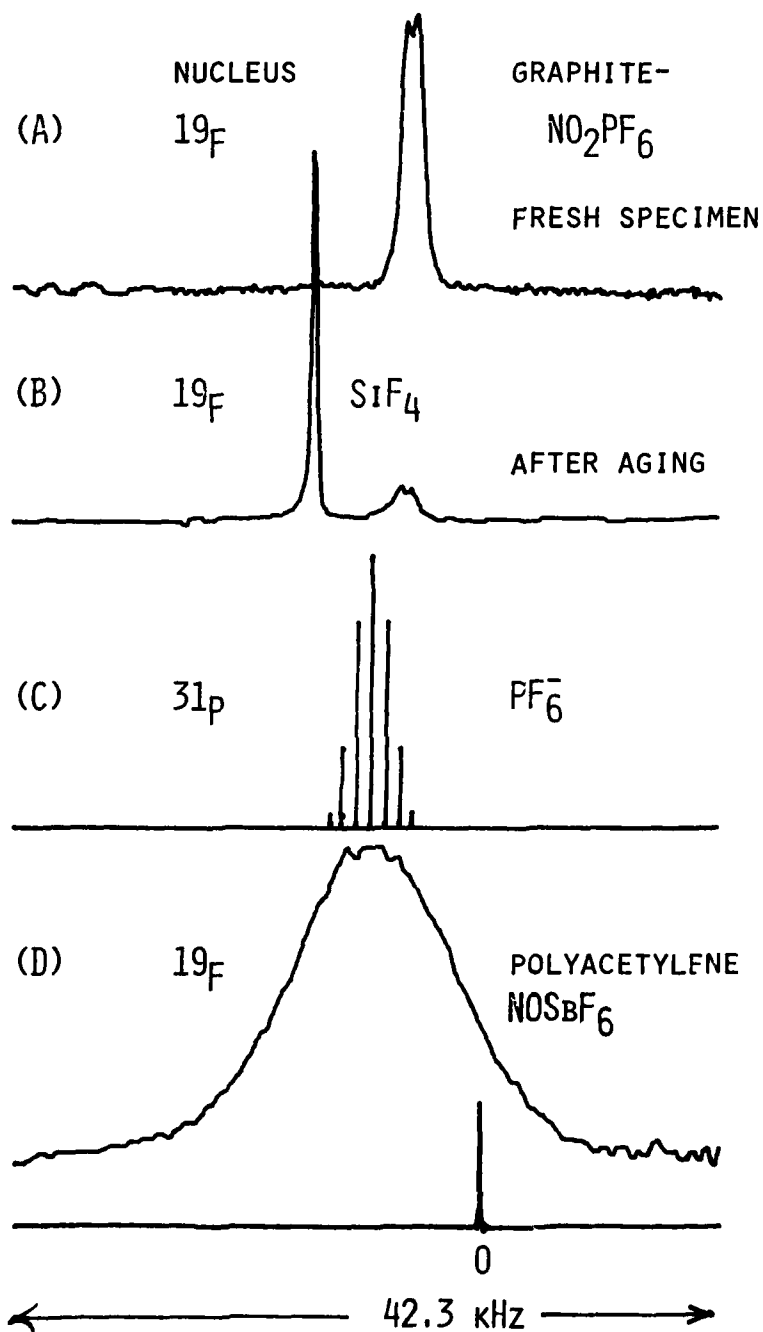


Fig. 7. Fluorine-19 NMR spectra for a graphite- PF_6^- Stage II compound, (a) and (b) and for a polyacetylene- SbF_6^- compound (d). The theoretical phosphorus-31 spectrum for the PF_6^- ion is indicated at (c). The scan width in kHz applies to all spectra.

constants is possible. Therein lies our prime interest in this compound, although it also is reputed to be of high conductivity (9). Fig. 7b shows that over a period of time this compound reacts with the glass ampoule to form SiF_4 , presumably due to traces of water or HF.

The doublet implies that all ^{19}F are equivalent and are bound to a nucleus of spin 1/2, i.e. to phosphorus. But we can use this same coupling to actually count the number of equivalent fluorines bound to the phosphorus. We do this by recording the ^{31}P NMR spectrum. A theoretical spectrum for six fluorines bound to phosphorus (based on the literature values of the $^{31}\text{P} - ^{19}\text{F}$ coupling constant for aqueous PF_6^-) is given in Fig. 7c. The spectrum contains seven lines symmetrically disposed with splitting J_{PF} and with binomial intensity. For PF_5 the spectrum would only contain six lines with a different splitting. We have just carried out this experiment and verified that the PF_6^- ion is the only species present (25).

Fig. 7d shows the ^{19}F spectrum for polyacetylene doped by reaction with NOSbF_6 . The linewidth is practically the same as for polyacetylene doped with AsF_5 (to be discussed below), and the presumption is that if PF_6^- were doped into polyacetylene each line of the ^{19}F doublet or of the ^{31}P septet (or sextet) would have the same broadening as seen in Fig. 7d. This would of course render these multiplets unresolved and thus render this identification scheme, based on multiplet structure and splitting, unusable in polyacetylene. We presently believe that the ^{19}F linewidth for the SbF_6^- ion (or whatever) is due to surrounding protons of the polyacetylene structure. Thus we have under synthesis deuterio-polyacetylene doped with PF_6^- , SbF_6^- , and AsF_5 . If the line narrows by a factor of 1/6 on deuteration as compared to Fig. 6d, then protons are indeed the source of linewidth. And this narrowing should be just sufficient to allow resolution of the ^{31}P multiplet.

In conclusion, the PF_6^- ion, more specifically the ^{31}P nucleus, is a unique probe into the interior space of graphite and polyacetylene. Its properties must be exploited.

AsF_5 In Graphite Fibers and Polyacetylene. AsF_5 as an intercalant is in many ways complementary to SbF_5 , as pointed out in the introduction. Yet the changes in conductivity produced by both intercalants are similar (36). An important implication of the above is that all of the arsenic (fluoride) species, AsF_3 , AsF_5 , and AsF_6^- are independent molecular or ionic species, and there is reason to expect each, if present, to show its own chemical shift if a temperature can be found at which fluorine exchange between the species is not fast.

Spectra for AsF_5 in graphite fibers and in polyacetylene are shown in Fig. 8. For two specimens of pitch-based fiber (e.g. Fig. 8a), a single line is found which can be ascribed to AsF_5 or AsF_6^- , but not to AsF_3 . Thus either fast exchange or a single species is implied. For the polyacrylonitrile (PAN) based fiber, two lines are seen

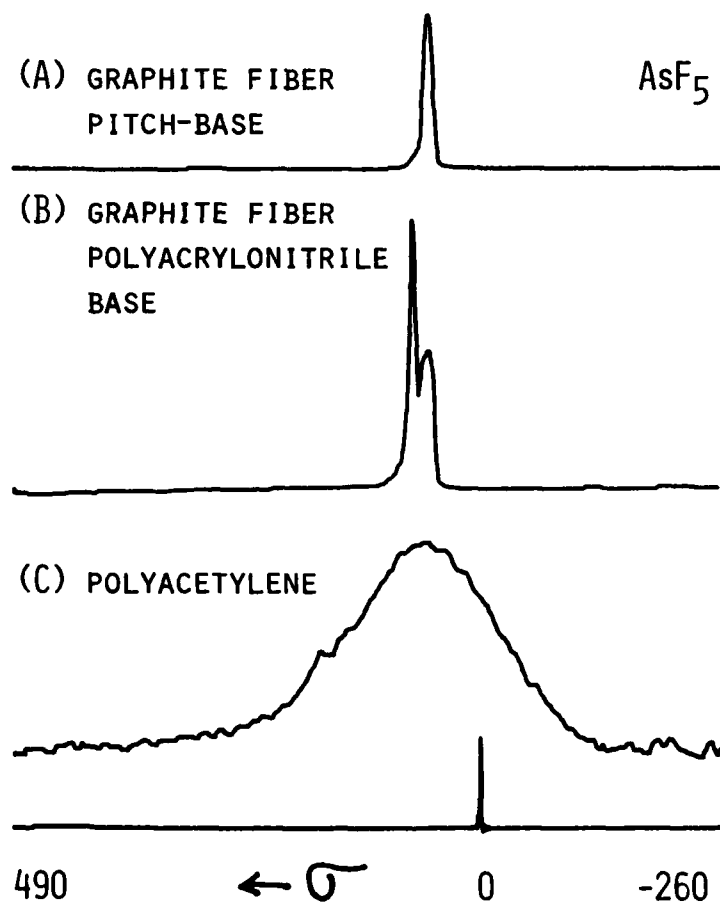


Fig. 8. Fluorine-19 NMR spectra for AsF₅ intercalated in pitch-based graphite fibers (a), polyacrylonitrile-based fibers, (b) and in polyacetylene (c).

bracketing the AsF_5 - AsF_6^- region (Fig. 8b). The polyacrylonitrile-based fibers retain several percent of nitrogen (37), but are otherwise similar in mechanical and crystallographic aspects to the pitch-based fibers. Thus the origin of the two lines is unclear, but their existence must eventually lead to chemical information. Temperature effects should be useful. Do the lines coalesce at high temperature due to fast fluorine exchange? An important NMR experiment for the AsF_5 -graphite/graphite fiber systems is to react the graphite with a fixed amount of AsF_5 in a closed system so that all products are retained in the volume actually examined in the NMR experiment. Nothing should be pumped off.

The spectrum for AsF_5 in polyacetylene is shown in Fig. 8c, and it consists of a broad line centered at the pitch based fiber peak. The spectrum is for a pumped specimen. For a non-pumped specimen there is a somewhat narrower peak of about 10% relative intensity superimposed on the broad peak. This narrower peak spontaneously disappears over time with the formation of SiF_4 ; hydrolysis again.

Fig. 1 shows the relative size of the SbF_6^- ion with respect to the polyacetylene chains viewed end on. It is clear that the intercalant species are quite large with respect to any vacant site in the lattice, and the question can legitimately be posed as to whether the "intercalants" are in the polyacetylene lattice or adsorbed on the surface of the 400 Å diameter polyacetylene fibers. We believe that the intercalants AsF_5 and SbF_6^- are actually within the lattice because the linewidth can be accounted for on the basis of a spherical molecule rotating rapidly in place surrounded by eight near-neighbor protons. See the second moment summary in Table I. In other words, protons are the complete source of the linewidth. This can neatly be checked by using deuterio-polyacetylene as host, whereupon the AsF_5 linewidth should decrease by a factor of 1/6. We have found that the linewidth is independent of temperature from room temperature down to 150K; the inverse linewidth is presented as T_2 in Fig. 9. Thus the width is characteristic of some rigid lattice condition, and our calculation of linewidth, above, in terms of a theoretical second moment (17) is a valid procedure.

The spin lattice relaxation time as a function of temperature is shown in Fig. 9 as well as an extrapolation to lower temperatures based on the motional model of rapid isotropic AsF_5 motion at a fixed site in polyacetylene. We expect to find a T_1 minimum to corroborate the rotational model. Likewise, at still lower temperatures the line should broaden (T_2 should decrease, Fig. 9) as the rotational motion effectively ceases. In principle the line should begin to narrow with an increase in temperature at some point above room temperature due to molecular translation, but we are loath to raise the temperature for fear of causing irreversible changes in the specimen. Thus we propose to use rotating frame relaxation (schematically indicated in Fig. 9 as $T_{1\rho}$.)

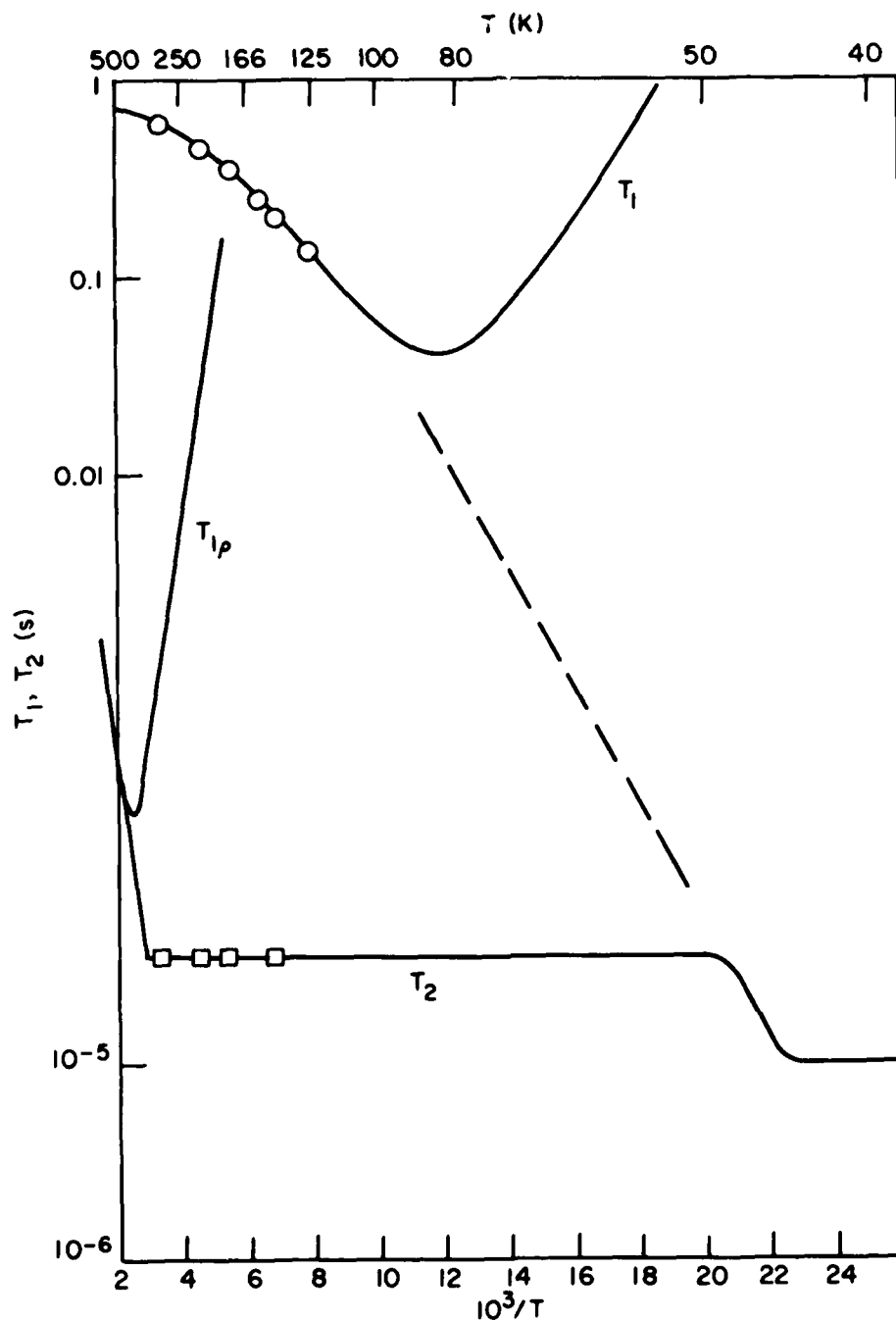


Fig. 9. Measured relaxation times T_1 and T_2 vs reciprocal temperature for ^{19}F nuclei of AsF_5 intercalated in polyacetylene. The schematic course of the rotating frame relaxation time, $T_{1\rho}$, vs $1/T$ is indicated. See text.

Table I: ^{19}F NMR second moments for octahedral hexafluoride molecules/ions in solids where isotropic rotation is allowed or postulated: intramolecular contribution is zero.

<u>Molecule/ Ion</u>	<u>Solid</u>	<u>Second Moment (G^2)</u>	<u>Ref.</u>
SF_6	SF_6	1.42 G^2	38
SiF_6^-	$\text{Mg}(\text{H}_2\text{O})_6\text{SiF}_6$	$\sim 1 \text{ G}^2$	39
AsF_6^-	KAsF_6	1.3 G^2	27
AsF_5	Polyacetylene	1.35 G^2	This work
SbF_6^-	Polyacetylene	1.43 G^2	This work

to find out about diffusion (40); here certain experimental variables allow a decision as to whether the rotating AsF_5 is diffusing with respect to a sea of protons (unlike nuclei) or of fluorines (like nuclei) (40).

Thus the variety of NMR experiments, the temperature, and composition variables should allow characterization of molecular species and motion. Even now we can suggest from our model an upper limit to the diffusion coefficient of $10^{-11} \text{ cm}^2/\text{sec.}$; this implies a loading (or unloading) time of not less than 0.1 s if there are no rate limiting surface reactions. Again this is an assessment of stability.

CONCLUSIONS

The principal difference between the behavior of intercalants in graphite and in polyacetylene that we have found is that translational diffusion of the coefficient group V fluoride intercalants in graphite is at least five orders of magnitude greater between the graphite layers than in the polyacetylene. Nevertheless, the mean time between encounters of an intercalant molecule and the host surface is about the same for both hosts, if the available crystal sizes are considered; thus respective stabilities of the compounds based on this criterion are about the same. As far as establishment of the chemical species present is concerned, no clear differences between polyacetylene and graphite have been found in these NMR studies; because of the greater mobility of intercalants in graphite and the resultant narrower lines, the potential use of high resolution NMR techniques is much more

attractive for analysis of intercalants in graphite than in polyacetylene. The most simple high resolution NMR analytical studies are those involving fluorides of phosphorus, for which the J coupling occurs; we have verified that the PF_6^- ion exists exclusively in graphite compounds prepared by reaction with NO_2PF_6 . For AsF_5 and SbF_6 in polyacetylene, the linewidth is consistent with a rapidly rotating molecule fixed in position in a lattice of protons. The benefits of extension of the data suite by (a) use of a broader temperature range, (b) use of perdeuteropolyacetylene, and (c) use of other NMR experiments are pointed out.

ACKNOWLEDGEMENTS

It is a pleasure to acknowledge the manifold help of David Weber, Patrick Brant, Joseph Reardon, Paul Waters, John Ferraris, Gerald Miller, and F. Lincoln Vogel, who should perhaps all be coauthors hereon. Specific assistance is indicated in the references.

REFERENCES

1. F. L. Vogel and C. Zeller, in "Molecular Metals", W. Hatfield, Ed., Plenum, 1978, p.289.
2. A. G. MacDiarmid and A. J. Heeger, *ibid*, p.161.
3. N. L. Jarvis, personal communication.
4. H. A. Resing, F. L. Vogel and T. C. Wu, *Mat. Sci. Eng.*, 41, 113 (1979).
5. C. K. Chiang, C. R. Fincher, Y. W. Park, A. J. Heeger, H. Shirakawa, B. J. Louis, S. C. Gau and A. G. MacDiarmid, *Phys. Rev. Lett.*, 39, 1098 (1977).
6. E. E. McCarron and N. Bartlett, Preprint, 1980.
7. W. C. Forsman, Extended Abstracts of 13th Biennial Conf. on Carbon, 1977, p. 153.
8. P. Brant, personal communication.
9. F. L. Vogel, personal communication.
10. Graphite can be fluorinated to the extent $\text{CF}_{1.12}$. See P. Kamarchik and J. L. Margrave, *Accts. Chem. Research*, 11, 296 (1978).
11. E. L. Muetterties and W. D. Phillips, *J. Am. Chem. Soc.* 81, 1084 (1959).
12. T. C. Wu, F. L. Vogel, L. A. Pendry, and C. Zeller, preprint.

13. G. S. Parry, Mat. Sci. Eng., 31, 99 (1977).
14. R. H. Baughman, S. L. Hsu, G. P. Pez, and A. J. Signorelli, J. Chem. Phys. 68, 5405 (1978).
15. D. Weber, personal communication.
16. N. Bloembergen, E. M. Purcell and R. V. Pound, Phys. Rev. 73, 679 (1948); see also A. Abragam, "Principles of Nuclear Magnetism", Oxford, 1960.
17. J. H. Van Vleck, Phys. Rev. 74, 1168 (1948).
18. C. P. Slichter, "Principles of Magnetic Resonance", Second Edition, Springer, Berlin, 1978.
19. J. Bacon, P.A.W. Dean, and R. J. Gillespie, Can. J. Chem. 47, 1655 (1969); see also Ref. 11.
20. A. J. Edwards and P. Taylor, Chem. Commun. 1971, P. 1376.
21. C. K. Chiang, C. R. Fincher, Y. W. Park, A. J. Heeger, H. Shirakawa, B. J. Louis, S. C. Gau, A. G. MacDiarmid, Phys. Rev. Lett. 39, 1098 (1977).
22. H. A. Resing, J. P. Reardon, D. C. Weber, P. Brant, F. L. Vogel and T. C. Wu, Proceedings of the NATO School on Magnetic Resonance in Colloid and Interface Science, Reidel, Dordrecht, 1980, in press.
23. A. Avogadro and M. Villa, J. Chem. Phys., 66, 2359 (1977).
24. G. S. Parry, Mat. Sci. Eng., 31, 99 (1977).
25. G. R. Miller, H. A. Resing, F. L. Vogel, A. Pron, and T. C. Wu, manuscript in preparation.
26. For a clear discrimination between the two processes see D. W. Asknes, S. M. Hutchison, and K. J. Packer, Mol. Phys., 14, 301 (1968).
27. E. R. Andrew, L. F. Farnell, and T. D. Gledhill, Phys. Rev. Ltr., 19, 6 (1967).
28. R. G. Kidd and R. W. Matthews, Inorg. Chem., 11, 1156 (1972).
29. R. Andrew, "Nuclear Magnetic Resonance", Cambridge, 1954.
30. N. Boden, in "Plastic Crystals", J. N. Sherwood, Ed., Oxford, 1979.
31. H. Y. Carr and E. M. Purcell, Phys. Rev., 94, 630 (1954).

32. H. A. Resing, Proceedings of the NATO School on Magnetic Resonance in Colloid and Interface Science, Reidel, Dordrecht, 1980, in press.
33. M. Goldman and L. Shen, Phys. Rev. 144, 321 (1966).
34. C. S. Johnson, Jr. Adv. Mag. Res. 1, 33 (1965).
35. U. Haeberlen, J. D. Ellett, and J. S. Waugh, J. Chem. Phys., 55, 53 (1971).
36. B. R. Weinberger, J. Kaufer, A. J. Heeger, E. R. Falardeau, and J. E. Fischer, Solid State Commun. 27, 163 (1978).
37. C. N. Tyson, J. Phys. D: Appl. Phys., 8 749 (1975).
38. S. K. Garg, J. Chem. Phys., 66, 2517 (1977).
39. J. Dereppe, P. W. Lobo, and M. VanMeersche, J. Chim. Phys., 1964, 1076.
40. H. Stokes and D. C. Ailion, Phys. Rev. B16, 4746 (1977).